DEFENCE
SCIENCE & TECHNOLOGY

The Incorporation of Pitting Corrosion Damage into F-111 Fatigue Life Modelling

T. Mills, P. K. Sharp and C.Loader

DSTO-RR-0237

20021119 140

DEFENCE
SCIENCE & TECHNOLOGY

The Incorporation of Pitting Corrosion Damage into F-111 Fatigue Life Modelling

T. Mills*, P.K. Sharp and C. Loader

*Aerostructures Technologies, Pty. Ltd.

**Airframes and Engines Division
Aeronautical and Maritime Research Laboratory**

ABSTRACT

In this report, an Equivalent Crack Size (ECS) approach is assessed and implemented for corrosion pitting in D6ac steel. Relationships between physical corrosion morphology and fatigue life of laboratory coupons were established that allowed corrosion pits to be described as cracks to provide input for durability and damage tolerance analyses. Using the ECS relationship, fatigue lives were accurately predicted in complex coupons tested under spectrum loading. Details are provided on all the corrosion procedures, the developmental testing program, and the validation testing program. So far, the ECS model for corrosion pitting is only valid for areas of the structure that do not experience yielding. Examination of the application of ECS to cases that experience compressive and tensile yield, awaits final development of the appropriate analysis software. The impact of this research on F-111 fleet management can be quite positive by helping avoid unnecessary maintenance and helping to reach a life-of-type goal of 2020.

RELEASE LIMITATION

Approved for public release

AQ F03-02-0359

The Incorporation of Pitting Corrosion Damage into F-111 Fatigue Life Modelling

Executive Summary

The ageing of the F-111 fleet in conjunction with a significant increase in planned retirement date has presented a new challenge to the RAAF, namely: maintaining the level of safety from catastrophic failure while still being able to economically operate the fleet. Such a goal requires an in-depth understanding of the structure, materials, and possible failure modes. For instance, structural optimisation aimed to increase inspection intervals for critical structure (which will reduce the maintenance burden) should only be practiced if time-dependant failure modes, such as corrosion, will not become the new life-limiting scenario for that location.

Durability and damage tolerance analyses of structure assume initial cracks exist, which makes it easy to implement fracture mechanics and fatigue-based management tools. But how does one treat corrosion? It comes in so many shapes and sizes and it does not look anything like a crack (unless it is stress corrosion cracking, SCC). But experience shows us that corrosion can behave like a crack in that it can severely reduce fatigue performance in many instances.

Corrosion pitting is the most insidious type of corrosion affecting major structural components of the F-111, the D6ac steel comprising the wing carry through box, wing pivot fittings, and even the horizontal tail pivot shaft. All are vitally important to flight safety, and all of them pit. Fortunately, D6ac tends to pit in a geometrically simple, orderly fashion, which gives us a greater chance to model it as a crack. This research report focuses on methods to transform a corrosion pit into a crack. Once that is accomplished, then traditional crack growth modelling can be applied to determine a life. The elements of this approach, named the Equivalent Crack Size (ECS) model in the report, are summarised as follows:

- Laboratory coupons were fatigued under constant amplitude, and then the experimental lives were back-predicted using crack growth software to find an equivalent crack size for that life.

- Key features of real corrosion pits that generated the fatigue failures in laboratory coupons were characterised.

- These features were correlated to fatigue life of the coupons and, ultimately, the ECS for those coupons to make what is coined the "ECS distribution."

- The ECS distribution was validated on more complex coupons under spectrum loading with much success.

- Now, when corrosion damage is found in a real component, the key features of the corrosion damage can be measured, and an ECS can be calculated based on historical data (ECS distribution) from the coupon test program.

- By using a known stress spectrum for the part and an appropriate crack growth model, life from that ECS is calculated.

- In this way, residual life of the structure can be extracted from the basic as-detected damage dimensions.

The ECS provides a first approximation of life from a certain snapshot in time. For now, this approach does not take into account the possibility that the corrosion damage will continue to grow and evolve, thus changing the life prediction. This is important to recognise, since the purpose of the ECS modelling, in part, is to assess whether or not damage is safe to leave in place until either retirement or until a better maintenance opportunity. The adaptation of evolving damage states in this model requires knowledge of corrosion growth behaviour in D6ac steel, and others at DSTO/AMRL are working the corrosion kinetics issues.

The data presented in this report show that the ECS technique works well using a variety of specimen types and a variety of loading conditions. Success was met using two different specimen types containing a wide variety of corrosion pit sizes and tested using DADTA 2B load spectra scaled to four different peak load levels.

Currently, the ECS model is only valid for load cases that stay completely elastic. The most complex demonstration of the test program included a high-kt coupon with compressive yield stresses under the Cold Proof Load Test cycle, but the analysis software necessary to predict crack growth in elastic-plastic stress fields was not functioning completely at the time of the research. However, the testing has been completed, so the results can be validated once the software is ready.

The results of this program are significant and useful. Being able to predict the pitting/fatigue behaviour of D6ac steel in the F-111, enhances the safety of the fleet. The informed decisions surrounding dealing with failure modes such as corrosion will allow the F-111 to be managed more economically. The ultimate benefit for the RAAF will be reduced aircraft down time and increased availability.

Authors

T. Mills
Aerostructures Technologies, Pty. Ltd.

Thomas Mills, Principal Engineer--Aerostructures, graduated from the University of Missouri in 1991 with a Bachelor of Science in Mechanical Engineering. Graduate studies earned him Master of Science and PhD degrees in Mechanical Engineering from the University of Utah, ending in 1997. From there, he joined the Air Force Research Laboratory, Wright-Patterson AFB Ohio, where for three years he researched both corrosion/fatigue interactions in aluminium and bonded composite repairs of aluminium aircraft structure. In April 2000, he moved to Australia to work for Aerostructures located at AMRL, Fishermans Bend where his primary responsibility is to incorporate corrosion into the damage tolerance assessment of the F-111 strike aircraft as part of the Sole Operator Program.

P. Khan Sharp
Airframes & Engines Division

Khan Sharp, Senior Research Scientist. Graduated from Monash University in 1987 having obtained a Materials Engineering Degree with Honours. In 1990, he completed a Masters of Engineering Science degree and commenced work in the Fatigue and Fracture Detection and Assessment area at Fishermans Bend. Over the past 10 years he has been involved in the metallurgical investigation of aircraft structures and components, fractographic analysis of fatigue surfaces and research into fatigue crack growth and fracture of aircraft materials. During that time he has published over 40 reports and papers. He has completed extensive research into novel methods of retarding crack growth and innovative NDI methods. In 1999, he was awarded a Research Scientist Fellowship to study at the US Air Force Research Laboratory. He presently manages the Structural Implications of Corrosion task and conducts research on fatigue and fracture.

C. Loader
Airframes & Engines Division

Christopher Loader, Professional Officer, graduated from Monash University in 1998 with a Bachelor of Science majoring in Materials Science and Chemistry and a Bachelor of Engineering with Honours in Materials Engineering. Since arriving at Fishermans Bend two years ago, he has worked several programs aimed at better understanding corrosion-initiated fatigue in a variety of aluminium and steel alloys used in the aircraft industry.

Contents

Acronyms

AMARC	Aircraft Maintenance and Reclamation Centre
CPLT	Cold Proof Load Test
DADTA	Durability and Damage Tolerance Analysis
ECS	Equivalent Crack Size
EDX	Energy Dispersive X-Ray
EIFS	Equivalent Initial Flaw Size
FFVH	Fuel Flow Venthole
HE	Hydrogen Embrittlement
LEFM	Linear Elastic Fracture Mechanics
LMTAS	Lockheed-Martin Tactical Aircraft Systems
Metric	a measurable pit morphology parameter (e.g. pit depth, pit area, etc.)
NDI	Non-Destructive Inspection
PDM	Programmed Depot Maintenance
POD	Probability of Detection
RAAF	Royal Australian Air Force
SCC	Stress Corrosion Cracking
SFH	Simulated Flight Hours
SMF	Stress Multiplication Factor
USAF	United States Air Force
UTS	Ultimate Tensile Strength
WCTB	Wing Carry Through Box
WPF	Wing Pivot Fitting
YS	Yield Strength

1. Introduction

With the retirement of all F-111 variants by the United States Air Force (USAF), the Royal Australian Air Force (RAAF) has become sole operator of the F-111 aircraft. The RAAF fleet is planned to remain operational until the year 2020. However, the structural sensitivity and complexity of the F-111 contributes significantly to the costs of continued fleet operations. As such, current structural integrity efforts for the F-111 are focused on reducing maintenance burden whilst ensuring that all possible failure modes are correctly accounted for in the type's Durability and Damage Tolerance Analysis (DADTA).

A good example of a program designed to reduce long-term maintenance burden is the optimisation of the Fuel Flow Vent Holes (FFVH) in the Wing Pivot Fitting (WPF) [Heller, Burchill, McDonald and Watters 2001]. These highly fatigue critical locations demand inspection as often as 500 hours. Shape optimisation to alleviate stress can relieve this high inspection burden significantly and perhaps raise the inspection interval for that region as high as 2000 hours.

Such an increase in inspection interval is only viable if other failure modes, not previously considered, do not become a threat to flight safety as a result. One failure mode that needs particular attention under such a scenario is corrosion. Corrosion has caused problems in critical areas on the aircraft. In particular, corrosion pitting has been found in the F-111 Wing Pivot Fitting (WPF) on numerous occasions, and this is a significant concern given the fact that the WPF is very sensitive to mechanical damage.

The lack of adequate techniques to analyse corrosion fatigue interactions [Cole, Clark and Sharp 1997] gave rise to an AMRL research program into the effects of pitting on the fatigue behaviour in D6ac steel. The program contains several phases all of which are detailed in this report. Elements of the program follow:

- Constant amplitude fatigue of simple pitted coupons--these coupons contained pits in a flat surface, so no other structural details, such as holes, influenced the fatigue life. These coupons and the associated program will be referred to as 'low-k_t' throughout this report.

- Extensive fractography of the failed low-k_t specimens--crack growth rates in some specimens and key pit features in all specimens were measured to help develop the Equivalent Crack Size (ECS) model described shortly.

- Evaluation of material models and selection of appropriate crack growth modules based on stress levels--some load cases in the F-111 require elastic-plastic analysis, where other cases are purely elastic.

- Development of the ECS for pitting corrosion in D6ac steel.

- Use of ECS to predict lives in more complex fatigue specimens--these specimens were simulated FFVH coupons that feature a high stress concentration (hereafter referred to as high-k_t coupons). These high-k_t coupons served to validate the ECS data developed to date.

The key result of this effort has been to implement a method to incorporate corrosion damage into specific fatigue life analysis technique. The analytical procedure adopted in these experimental efforts has been named the ECS model, and it is essentially an application of the Equivalent Initial Flaw Size (EIFS) approach, Manning et.al, from the early 1970s.

The model will be discussed in detail in the next section, but a summary of the approach is as follows:

- Key features of real corrosion pits that generate fatigue failures in laboratory coupons are characterised.

- These features are correlated to fatigue life of the coupons and, ultimately, the ECS for those coupons.

- When corrosion damage is found in a real component, the key features of the corrosion damage can be measured, and an ECS is calculated based on historical data from the coupon test program.

- By using a known stress spectrum for the part and an appropriate crack growth model, life from that ECS is calculated.

- In this way, residual life of the structure can be extracted from the basic as-detected damage dimensions.

The ECS provides a first approximation of life from a certain snapshot in time. For now, this approach does not take into account the possibility that the corrosion damage will continue to grow and evolve, thus changing the life prediction. This is important to recognise, since the purpose of the ECS modelling, in part, is to assess whether or not damage is safe to leave in place until either retirement or until a better maintenance opportunity. The adaptation of evolving damage states in this model requires knowledge of corrosion growth behaviour in D6ac steel, and others at DSTO/AMRL are working the corrosion kinetics issues.

2. Background

This chapter describes some of the basics associated with this research program. Elements include a discussion of the history of corrosion problems in the F-111, especially as relevant to safety of flight, as well as discussions on corrosion pitting in D6ac steel and the creation of service-representative damage in the laboratory. Also, an extended discussion of the Equivalent Crack Size (ECS) concept, the focus of this report, is offered at the end of this chapter.

2.1 Service failures in F-111 from corrosion

When the F-111 entered service with the USAF in the late 60s, a number of structural failures occurred in the D6ac steel components both during service and during full-scale fatigue testing. The first set of failures occurred from manufacturing flaws present in the components, with most of the cracks originating in boltholes for Taper-Lok fasteners. The failures occurred in the most critical components of the aircraft manufactured from the D6ac steel, namely in the Wing Carry Through Box (WCTB) and in the in the Wing Pivot Fittings (WPF). As the length of service of the F-111s increased, the failures originating from manufacturing flaws were replaced by failures caused by degradation of the material in service.

Difficulties with inspecting the WCTB, WPFs, and horizontal tails in the F-111, largely because of very small critical crack sizes, resulted in the development of the cold proof load test (CPLT) to prevent in-flight failures. General Dynamics initiated the first phase, the Recovery Program, after the loss of aircraft 67-049. The accident aircraft was an F-111A, which had accumulated just over 100 flight hours; it crashed on the Nellis AFB range on 22 December 1969 when a wing separated in flight.

In its latest form, the CPLT involves maximum negative and positive g excursions at both minimum and maximum wing sweep at a temperature of -40°C. The principle of the CPLT is simple enough—the toughness of the steel is significantly reduced at low temperatures, and, therefore, any failure should occur during the cold-proof load test rather than in service. The test thus allows a 'safe' period in service before re-test, this period being based on the time required to grow a crack which just passes the CPLT to the size required to cause failure in service.

The CPLT, the core of the Recovery Program, has since been repeated fleet-wide in efforts known as II-SIP and III-SIP. A report by Mills, et al. (2001), gives a thorough history of D6ac failures in the F-111, but for the purposes of this research report, only the failures (or imminent failures) resulting from corrosion are summarised.

The first recorded corrosion failures happened in 1971 when a Recovery Program F-111A suffered catastrophic failure in the lower plate of the WCTB during the CPLT. The crack completely ruptured the lower plate along with the front and rear spars.

This failure emanated from a stress corrosion crack at a Taper-Lok hole that most likely resulted from improper cleaning during assembly [Laffe and Sutherland 1994]. The failure occurred at 57.5% of the maximum +7.3 g load [Buntin 1971].

As part of the CPLT process, many pre-test inspection programs have been implemented over the years. These inspections are designed scrutinise problem areas before the CPLT is conducted to prevent failures during the test. These inspections have averted costly failures and highlighted new problems. For instance, cracks were found in the No. 2 stiffener runout in the upper WPF of two Australian F-111Cs (A8-148 and A8-109) [Cox 1985]. In both cases, the cracks initiated from corrosion pits and the initial fracture was intergranular before developing into a more typical striated fatigue crack. However, the extent of the intergranular fracture was only one grain deep and did not contribute significantly to the overall crack length. The intergranular crack growth probably occurred by a stress corrosion cracking (SCC) mechanism. The fracture in A8-109 started from three separate pits, and the cracks initially grew at approximately the same rate before joining to form one large crack. Pit/crack interaction is shown in Figure 1 a & b.

a)　　　　　　　　　　　　　　　b)
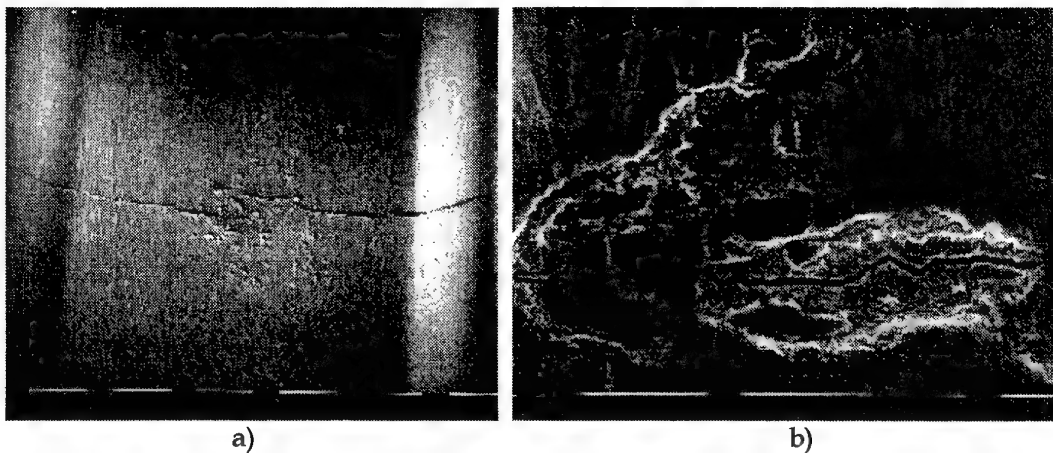
Figure 1 a & b. Pitting-nucleated cracks in F-111 stiffener runout.

Later, in 1988, an F-111E suffered failure of the horizontal stabiliser pivot shaft fitting; the cause was a stress corrosion crack. The damage formed at a tooling hole in the top of the fitting. This location was added to the inspection package for future programmed depot maintenance (PDM) [Laffe and Sutherland 1994].

An examination of an F-111E (USAF 68-043) WCTB in 1991 revealed two cracks in the upper plate. These cracks originated from pitting corrosion in Taper-Lok holes [Nguyen 1991]. The fracture mode was predominantly intergranular and was attributed to stress corrosion cracking. In some regions of the crack front, there was no evidence of fatigue crack growth, and where present, the fatigue region was still

extremely short (~40 μm long). In this instance, the cracks were found during a teardown inspection of the WCTB after 4239 flight hours.

A clearer picture of the origin and mode of cracking observed in the critical D6ac components is emerging. Up to the 1980s, the failures and cracks originated from problem areas generated or left over from the manufacture of the components. A number of these failures occurred in the CPLT, thus preventing almost certain in-flight catastrophic structural failures. Since the early 1980s, most of the cracks were observed to originate from damage sustained in service, often in the form of pitting corrosion. Intergranular SCC sometimes followed the pitting corrosion, before developing into a fatigue crack. The presence and extent of SCC probably depended on the local stress distribution.

Another cracking mechanism originated from the compressive overload, which resulted in localised compressive yielding during high-g manoeuvres and/or during CPLT. Upon removal of the compressive load, the yielded areas contained residual tensile stresses of sufficient magnitude to initiate and propagate SCC and/or fatigue cracks. The possibility of this damage continuing to accumulate is real, since CPLT is a mainstay of F-111 fleet management. Combinations of pitting and these residual tensile stresses could continue to be a serious problem.

2.2 Corrosion pitting in D6ac

D6ac steel, used in structural applications in the F-111, has minimal corrosion resistance under most environments. Thus, D6ac steel on the F-111 aircraft is, in most components, protected by cadmium plating. The breakdown of this plating, through erosion, abrasion or polarisation, will lead to pitting in the steel. This method of pit formation in these regions is not governed by the same mechanisms as are often discussed in papers dealing with pitting corrosion. It is important, however, to understand the factors affecting the nucleation of pitting corrosion on bare metal in order to produce pitting on D6ac steel in accelerated tests.

The mechanisms of pit nucleation in steels discussed by Loader and Sharp (2001) are relevant to those few locations of unprotected D6ac steel in the F-111 and are important given the tendency for these areas to be in highly stressed regions of the aircraft structure where the degradation of fatigue life by pit nucleation cannot be tolerated.

Initial studies by General Dynamics [Kendall 1971] found pitting to take the form of circular holes. The maximum sizes reported for deionised water and salt water were 30 microns and four microns, respectively. Although the pits developed very quickly (less than 24 hours in the distilled water and less than eight hours in the salt water), they size was quickly capped by general corrosion mechanisms. It appears that the pitting and the general attack were competing. In the distilled water, pit depths reached 30 microns and then general attack started and kept the pit sizes stable. In the more severe environment of salt water, it would be natural to assume more severe

pitting, but as can be seen from the results, this was not the case. It is hypothesised that the general attack begins much sooner and progresses much faster in the salt water environment; therefore, the pit depths cap at a much smaller value.

Pitting damage can take many forms, from uneven local corrosion to narrow pits and crevices as characterised by Melchers (1994), and shown below in Figure 2. The main contributors to pit nucleation in high strength steels (opposed to general corrosion) are manganese sulphide (MnS) inclusions (Figure 3). The conclusion that the inclusions themselves are cathodic has been investigated by a number of authors and proved incorrect. Srivastava and Ives (1987) exposed a sample corroding about a sulphide inclusion to a solution of 3% cupric chloride and found that copper precipitated on the matrix close to the sulphide inclusions but not over the inclusion. This implied that the inclusions themselves were anodic. This leads to dissolution of the matrix surrounding the inclusion providing greater opportunity for multiple inclusions to 'link up' and form deep pits.
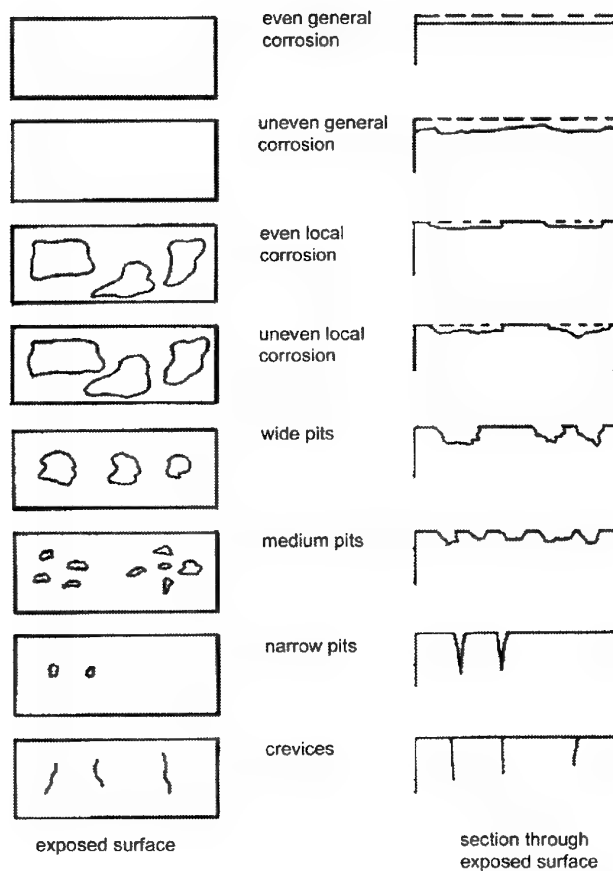
Figure 2. Types of Corrosion [after Melchers, (1994)].
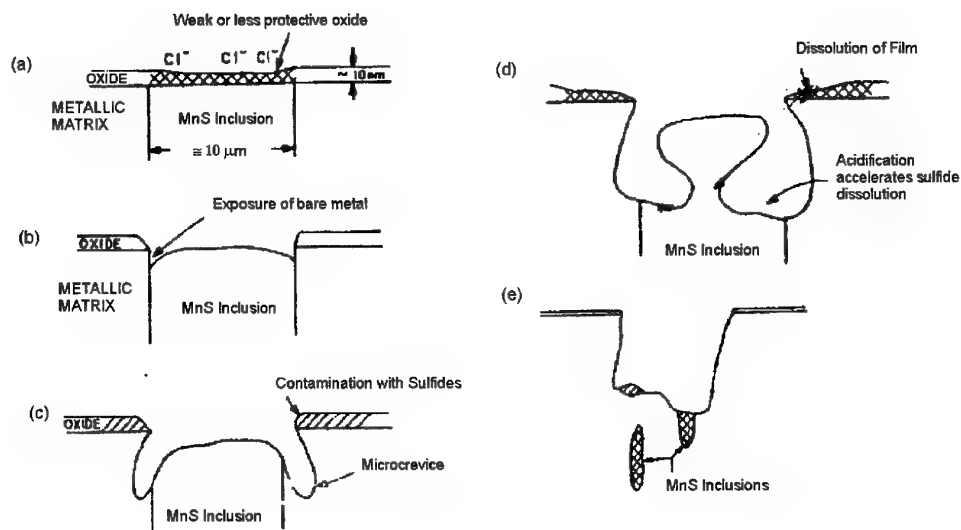
Figure 3.. Schematic representation of the initiation and propagation of pitting corrosion at MnS inclusions. (a) Dissolution of the film above the inclusion promoted by (1) galvanic action between the protective oxide of low conductivity and the oxide above the inclusion and (2) preferential adsorption of chlorine ions. Both the weak oxide and the inclusion are anodic to the metallic matrix. (b) Dissolution of the sulphide inclusion. (c) Propagation of localized attack. The bare metal becomes anodic to the less conductive MnS inclusion. Acidification by hydrolysis in the occluded region stimulates further sulphide dissolution and propagation of pit-type attack. (e) Propagation of macro-pits {Eklund (1994)].

Srivastava and Ives supported a proposal by Eklund (1994) that the steel is initially cathodic with respect to sulphides during the initial stages of attack when the sulphides are polarised to the potential of the oxide film. The potential difference progressively decreases and reverses with the exposure of bare metal. Sulphide ions produced by the electrolytic dissolution of the sulphide inclusions immediately adsorb on the nearest oxide covered surface, while hydrolysation of the metal cations produces a localised acidity that leads to autocatalytic behaviour that propagates the pit.

Initial studies using D6ac steel, which were polished then immersed in ionised water for periods up to two hours, showed evidence of this type of attack at the interface between the MnS inclusions and the matrix. The composition of the inclusions was determined from EDX measurements made on the SEM microscope. This is shown in Figure 4. Pit formation at these inclusions is shown in the scanning electron micrograph in Figure 5a and the optical micrograph in 5b.
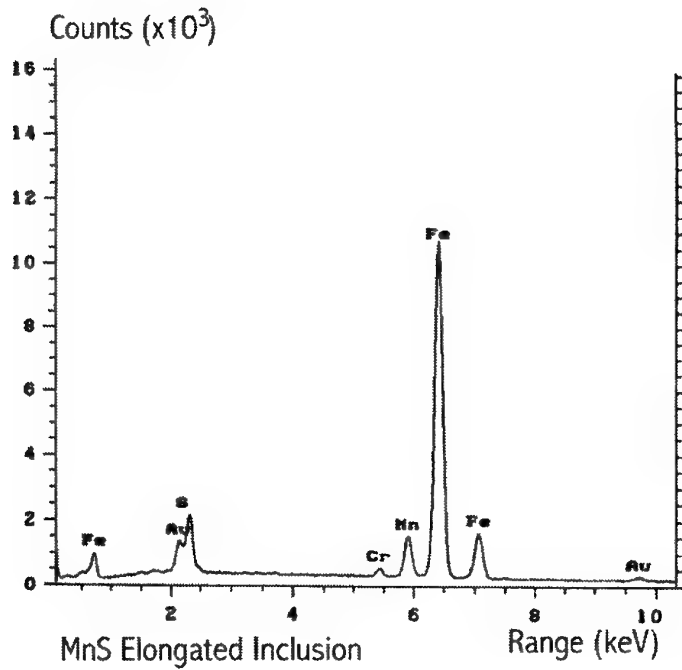
Figure 4. EDX spectrum for MnS inclusions in D6ac.

a)   b)
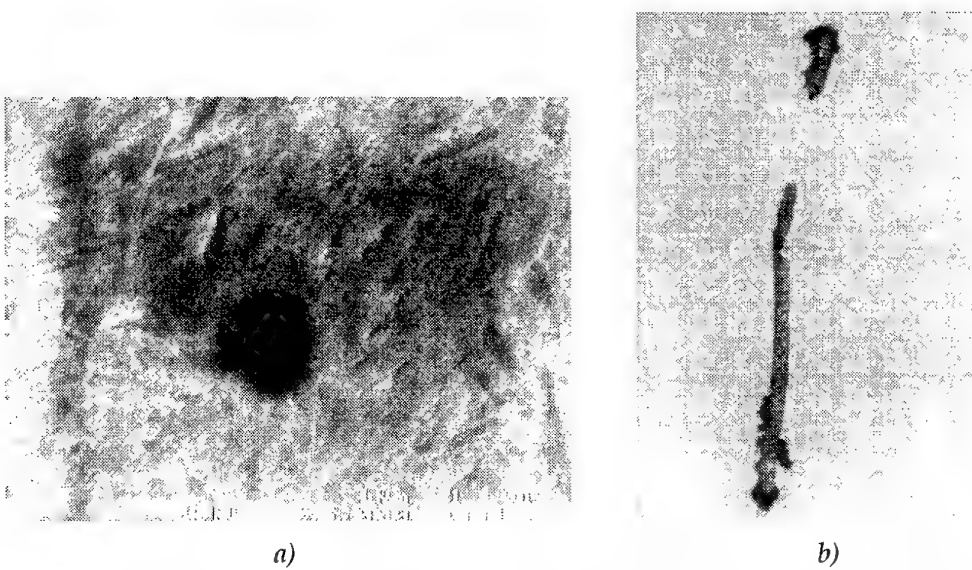
Figure 5. Initiation of pitting corrosion at the interface of the metal matrix and MnS inclusions in D6ac steel---a) SEM, b) optical microscope.

2.3 Recreating service corrosion for laboratory specimens

2.3.1 Corrosion protocol requirements

The need to quickly produce controlled amounts of corrosion on fatigue specimens of D6ac steel required environmental conditions very different from those present in the aircraft. The corrosion protocol developed for pitting in D6ac had to meet the following five requirements:

1. Corrosion had to be produced within a limited time frame.

2. General corrosion had to be undetectable.

3. Crevice corrosion had to be minimal.

4. Production of corrosion had to be limited to a controlled area.

5. The corrosion had to be reproducible.

Issues and approaches for these five requirements are discussed where appropriate in the following sections dealing with different corrosion techniques, namely: natural, potentiostatic, and galvanostatic. A detailed discussion of the actual procedures can be found in a report by Mills and Loader (2000).

2.3.2 Natural corrosion

In-service corrosion, for the most part, occurs when the cadmium plating that protects the D6ac steel from corrosion breaks down. This allows the pits to grow in environments that would normally result in general corrosion of the steel, making it difficult to recreate the corrosion process in the laboratory without long operating times. It would have been possible to cadmium plate the fatigue specimens and then either artificially or naturally degrade the plating to allow for pitting, but this would have caused one of two problems. Artificial breakdown of specific areas would have resulted in artificial control over the pit spacings and, thus, non-representative corrosion. Chemical or natural breakdown of the cadmium plating would have contravened requirement 1, because it would have taken too much time.

At first, basic immersion exposure was tried to allow natural pitting to develop in the specimens. Unfortunately, D6ac steel, unlike stainless steels, does not readily produce a passive film. High pH or passivating chemicals are required to allow pitting corrosion to without the occurrence of general corrosion. No solution was found that provided pitting corrosion without the presence of either general corrosion or crevice corrosion (violating requirements 2 and 3).

2.3.3 Potentiostatic corrosion

The next approach tried for producing pits in D6ac was electrochemical in nature. The idea was to provide a driving force to cause pit formation and propagation without general attack. The electrochemical approach made up for the lack of cadmium plating and aimed to create a corrosion morphology representative of that present in D6ac with a damaged protection scheme.

The first step in the electrochemical process was to find an electrolyte that produced a very strong passive layer and that remained passive on the surface of the D6ac unless a current was applied. This eliminated the risk of corroding areas unintentionally if some electrolyte came into contact with areas not targeted for corrosion (requirement 4). A strong passivating electrolyte can be determined by measuring the difference between the corrosion potential (the point at which the material changes from anodic to cathodic behaviour), and the pitting potential.

The pitting potential was determined by conducting potentiostatic scans of D6ac steel exposed to a variety of electrolytes. Through anodic polarisation, a threshold value of potential below which pitting does not occur was determined. By measuring the hysteresis between increasing and decreasing potential, it is possible to define a range in potential between which existing pits will grow but no new ones will nucleate. Literature references to these potentials are not consistent, though they are commonly called the pitting nucleation potential, E_{NP} and the pitting protection potential E_{PP}.

During the potentiostatic scans, different concentrations of inhibiter and salt were tested until a combination that produced strong passive layer was discovered. The electrolyte selected from these experiments was 0.1 M Sodium Chloride (NaCl) with 1000 ppm of Sodium Nitrite ($NaNO_2$) at pH 10.

With the electrolyte selected, the next goal was to try to generate highly predictable and reproducible pitting damage. However, producing corrosion that met the five requirements of the protocol was not so easily done.

Potentiostatic corrosion attempts led to a system that tended to be extremely sensitive, with large variations in the corrosion current occurring between specimens. This led to some specimens giving very high corrosion currents, which caused general corrosion, while others produced very low currents, for the same set up.

The low growth rates of the corrosion produced a very strong and cohesive corrosion product that provided a site for self-propagating filiform corrosion. This developed where the corrosion product provided an interface under which an active site could react to produce more corrosion product. This extended the interface and moved the active site with time and resulted in wormlike trails of corrosion extending across the surface of the specimen (Figure 6).

Figure 6. 'Wormlike' self-propagating filiform corrosion on the surface of D6ac steel.

Crevice corrosion proved problematic initially. The cell set-ups used a rubber O-ring to isolate the area to be corroded and provided a site for crevice corrosion, which occurred preferentially to any pitting corrosion. This problem was overcome by using different masking agents to isolate the area to be corroded. The O-ring then contacted only the masking agent preventing the crevice corrosion, while the masking agent wet the surface of the steel and did not provide a site for crevice corrosion. The masking agent required both mechanical strength to prevent the O-ring from penetrating and had to wet the steel and provide a barrier to the electrolyte. Araldite (a two-part adhesive) and Macdermid Ferro Stop-Off Lacquer (a masking agent) were used for this purpose. See the report by Mills and Loader (2000) for more details on this procedure.

The Araldite was used to mask off the immediate area to be corroded, and because of its ease of use, the stop-off lacquer was used to wet all other areas to be protected going from the Araldite outwards. The Araldite wetted the surface much better and eliminated all risk of crevice corrosion. The stop-off lacquer was effective at stopping electrolyte penetration, but it was not effective at stopping crevice corrosion where the electrolyte had access to a free edge of the masking agent. That is why the Araldite was used for that interface locally.

2.3.4 Galvanostatic corrosion

Galvanostatic corrosion was attempted next, with better success. Initial attempts to produce a minimum pit density by controlling the corrosion rate with a two-stage current density profile were unsuccessful. The initial high corrosion rate was expected

to allow both the start of pitting and pit growth, while the lower corrosion current was expected to allow only pit growth (nucleation of pits, as has been discussed, requires a higher potential than the growth of the pits). This proved impossible to gauge because the lower corrosion current resulted in minimal continued pit growth, the start of general corrosion, or the production of the self-propagating filiform corrosion. Therefore, a single current density was chosen, and trials showed a power law growth that was reproducible (requirement 5), and easily predicted with a high degree of accuracy.

Determination of the power law curve for the galvanic corrosion of D6ac steel was accomplished using 10 specimens at each of three corrosion times, all with a current density of 1000 mA/mm². Figure 7 shows the results of those experiments.

This power law was also used to predict corrosion depths using different current densities for the much smaller areas used in specimens representative of areas on the F-111 Wing Carry Through Box, and on the AMARC wing used in a fatigue test at AMRL Fishermans Bend [Mills and Loader 2000].
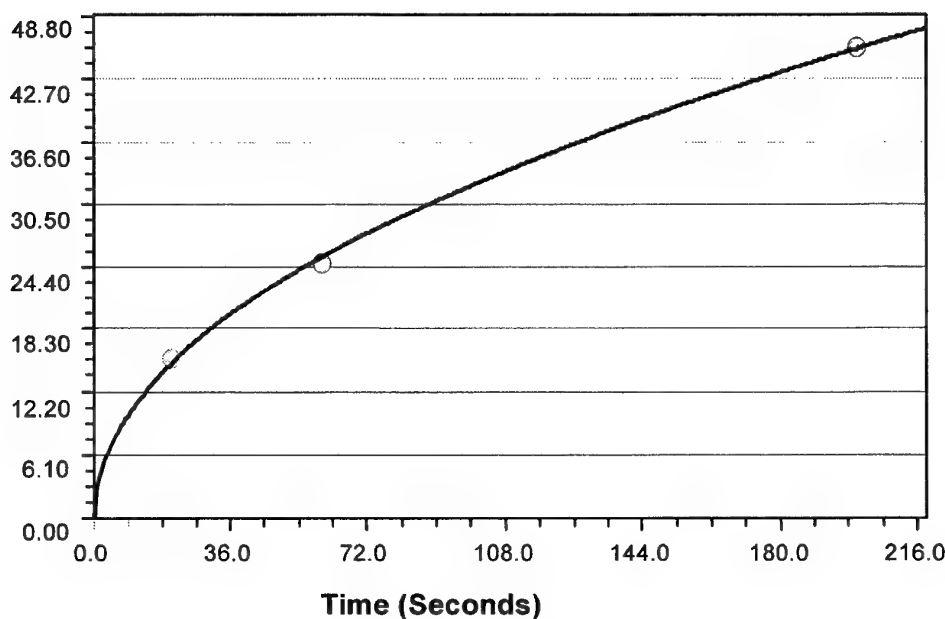
Figure 7. Power law prediction of pitting corrosion depth following the rule $D = 3.3t^{0.5}$ where D is the maximum pit depth in microns, and t is time of corrosion in seconds.

As described in more detail in the report by Mills and Loader (2000), the power law (from Figure 7) was used successfully to predict corrosion pit depths for laboratory applications. Figure 8 shows the predicted versus actual pit depths. The power law seemed to be slight conservative in most cases, in the sense that it really gave a 'minimum' maximum pit size. In other words, the largest pit in the sample was essentially guaranteed to at least be the target depth. Often times, the actual pit depths were somewhat deeper. This did not cause a problem, though.

2.4 The ECS concept

The Equivalent Crack Size concept is not new. As mentioned previously, it stems from much early work into the Equivalent Initial Flaw Size concept. Practically, the move away from the word 'flaw' can largely be attributed to litigation brought on by using words that imply 'defective,' and the concept surrounding 'initial' shows the roots of the concept in describing the initial quality of a manufactured component. The term 'initial' could also be used to describe the fact that the equivalent flaw is used as the starting point of a traditional fatigue analysis.

Renaming the concept from EIFS to ECS may seem like semantics, but the term ECS goes a long way towards an accurate description. In ECS, we are taking some detected discontinuity and equating it to a crack for the purpose of fatigue analysis. The damage might be an accidental scratch or nick, a corrosion pit, a fretting scar, or perhaps even some discontinuity caused by the manufacturing process of the material or component itself.

In the case of ECS as used in this report, the concept captures a method for relating corrosion pitting to an equivalent crack. Other terminology in the literature refers to Equivalent Pit Size or Equivalent Corrosion Damage models, but in fact, the corrosion damage is the real damage, not the equivalent. What the corrosion damage is equivalent to in every single analysis is a crack.

Although the concept may sound simple enough—find a corrosion pit and treat it like a crack using some growth model—the amount of work required to generate this information is often seen as prohibitive. So many variables in corrosion geometry can have such a profound effect on ECS distributions that it appears that a new distribution would need to be developed for each new application. This is true in many cases. The morphology of crevice corrosion is different to that of pitting, which differs from exfoliation or intergranular attack, and so on.

Fortunately, the type of corrosion of concern in the F-111 is pitting in D6ac steel. As mentioned before, the damage morphology is fairly uniform in this material, since the driving force for corrosion pitting in this material is the galvanic couple between the protective cadmium plating and the bare steel where the plating has locally broken down.
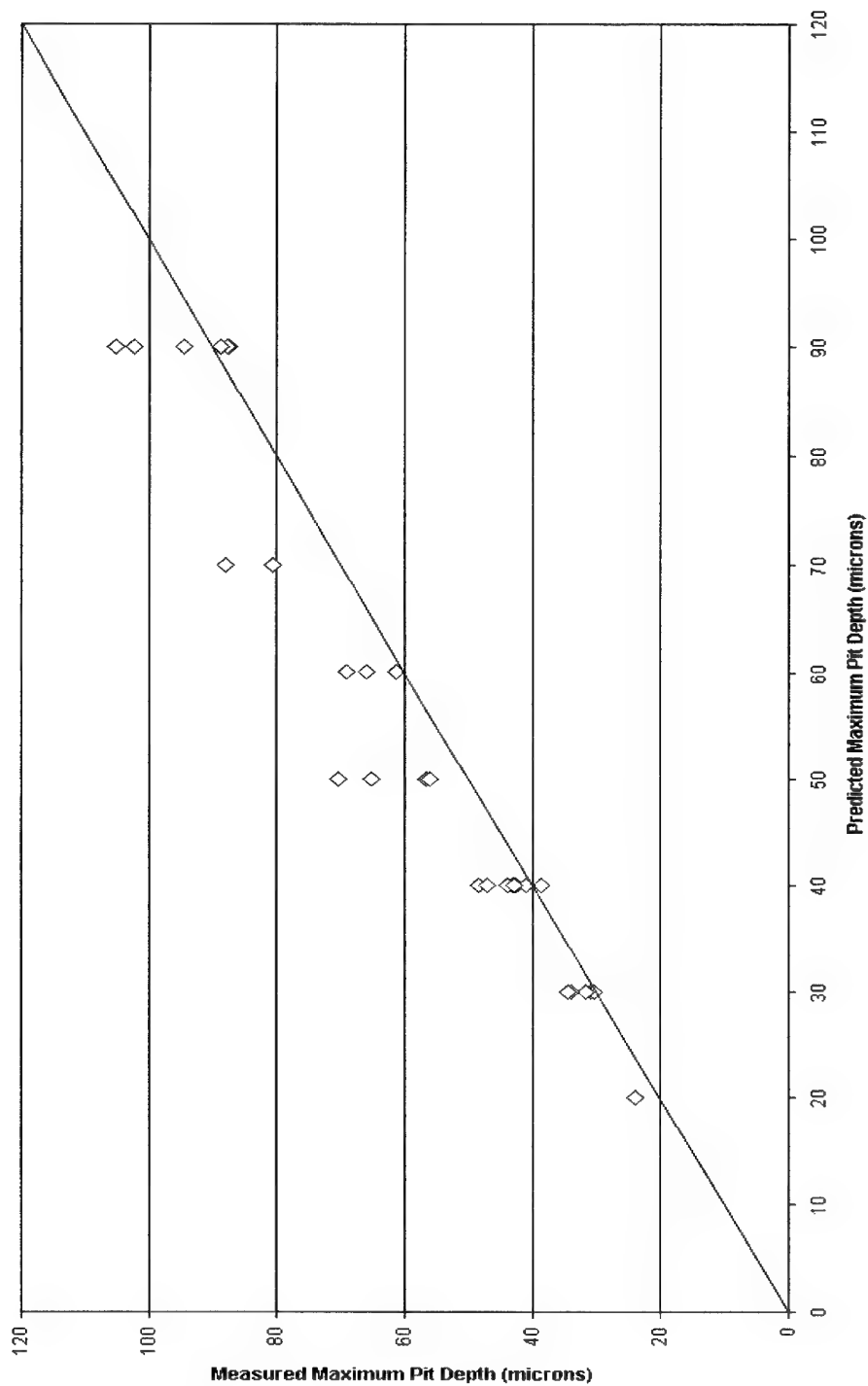
Figure 8.   Measured vs. predicted maximum pit sizes produced in D6ac steel using the DSTO/AMRL-developed pitting corrosion procedure.

The pits that develop are very hemispherical in shape, which makes them very well behaved from a fatigue point of view and from a non-destructive inspection perspective. The pit geometry in D6ac steel, being hemispherical, is quite open, unlike some of the sharp, tortuous pit geometries found in some aluminium alloys (Sharp 2001). Thus, the pits in the steel are relatively easy to measure in terms of depth and aspect ratio, which so happen to be the features that correlate best with the laboratory fatigue results described in Chapter 3.

The basics of applying the ECS concept are summarised here, and the individual steps as applied to this program are shown in detail throughout Chapter 4.

- Key features of real corrosion pits that generate fatigue failures in laboratory coupons are characterised.

- These features are correlated to fatigue life of the coupons and, ultimately, the ECS for those coupons.

- When corrosion damage is found in a real component, the key features of the corrosion damage can be measured, and an ECS is calculated based on historical data from the coupon test program.

- By using a known stress spectrum for the part and an appropriate crack growth model, life from that ECS is calculated.

- In this way, residual life of the structure can be extracted from the basic as-detected damage dimensions.

It should be clear from reading this summary just how much work was involved in developing the ECS for corrosion pitting in D6ac steel. First, fatigue tests were necessary using corroded coupons. The development of the corrosion procedure used to introduce realistic damage (representative of that found in the fleet) in the laboratory coupons was a major effort in its own right, as can be seen from the discussion in Section 2.3.

Once the tests were complete, extensive fractography was necessary to establish two things, namely: the features and geometries of the pits that caused fatigue failures and the growth rates of the cracks. The growth rates of the cracks were necessary to ensure that the material model selected, (which is fed into a crack growth engine for life prediction) describes the laboratory behaviour of the specimens.

When the pit features of interest were correlated with the ECS distribution derived from the combination of material model and experimental fatigue life results, then the application of the concept had to be validated. Again, this required more predictive modelling and experimental verification of those results.

Hopefully, this discussion helps illustrate why the ECS concept is not widely used to date. However, this report also strives to illustrate that given the appropriate resources, this technique can be quite powerful. In this case, the success has been greatly aided by the nature of the pits in D6ac steel.

3. Low-k_t Fatigue Experiments

The first stage in developing the Equivalent Crack Size (ECS) data for corrosion pitting in D6ac required a constant amplitude fatigue program. Low stress concentration (low-k_t) specimens were chosen to take advantage of the tight control exhibited in the generation of corrosion pits. By using a low-k_t specimen, it was possible to ensure that the largest pit was always in the area of maximum stress, since all areas of a gauge section saw the same stress. Had the specimens had a stress concentrator in them, such as a hole, it would not have been possible to ensure that the largest pit was in the area of peak stress.

The purpose of these tests was to develop a relationship between a pit "metric" and fatigue life. The entire ECS *vs.* pit parameter relationship was developed from these tests.

3.1 The specimens

D6ac steel, like many alloys, has changed extensively over the years, in that newer alloys are typically cleaner, tougher, and more fatigue resistant. This was a primary concern for this program, as the goal was to investigate the behaviour of F-111 grade material to pitting corrosion fatigue. Fortunately, AMRL had purchased large quantities of bar stock during the F-111 recovery program, and such stock was inventoried prior to the commencement of these tests. During the inventory process, it became apparent that large numbers of specimens were commissioned and produced in the 1970s, and were never tested. Conservation of the remaining bar stock meant that these specimens could provide a source of material for the low-k_t fatigue tests planned as part of the current program. Critical mechanical properties of D6ac steel from this era follow:

- UTS   1517-1655 MPa (220-240 ksi)
- YS   1310 MPa (190 ksi)
- K_c 122 MPa $\sqrt{m}$ (110 ksi $\sqrt{in}$)
- K_{Ic} (low)   46.5 MPa $\sqrt{m}$ (42 ksi $\sqrt{in}$)
- K_{Ic} (high)   75 MPa $\sqrt{m}$ (67.5 ksi $\sqrt{in}$)

The reason two values for plane strain fracture toughness are given is because a processing change in the D6ac used in the F-111 resulted in widely varying toughness values. For all the analyses in this report, the higher value is used. Changing the value to the lower number affects the final crack size more than the total life.

Three specimen types were found that were suitable for axial fatigue testing. These were all flat axial fatigue specimens of varying geometry. All of these specimens had some common features:

- The specimens were narrow-waisted such that the grip ends were thicker than the centre sections.

- The gauge length of the specimens was in the as-machined state

- The grip ends were set up for pin loading.

Searching through records showed that these specimens were known as SC97, SC97R1 and SK16359 flat axial fatigue specimens.

The SK16359 specimens were so large that the loads necessary to test these specimens in the low-k_t condition would have required a 1MN-capacity load frame. For this reason, those specimens were rejected. The SC97R1 specimens were very similar to the SC97 specimens and were also much smaller than the SK16359 specimens, so load requirements were much lower, and the SC97R1 specimens were available in greater numbers than the SC97 specimens. Figure 9 is a converted engineering drawing showing the tolerances used in the initial manufacture.

During the early part of the low-k_t test program, fatigue tests on these specimens showed up a number of problems in the original specimen design that had to be rectified to avoid failure outside the gauge section. The maximum stresses in the program were quite high (1351 MPa, 196 ksi), and as such many features of the specimen were all too eager to cause cracks. The most problematic areas were:

1. Sharp edges — to prevent the formation of fatigue cracks at the edges of the specimens, all specimen edges through the gauge section had to be rounded to a 2mm radius. This was accomplished by grinding followed by polishing with successively finer grades of silicon carbide paper.

2. Machined Faces and Undercutting — the faces of the gauge sections appeared to have been surface ground or fly cut after the production of the fillets. Even though the drawing called for smooth transition between the fillet radius and gauge section without undercutting, a marked step of undercut was present in this area. It is presumed that the specimens found for this new program had never been completely finished, so an automatic polishing machine, purpose-built for these specimens during their initial manufacture, was pressed into service to remove the undercut. The spring loaded polishing machine allowed the entire face and filleted corner to be polished with minimal operator assistance. The polishing at the edge of the fillet, though improved, was not as good as the bulk of the specimen gauge length.

3. Stress Concentration — the main stress concentrator for these specimens was intended to be the corrosion pits in the flat faces. However, the stress concentration caused by the filleting from the grip to the face was calculated at approximately 1.05. This small amount was enough to promote crack growth at

the edge of the fillet. (The presence of an undercut, and the difficulty in polishing the base of the fillet exacerbated this problem.) Shot peening alleviated this difficulty by retarding crack growth in all areas save for the small area of corrosion. This method was not fully effective, and additional samples were required to replace those that still failed from the peened areas.
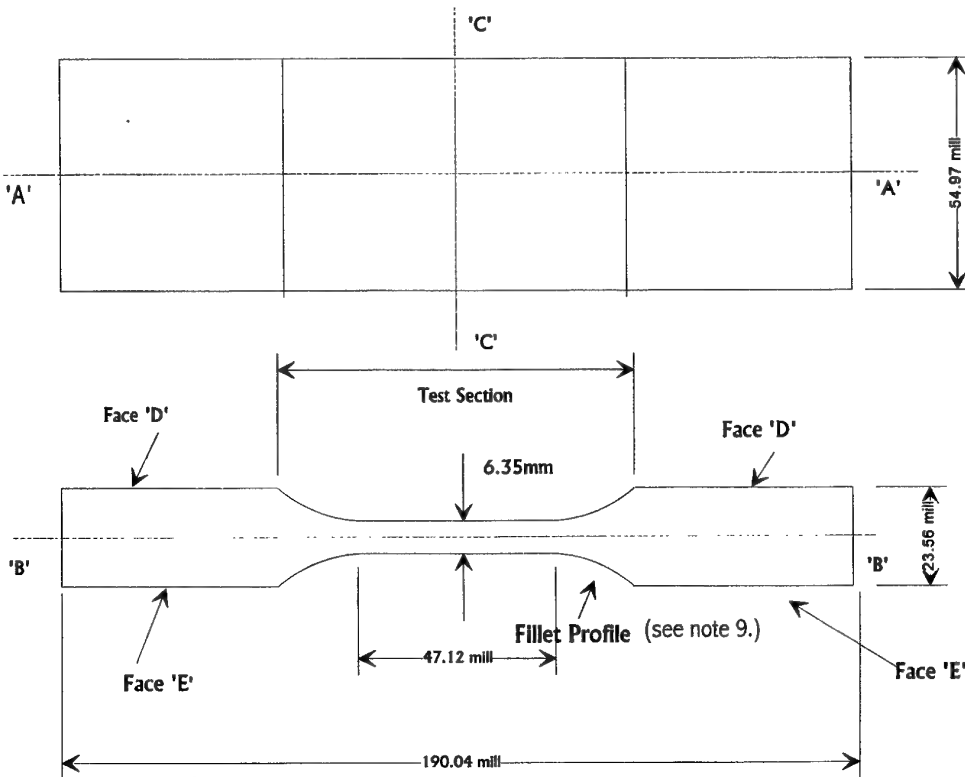
1. General Tolerances to be +/- 0.5mm.
2. Test Section to be symmetrical about 'A-A' and 'B-B' to within 0.025mm.
3. Transition from Fillets to 6.35mm thickness must be smooth and without undercutting.
4. Faces of Specimen are not to be marked or damaged in any way.
5. Face 'D' to be parallel to face 'E' within within 0.025mm.
6. Remove all sharp edges except on test section.
7. Rough Machining to be done symmetrically.
8. Finish on Test Section to be free from chatter marks. Roughness to be 0.4-0.8 μm.
9. Fillet Profile: 25.4mm

Figure 9. Converted Engineering Drawing of SC97R1 flat axial fatigue specimen.

3.2 Test conditions

The tests were carried out under constant amplitude loading[1] at three different maximum stress levels. These stress levels were typical of those found in the WCTB.

- 1351 MPa (196 ksi),

- 1214 MPa (176 ksi), and

- 1144 MPa (166 ksi).

A frequency of 10 Hz and a stress ratio of 0.1 were used for the tests.

Plastic sheets were fixed to both grips following the insertion of the sample, with desiccant held in containers within the confined area. The purpose of the desiccant was to provide a dry environment to preclude any chemical corrosion fatigue interaction during testing. Use of desiccant consistently held relative humidity levels below 25%.

To aid in crack growth rate determination, a digital camera (Kodak Megaplus, 8 bit camera with a resolution of 1317 x 1035 pixels) was used to monitor the corroded area during cycling. A hole in the plastic sheet allowed access to the specimen for the camera lens, and a scale was added to the sample below the area of interest.

Lighting for the camera was provided by fluorescent tubes placed within the contained area. These lights were set in order to highlight the growing crack and were adjusted prior to the testing using a sample that failed from the radius in the developmental stage of the experiment. This sample contained cracks in various stages of growth on the surface of the specimen, making optimisation of the lighting conditions for this work possible. Images were taken at set intervals, with the specimen held at a load approximately one third of the maximum load used for each test for the duration of the image capture.

Pitting to predetermined depths was produced using the galvanostatic electrochemical method detailed in section 2.3.4. More description of the method can be found in a report by Mills and Loader (2000).

3.3 Test matrix

As was mentioned earlier, three levels of maximum stress were used for the experiments. Also, seven levels of pitting were used among the specimens, although one of the pit depths (20 microns) was so shallow that only one successful test was

---

[1] Some tests used marker loads, but for all intents and purposes, the tests were constant amplitude.

completed at this level. In the other tests at 20 micron pit depths, the specimens failed from other specimen features (discussed in section 3.1).

For the first batch of samples, the specimens were numbered according to the following formulae: D6-X-Y. In this designation, X was a letter indicating the stress level used, and Y was a letter indicating the level of pitting produced on the sample. Plans for a fourth higher stress (level A) were rejected leaving the stress levels as:

- B--1351 MPa, 390kN

- C--1214 MPa, 350 kN

- D--1144 MPa, 330 kN

The maximum pit depths for the different levels for the original test matrix were:

- A and B — 10 microns (0.0004 inch)

- C and D — 20 microns (0.0008 inch)

- E and F — 30 microns (0.0012 inch)

- G and H — 40 microns (0.0016 inch)

- I and J — 50 microns (0.002 inch)

The times of corrosion to the different pit depths were determined from the power law relationship in Figure 7, section 2.3.4.

Putting the specimen naming convention together, for example, sample D6CF was tested at 1214 MPa (R = 0.1), had a maximum pit depth of approximately 30 microns, and a corrosion time of 270 seconds.

The original test matrix, using the variables above, included 30 tests. However, many specimens failed from sources other than the pitting, and these were repeated where possible. Thus, some specimens have a '2' or '3' as part of their specimen ID as repeats.

At the end of that test program, only 12 successful tests were completed. A few other specimens were added that had IDs ending with 'K' and 'L'. These were add-on specimens necessary to increase the amount of data for 30 and 40 microns, respectively. Of the original tests, none of the specimens with 10 micron pits (A and B), and only one of the specimens with 20 micron pits (C and D) failed from corrosion.

The addition of the 'D6*K' and 'D6*L' levels of corrosion filled the test matrix out to 16. However, still more were deemed necessary to get a good feel for pitting influences.

Since smaller pit depths were not effectively causing corrosion damage, several specimens were added that had target pit depths of 60, 70, and 90 microns (0.0024, 0.0028, and 0.0036 inch, respectively). An additional 14 specimens were tested with these configurations, bringing the total to the original 30 desired. These specimens were never given a 'D6**' ID number. Instead, they are identified by the number stamped in them from when they were first made. These specimens all start with the code 'EK', 'EL', or 'EM' in their ID numbers.

Table 1 shows the completed test matrix as sorted by maximum stress level. The pit sizes shown are those predicted based on the exposure time and only includes specimens that properly failed from the corrosion pits. In future sections of this report, pit sizes that are reported are actual, not predicted.

3.4 Fatigue life results

As discussed in the previous section, the constant amplitude matrix was essentially completed in two separate phases. The specimens in the first phase contained pits varying in size up to 50 microns (0.002 inch). These smaller pits performed their function well at the two lower stresses, but at the highest stress, the smaller pits just didn't have enough influence to ensure that failure would always be caused by corrosion. The specimen design was so sensitive to damage, that virtually any geometric feature caused failure at the higher stress. Sources of failure included pockmarks from the peening, the undercut near the fillet radii at the grip ends, specimen corners, and other accidental surface 'damage.'

At the end of the first program, only four successful tests had been completed at the high stress level. As such, it was decided that some more specimens should be included at the high stress level to fill out the matrix. To ensure that these specimens failed from corrosion damage, the pit size was increased markedly to include sizes in the 70-100 micron (0.003-0.004 inch) range. To finish rounding out the matrix, some more specimens were tested at the middle and low stress level with these larger pits.

Table 2 shows tabulated fatigue results for all the successful tests, where failure originated from corrosion damage. The average fatigue lives for the 1351 MPa, 1244 MPa, and 1144 MPa stress levels were 9639, 27 482, and 44 175 cycles, respectively. Specimen ID numbers that begin with 'D6' are from the original test program, where specimen ID numbers that begin with 'E' are from the second phase and are specimens with the deeper pits.

Figure 10 shows the fatigue results as a stress life curve. As expected, scatter increased at lower stress levels. Included in Figure 10 are data points for specimens that failed from features other than corrosion damage. They are denoted by the X symbols.

Table 1. Constant amplitude fatigue test plan.

Stress Level (MPa)	Specimen ID	Target Pit Depth (μm)
1351	D6BF	30
	D6BG	40
	D6BH	40
	D6BJ3	50
	EM56CC	70
	EK14AL	70
	EM56CA	90
	EL1CL	90
1214	D6CF	30
	D6CG	40
	D6CH	40
	D6CI2	50
	D6CJ2	50
	D6CK2	30
	D6CL	40
	EM55CB	30
	EL1CK	40
	EM56BB	60
	EK7AL	90
	EM56CK	90
1144	D6DC	20
	D6DG	40
	D6DJ	50
	D6DK	30
	D6DL	40
	EM56BC	40
	EK10AL	60
	EK15AM	60
	EM56BF	90
	EM55BG	90

3.4.1 Influence of stress on scatter

As is typical of fatigue, scatter was quite low at the highest stress, 1351 MPa (196 ksi). At this high level, almost every little specimen detail is a potential crack-starter, and so it is reasonable to expect very small variations in life. Indeed, specimens that failed from nicks and scratches had the same life as specimens that failed from corrosion pits. By using deep pits (70-100 microns), however, it was possible to drop the life still further. This increased scatter at this stress level and all the others as well. This fact is discussed in the next section. The standard deviation for this level was 3469 cycles on a mean of 9639 cycles.

At the middle stress level, 1214 MPa (176 ksi), scatter increased substantially, but the incidence of specimens failing from non-corrosion damage dropped off. Again, the deeper pits used in the second phase of the testing influenced the scatter. The standard deviation for this level was 11 225 cycles on a mean of 27 482 cycles.

At the lowest stress level, 1144 MPa (166 ksi), scatter increased further still until the ratio of maximum to minimum life was over five. As with the other stress levels, the deeper pits influenced life substantially. This will be discussed shortly. The standard deviation for this level was 19 937 cycles on a mean of 44 175 cycles.

3.4.2 Influence of pit depth on scatter

The decision to use deeper pits in the second phase (designed to fill out the test matrix) flowed from a number of different observations.

- Only a limited number of specimens remained that had been adequately prepared for fatigue testing.

- Previous experience with the problematic stress level, 1351 MPa (196 ksi), indicated that it would take two or three tests to get one good data point using the pit sizes incorporated in the first phase. This was highly undesirable because of the point raised in the above bullet.

Some of the in-service damage detected in the F-111 was deeper than the pits examined in the first phase of testing, so data at still-deeper sizes was sought to increase the capability of any models developed later.

Using the deeper pits in the second phase did tend to increase scatter, though. The next batch of tables illustrates this point quite well. By merely ordering the fatigue lives in accordance with increasing pit size, two distinct families became apparent at each stress level. Statistical t-test analyses were conducted to test for differences in means, and sure enough, at the dividing lives selected for each stress level, the populations were statistically significantly different at an alpha of 0.05.

Table 2. Fatigue life by stress level and specimen ID.

Stress Level (MPa)	Specimen ID	Fatigue Life
1351	D6BF	12 394
	D6BG	13 764
	D6BH	12 368
	D6BJ3	11 913
	EM56CC	9586
	EK14AL	5956
	EM56CA	5196
	EL1CL	5933
	Mean:	*9639*
	Standard Deviation:	*3469*
1214	D6CF	45 507
	D6CG	29 513
	D6CH	22 960
	D6CI2	21 629
	D6CJ2	18 700
	D6CK2	44 183
	D6CL	34 019
	EM55CB	33 789
	EL1CK	34 622
	EM56BB	9954
	EK7AL	15 954
	EM56CK	18 955
	Mean:	*27 482*
	Standard Deviation:	*11 225*
1144	D6DC	58 910
	D6DG	56 313
	D6DJ	26 421
	D6DK	76 254
	D6DL	50 672
	EM56BC	64 000
	EK10AL	23 969
	EK15AM	33 953
	EM56BF	36 410
	EM55BG	14 846
	Mean:	*44 175*
	Standard Deviation:	*19 937*
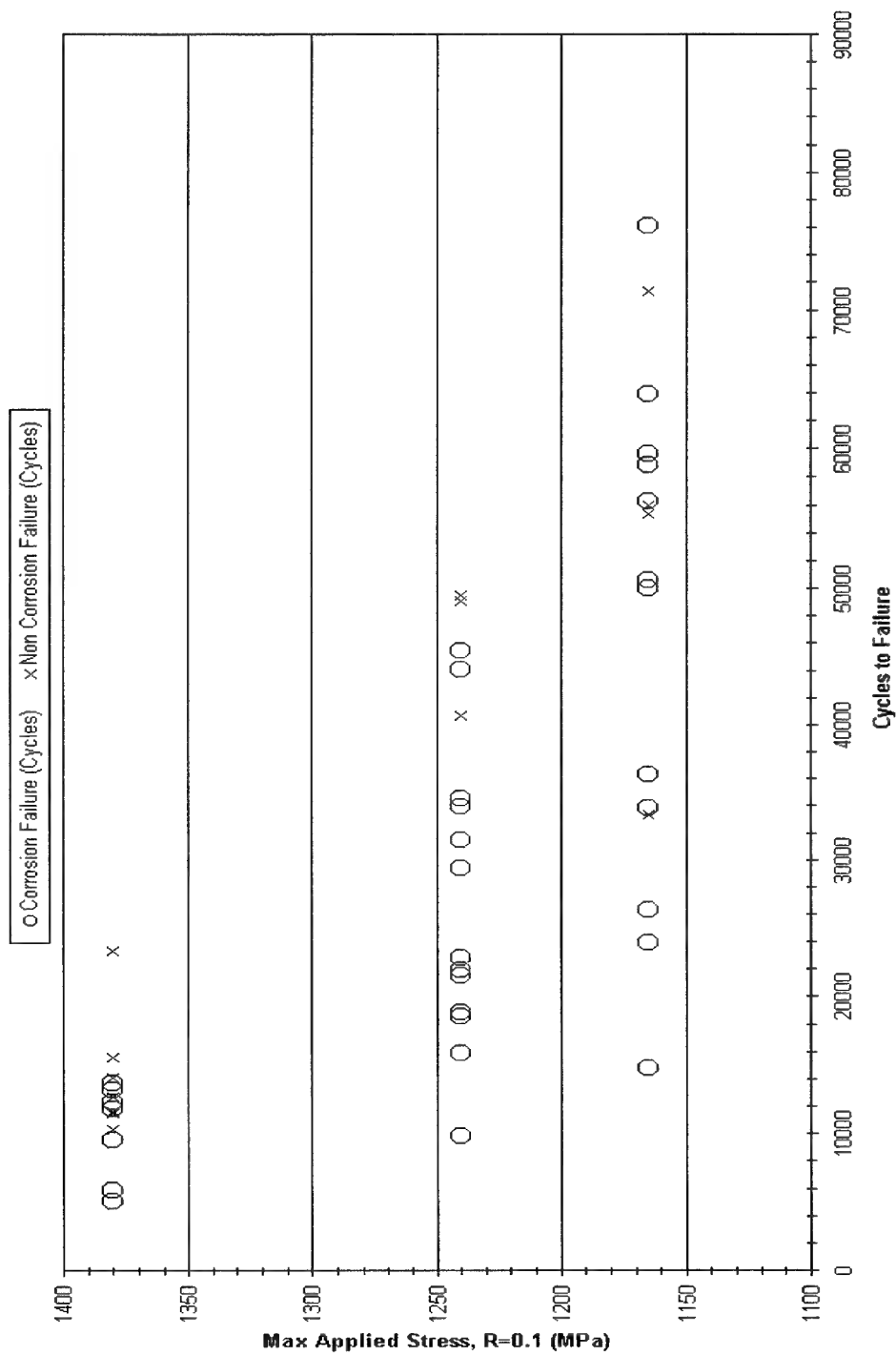
Figure 10. Maximum applied stress vs. cycles to failure for constant amplitude fatigue experiments.

Tables 3 and 4 pertain to the 1351 MPa (196 ksi) stress, Tables 5 and 6 pertain to the 1214 MPa (176 ksi) stress, and Tables 7 and 8 pertain to the 1144 MPa (166 ksi) stress. At the highest stress, pits 80 microns and above degraded life much more severely than at the lesser depths. Similarly, the cut-off seemed to be at 45 microns for the middle stress level and about the same at the lower stress level.

At the high stress level, the cut-off was at a significantly larger pit size; this is best explained by the fact that at smaller pit sizes, numerous sources were generating cracks. However, once the larger pits were used, the only features that caused cracks were the pits. Thus, only the deep pits ($d > 80$ microns) finally brought out the true effect of pitting and subsequent reduction in life. The lives at shallower pit depths were not truly indicative of pitting; it just so happened that pits caused the failure in those particular cases. As mentioned before, many other features caused failures as well.

Table 3. Fatigue life and pit depth for specimens tested at 1351 MPa (196 ksi).

Specimen ID	Cycles to Failure	Pit Depth (microns)
D6BF	12 394	30.4
D6BH	12 368	42.5
D6BG	13 764	48.4
D6BJ3	11 913	65.0
EM56CC	9586	80.4
EK14AL	5956	87.2
EL1CL	5933	87.9
EM56CA	5196	94.4

Table 4. Results of t-test for difference of means, 1351 MPa (196 ksi) data, $\alpha = 0.05$.

	Group 1, 30-65 microns	Group 2, 80-95 microns
Mean	12 610	6668
Variance	640 915	3 909 559
Observations	4	4
Pearson Correlation	-0.059	
Hypothesized Mean Difference	0	
Df	3	
t Stat	5.46	
P(T<=t) one-tail	0.0060	
t Critical one-tail	2.35	
P(T<=t) two-tail	0.0121	
t Critical two-tail	3.18	

Table 5. Fatigue life and pit depth for specimens tested at 1214 MPa (176 ksi).

Specimen ID	Cycles to Failure	Pit Depth (microns)
D6CK2	44 183	30.3
D6CF	45 507	30.8
EM55CB	33 789	31.6
EL1CK	34 622	34.0
D6CL	34 019	38.6
D6CG	29 513	43.2
D6CH	22 960	47.1
D6CJ2	18 700	55.9
D6CI2	21 629	56.4
EM56BB	9954	66.0
EK7AL	15 954	87.5
EM56CK	18 955	105.0

Table 6. Results of t-test for difference of means, 1214 MPa (176 ksi) data, α = 0.05.

	Group 1, 30-45 microns	Group 2, 45-105 microns
Mean	36 939	18 025
Variance	40 969 805	21 618 729
Observations	6	6
Pearson Correlation	0.3227	
Hypothesized Mean Difference	0	
Df	5	
t Stat	7.03	
P(T<=t) one-tail	0.0004	
t Critical one-tail	2.02	
P(T<=t) two-tail	0.0009	
t Critical two-tail	2.57	

Table 7. Fatigue life and pit depth for specimens tested at 1144 MPa (166 ksi).

Specimen ID	Cycles to Failure	Pit Depth (microns)
D6DC	58 910	23.7
D6DK	76 254	34.5
D6DL	50 672	41.0
EM56BC	64 000	42.9
D6DG	56 313	43.8
EK10AL	23 969	61.3
EK15AM	33 953	69.1
D6DJ	26 421	70.4
EM56BF	36 410	88.5
EM55BG	14 846	102.3

Table 8. Results of t-test for difference of means, 1144 MPa (166 ksi) data, $\alpha = 0.05$.

	Group 1, 23-45 microns	Group 2, 61-103 microns
Mean	61 230	27 120
Variance	93 606 032	73 515 617
Observations	5	5
Pearson Correlation	0.6131	
Hypothesized Mean Difference	0	
Df	4	
t Stat	9.43	
P(T<=t) one-tail	0.0004	
t Critical one-tail	2.13	
P(T<=t) two-tail	0.0007	
t Critical two-tail	2.78	
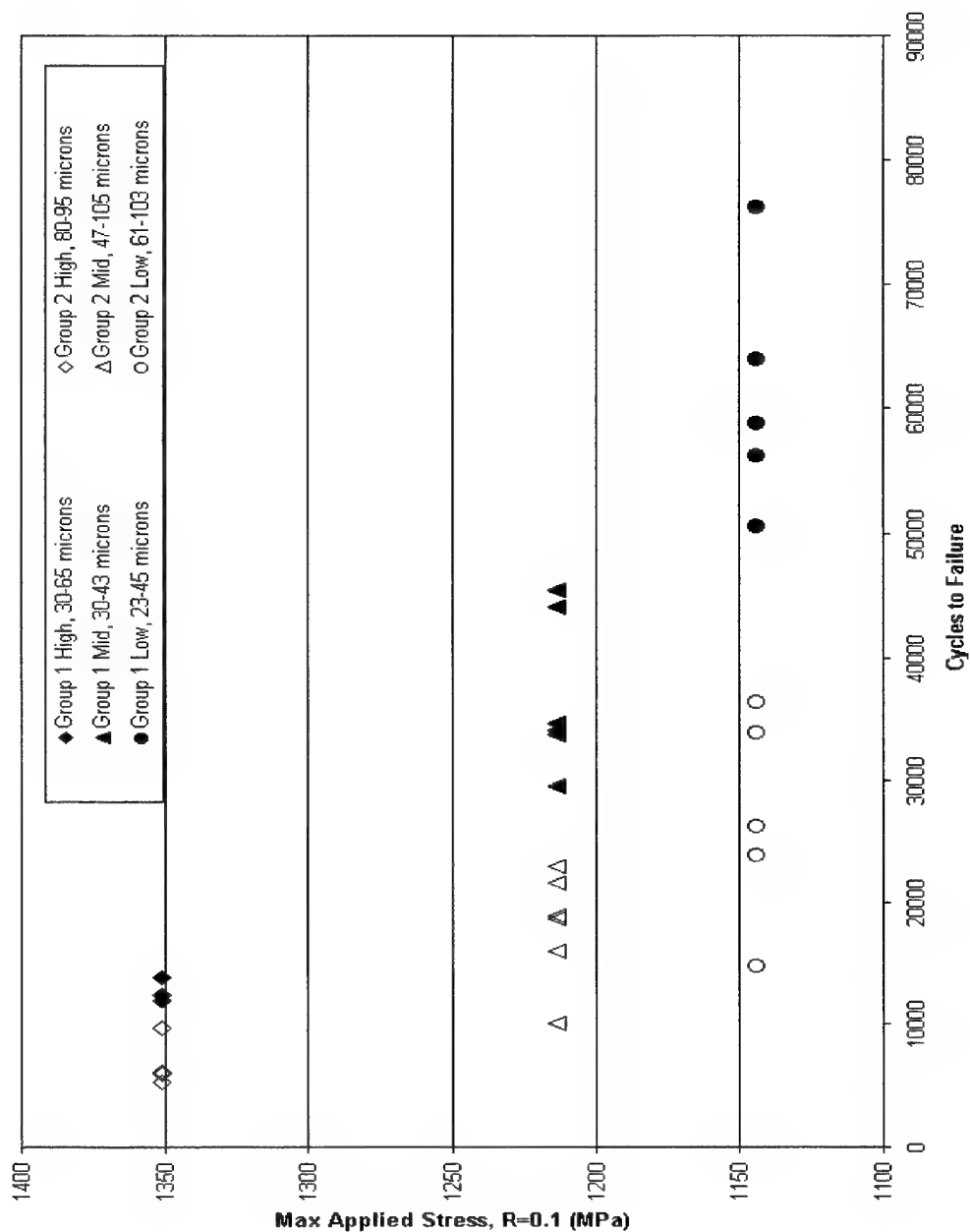
Figure 11. Maximum applied stress vs. cycles to failure for constant amplitude fatigue experiments showing that the pit size does influence the scatter at each stress level. Differences in means between Groups 1 & 2 are statistically significant at each stress at a level of $\alpha = 0.05$.

3.5 Summary of low-k_t fatigue program

This section of the report described a testing program that was used to establish the groundwork for Equivalent Crack Size (ECS) development in D6ac steel. The effort was centred on a constant amplitude fatigue program at three different stress levels using specimens with no stress concentration in the gauge section other than corrosion pits.

Corrosion pits of varying depth were used to provide variations in fatigue life that could be attributed to the different pit sizes. A number of observations came from this program, and they are summarised here.

- Three stress levels were tested in the low-K_t program, namely: 1351, 1214, and 1144 MPa (196, 176, and 166 ksi, respectively).

- As would be expected, the lowest stress exhibited longest fatigue lives and the most scatter, whereas the highest stress exhibited the shortest fatigue lives and the least scatter.

- It is believed that the scatter in the fatigue lives is not entirely attributed to that normally associated with fatigue, as the specimens contained pits of varying depth, and it is reasonable to expect that pit size influenced scatter.

- Statistical t-tests showed that at the middle and lowest stress levels, pits greater than 45 microns significantly affected the life relative to shallower pits.

- At the highest stress level, pits greater than 80 microns were required to start affecting the live beyond other geometric anomalies of the specimen, including scratches, peening marks, and design 'features' such as the undercut and the corners themselves. In other words, at 1351 MPa, corrosion pits were typically as likely to cause failure as any other stress concentrating features of the specimen.

- Comprehensive fractography was completed on all the specimens that failed from corrosion pits. The main goal was to completely document all pit features so that they could be correlated to fatigue life and ECS values as discussed in the next section.

- Some of the specimens contained marker bands (to mark the fracture surface), so that crack growth curves could be generated post-mortem for the material used in this program. Crack growth curves and the marker spectra are discussed in Section 4.

4. ECS Development

With the initial fatigue testing complete, the next portion of the model development involved determining the ECS that analytically produced the fatigue life of each laboratory coupon. The ultimate goal of this portion of the program was to generate ECS distributions and correlate them with pit features. This section of the report discusses the key elements of this procedure, to include:

- selection of material model,

- determination of ECS for all the constant amplitude specimens,

- fractography of the primary pits that generated fatigue failures, and finally

- correlation of the pit features with ECS.

4.1 Material models

The ECS concept requires some sort of material data input to generate life predictions. The most robust method is to generate a crack growth master curve for the actual specimens with which the ECS data were generated. Other material models can be used, too, if their behaviour seems to describe the actual crack growth in the coupons. A number of approaches were investigated in this program, and they are summarised in this section.

Master curves take large amounts of time and effort to generate, since it requires intensive fractography. With this in mind, it was decided to start the ECS investigation using a number of different material models available from the literature or computer codes to at least prove the concept at a basic level. The sources were two different curve fits of crack growth data for D6ac as found in Lockheed Document FZS-12-626 [Ball and Doerfler 1996], which were fits of comprehensive data generated by Feddersen et. al (1972). The first of those models is the Forman fit, which is a traditional Forman equation describing the data, and the second fit is a mean curve representation of the Feddersen data, and this fit was developed by Lockheed. As such, the second model is called the LMTAS (Lockheed Martin Tactical Aircraft Systems) Mean.

A third model was investigated briefly, and it was based on the NASGRO data set [Harter 2000], which is contained as a material library within the USAF's AFGROW computer code. AFGROW was used as the crack growth engine for all of the elastic crack growth analyses in this research effort.

An interesting aside needs to be mentioned here. AFGROW assumes no crack growth if the predicted rate drops below 2.54×10^{-12} mm/cycle (1×10^{-13} inch/cycle). In

addition, to generate an ECS, a material model is selected, and then the starting crack size is adjusted until the predicted life converges with the experimental life. However, using the first two models, Forman and LMTAS Mean, many of the attempts to determine the ECS for various specimens failed when AFGROW reported zero crack growth.

This phenomenon was tied to the threshold stress intensity (ΔK_{th}) values for crack growth as used by Lockheed. Both of these curve fits assumed a threshold stress intensity of 5.179 MPa $\sqrt{m}$ (4.752 ksi $\sqrt{in}$) at R=0 [Ball and Doerfler 1996]. In the attempts to converge to an ECS for many specimens, the assumed initial crack sizes were reduced to the point that the starting stress intensities for the modelling runs were below threshold.

After a little research, it was discovered that we were not the only ones to have encountered this difficulty, and in fact LMTAS did not use the experimentally measured threshold, but instead used a value of 2.18 MPa $\sqrt{m}$ (2.00 ksi $\sqrt{in}$) at R=0 [Walker 2000].

A more detailed discussion of threshold fatigue crack growth behaviour is provided in a report by Mills et al. (2001), but suffice it to say for the purposes of this report that the lower threshold had to be used to get ECS values that allowed predicted lives to converge with experimental lives. These two new models, known as the Modified Forman and Modified LMTAS mean were identical to the earlier models except they used the a threshold of 2.18 MPa $\sqrt{m}$ (2.00 ksi $\sqrt{in}$) at R=0. The following subsections provide the details of the individual models.

4.1.1 Modified Forman

The Forman equation takes the basic form of:

$$\frac{da}{dN} = \frac{C(\Delta K)^n}{(1-R)K_c - \Delta K} \tag{1}$$

where da/dN is the crack growth rate, C and n are curve fit parameters related to the material/environment combination, K_c is the critical toughness of the material, R is the stress ratio, and ΔK is the applied alternating stress intensity. The modified Forman parameters used in this research program were taken directly from the Ball and Doerfler (1996) document. The following conditions apply:

- D6ac Steel 1517-1655 MPa (220-240 ksi) heat treat

- long-transverse (L-T) grain orientation

- dry/lab air

The Forman curve derived for this material actually has two different 'sections' based on the stress intensity. For ΔK from threshold to 14.2 MPa √m (13 ksi √in), one equation applies, and for higher stress intensities, a second equation applies. These equations are:

$$\frac{da}{dN} = \frac{7.710 \times 10^{-9} (\Delta K)^{3.655}}{(1-R)110 - \Delta K} \, if (\Delta K_{th} < \Delta K \le 13ksi\sqrt{in})$$

(2)

$$\frac{da}{dN} = \frac{1.456 \times 10^{-7} (\Delta K)^{2.497}}{(1-R)110 - \Delta K} \, if (\Delta K > 13ksi\sqrt{in})$$

(3)

Figure 12 shows the equation graphically for a range of stress ratios.

4.1.2 Modified LMTAS mean

The desire to improve on the Forman fit drove LMTAS to develop mean curves to describe the Feddersen et al. (1972) data. In document FZS-12-626, the authors claim that the mean curves do a better job than the Forman equation at fitting the data, but at the same time LMTAS continue to use the Forman equation rather than tabular data derived from the mean fit.

This material model was input into AFGROW as custom-built tabular data. The material model is simply called Modified LMTAS Mean; the 'modified' identifies that the fatigue crack growth threshold has been lowered to 2.18 MPa √m (2.00 ksi √in) at R=0, as it was with the Modified Forman model.

Figure 13 shows the mean curves for three different stress rations, R = 0.1, 0.5, and 0.8. The tabular data are provided in Appendix A. The same basic data can be found in Lockheed document FZS-12-626 [Ball and Doerfler 1996]. Again, this data has been 'modified,' in that the threshold has been lowered by extending the lower linear portion of the crack growth curve.

4.1.3 NASGRO

The third empirical material model investigated for this exercise was the NASGRO model developed by Forman and Newman of NASA, de Koning at NRL, and Henriksen at ESA [Harter 2000]. The model has been implemented into the AFGROW computer code as follows:

$$\frac{da}{dN} = C\left[\left(\frac{1-f}{1-R}\right)\Delta K\right]^n \frac{(1-\frac{\Delta K_{th}}{\Delta K})^p}{(1-\frac{K_{max}}{K_c})^q}$$

(4)
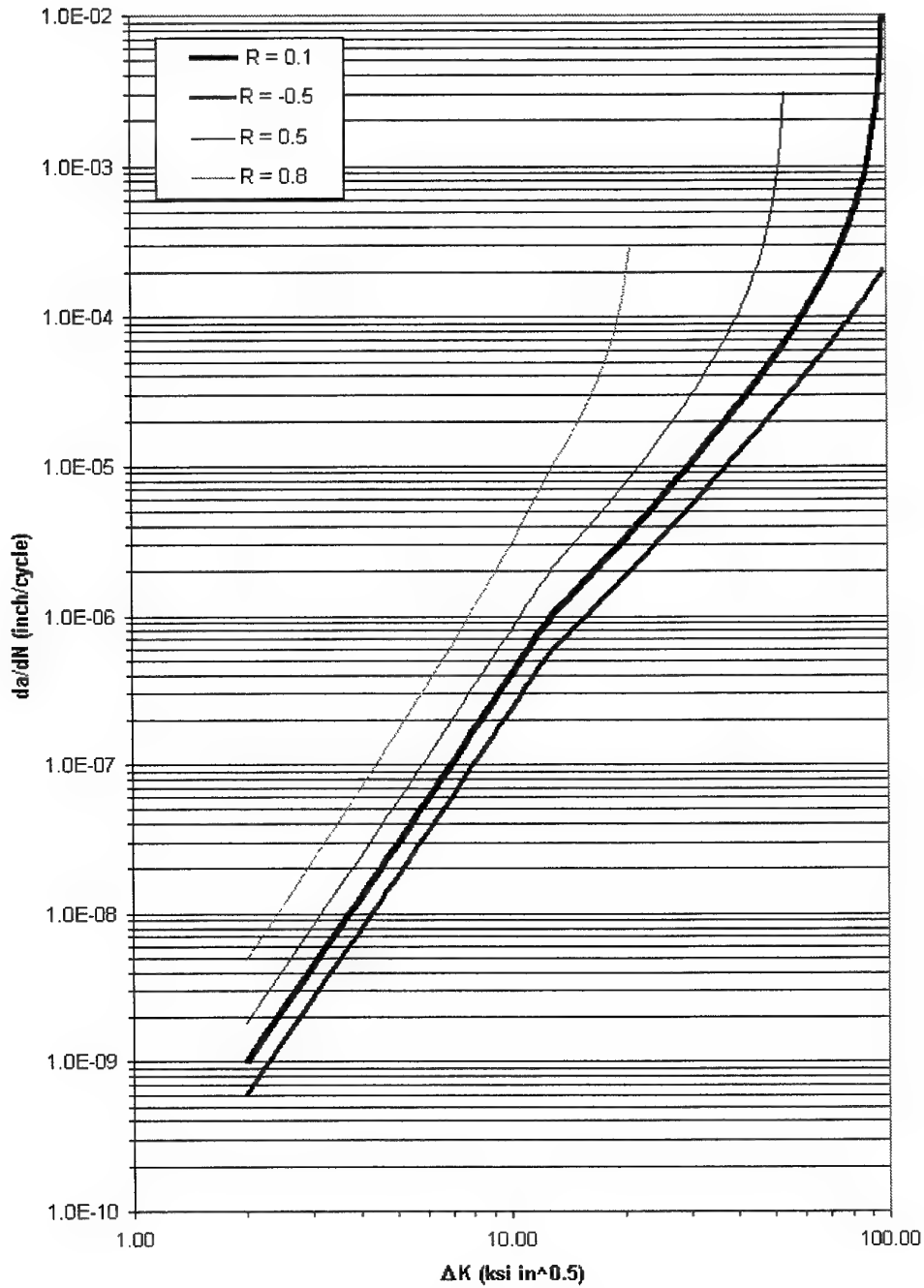
Figure 12. Modified Forman curve fit for D6ac steel, 220-240 ksi heat treat, L-T orientation, dry/lab air [Ball and Doerfler 1996].
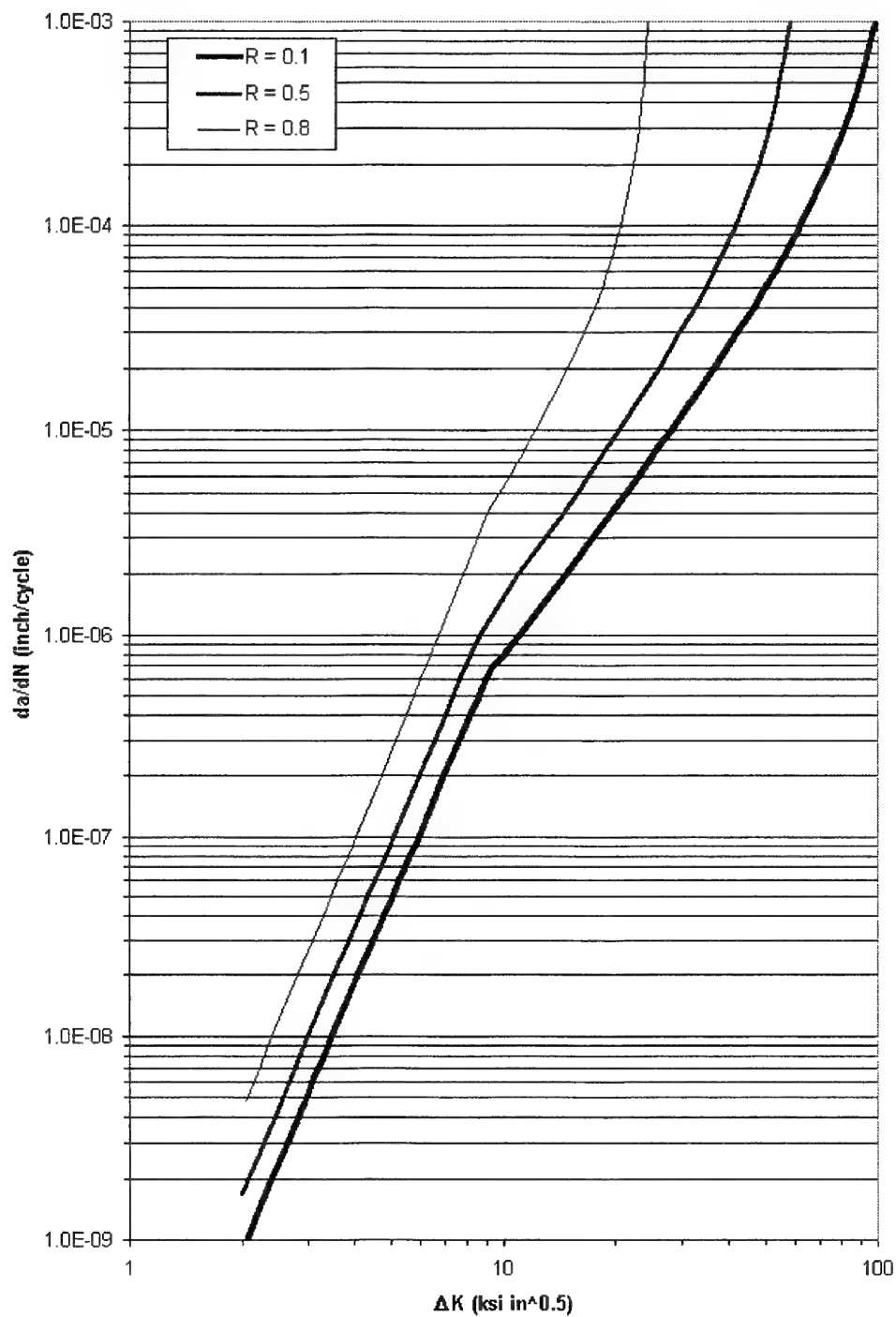
Figure 13. Modified LMTAS Mean curve fit for D6ac steel, 220-240 ksi heat treat, L-T orientation, dry/lab air [Ball and Doerfler 1996].

where C, n, ρ, q are all empirically derived and provided in the NASGRO material database, and

$$f = \frac{K_{op}}{K_{max}} = \left(A_0 + A_1 R + A_2 R^2 + A_3 R^3\right) \quad \text{for } R \geq 0 \tag{5}$$

$$= A_0 + A_1 R \qquad\qquad \text{for } -2 < R < 0$$

$$= A_0 - 2A_1 \qquad\qquad \text{for } R < -2$$

where,

$$A_0 = (0.825 - 0.34\alpha + 0.05\alpha^2)\left[\cos(\frac{\pi}{2} S_{max}/\sigma_o)\right]^{1/\alpha} \tag{6}$$

$$A_1 = (0.415 - 0.071\alpha) S_{max}/\sigma_o \tag{7}$$

$$A_2 = 1 - A_0 - A_1 - A_3 \tag{8}$$

$$A_3 = 2A_0 + A_1 - 1 \tag{9}$$

where α is the plane stress/strain constraint factor and S_{max}/σ_o is the ratio of maximum applied stress to the flow stress. All these values are provided in the database.

The other equation that applies to this model is the one for ΔK_{th}.

$$\Delta K_{th} = \Delta K_o \left(\frac{a}{a + a_o}\right)^{1/2} / \left(\frac{1 - f}{(1 - A_0)(1 - R)}\right)^{(1 + C_{th} R)} \tag{10}$$

where ΔK_o is the threshold stress intensity range at R = 0, a = crack length (a or c in AFGROW), a_o is the intrinsic crack length (0.0015 inch or 0.0000381 m), and C_{th} is the threshold coefficient. Both ΔK_o and C_{th} are provided in the database for each material.

The database-supplied values for the D6ac material (high toughness, K_{Ic} = 90 ksi √in) were:

- C = 3.2e-009
- n = 2.57
- ρ = 0.25
- q = 0.25

- $\Delta K_o = 4$
- $C_{th} = 0.8$
- $\alpha = 2.5$
- $S_{max}/\sigma_o = 0.3$

If more information is needed, readers are encouraged to consult the AFGROW online help. AFGROW is available free from the following website.

http://fibec.flight.wpafb.af.mil/fibec/afgrow.html

Figure 14 is a plot of *da/dN v ΔK* for D6ac using the NASGRO model.

4.1.4 Comparison of three material models

The effect that the varying behaviour in these material models has on calculated ECS values is profound. If nothing else, it illustrates the importance of picking an adequate material model in a research program and sticking with it. While two of the curves, Modified Forman and Modified LMTAS Mean, look quite similar, they produce very different results. The NASGRO equation produces a markedly different set of ECS values. Summaries of the ECS values derived using each of the three models at the three different stress levels used in the constant amplitude experiments are in the following three subsections. Figure 15 is an example of how the three models compare graphically at R = 0.1.

4.1.4.1 Model behaviour at high stress

The tables in this section summarise model performance at the high stress level, 1351 MPa (196 ksi). Table 9 shows the ECS values derived using the different material models in AFGROW. Table 10 is a summary of descriptive statistics for the ECS values arrived at by each model.

Finally, Tables 11-13 are t-test comparisons of the ECS values resulting from the application of each model. The t-test was performed on the means assuming a hypothesised mean difference of zero. In other words, it should be reasonable to assume that the means of each ECS distribution should be equal since the models are supposed to represent the same material. However, the results indicate otherwise. The results of all the models were significantly different from each other at an alpha of 0.05. In other words, there was a five percent chance of rejecting the null hypothesis when it was actually true.
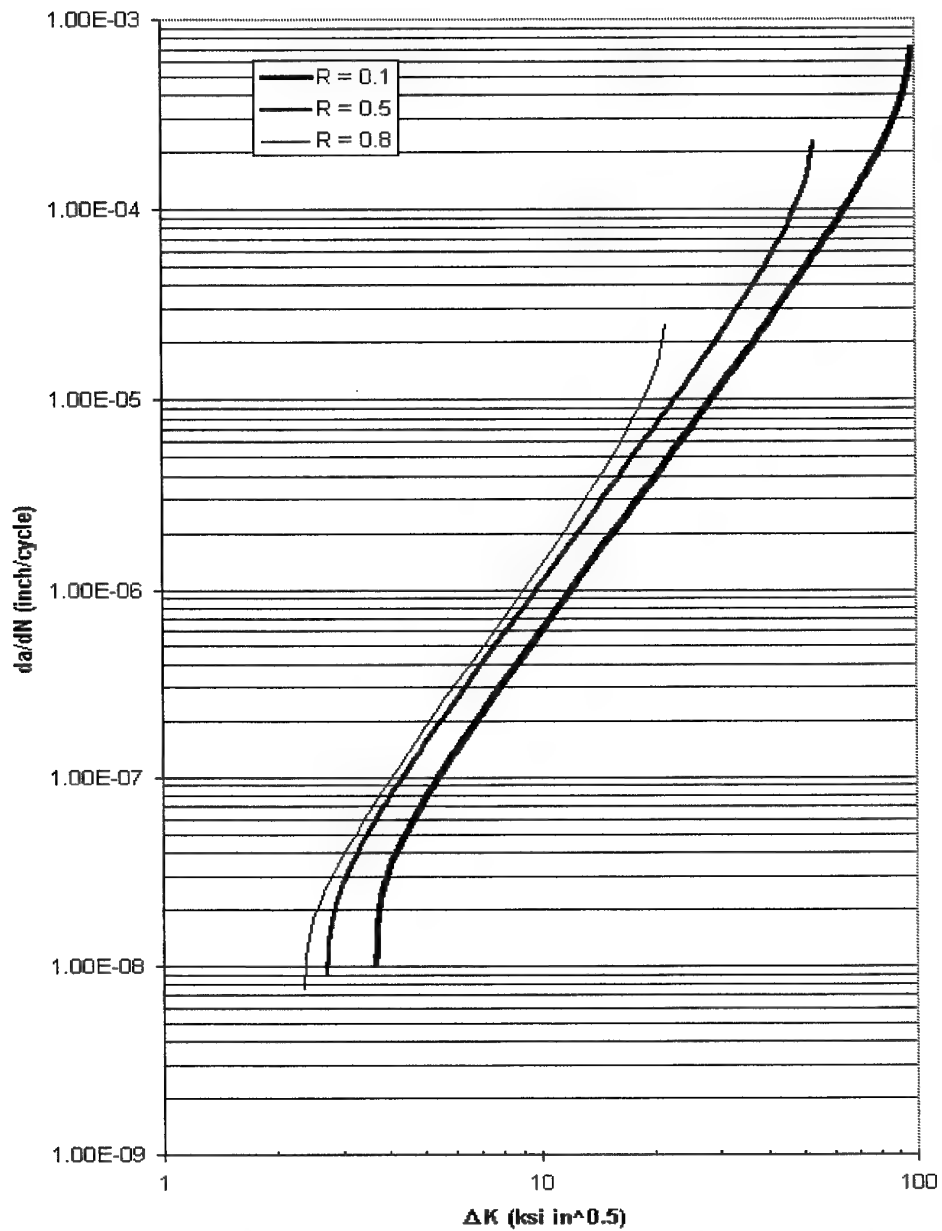
Figure 14. NASGRO material model for D6ac steel, 220-240 ksi heat treat, L-T orientation, dry/lab air as plotted using the equations found in the AFGROW online help [Harter 2000].
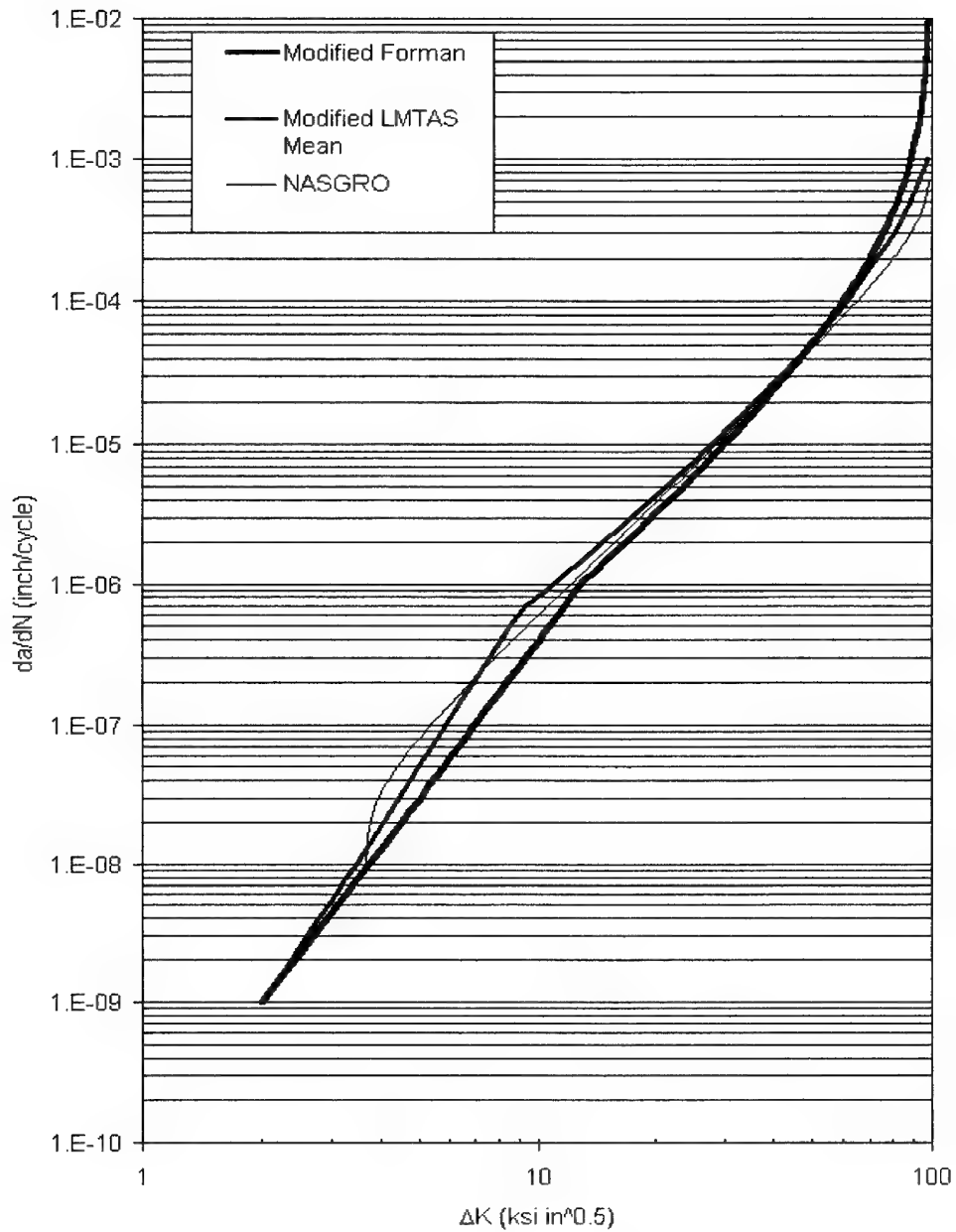
Figure 15. Comparison of the Modified Forman, Modified LMTAS Mean, and NASGRO material models for D6ac steel, 220-240 ksi heat treat, L-T orientation, dry/lab air, at R = 0.1.

Table 9. Comparison of ECS values (in microns) derived using Modified Forman, Modified LMTAS Mean, and the NASGRO material models for D6ac steel at 1351 MPa (196 ksi).

Specimen ID	Fatigue Life	ECS Forman	ECS LMTAS Mean	ECS NASGRO
D6BF	12 394	30.75	15.75	17.25
D6BG	13 764	27.50	14.00	13.25
D6BH	12 368	31.00	15.75	17.25
D6BJ3	11 913	31.25	15.95	20.32
EM56CC	9586	39.87	23.36	33.02
EK14AL	5956	96.52	63.50	93.98
EM56CA	5196	119.40	86.36	124.46
EL1CL	5933	96.50	63.50	93.98
Average	9639	59.10	37.27	51.69
Standard Dev	3470	38.12	29.04	44.81

Table 10. Descriptive statistics of the ECS values derived by each material model, 1351 MPa (196 ksi).

	ECS Forman	ECS LMTAS Mean	ECS NASGRO
Mean	59.10	37.27	51.69
Median	35.56	19.66	26.67
Std Dev	38.12	29.04	44.81
Range	91.90	72.36	111.21
Minimum	27.50	14.00	13.25
Maximum	119.40	86.36	124.46
Count	8	8	8

Table 11. Results of t-test for difference in means of the ECS values derived from the Modified Forman and the Modified LMTAS Mean material models at 1351 MPa (196 ksi). Means were significantly different at $\alpha = 0.05$.

	ECS Forman	ECS LMTAS Mean
Mean	59.10	37.27
Variance	1453.20	843.09
Observations	8	8
Pearson Correlation	0.998	
Hypoth Mean Diff	0	
df	7	
t Stat	6.64	
P(T<=t) one-tail	0.0001	
t Critical one-tail	1.89	
P(T<=t) two-tail	0.0003	
t Critical two-tail	2.36	

Table 12. Results of t-test for difference in means of the ECS values derived from the Modified Forman and the NASGRO material models at 1351 MPa (196 ksi). Means were significantly different at $\alpha = 0.05$.

	ECS Forman	ECS NASGRO
Mean	59.10	51.69
Variance	1453.20	2007.84
Observations	8	8
Pearson Correlation	0.999	
Hypoth Mean Diff	0	
df	7	
t Stat	3.01	
P(T<=t) one-tail	0.0099	
t Critical one-tail	1.89	
P(T<=t) two-tail	0.0197	
t Critical two-tail	2.36	

Table 13. Results of t-test for difference in means of the ECS values derived from the Modified LMTAS Mean and the NASGRO material models at 1351 MPa (196 ksi). Means were significantly different at $\alpha = 0.05$.

	ECS NASGRO	ECS LMTAS Mean
Mean	51.69	37.27
Variance	2007.84	843.09
Observations	8	8
Pearson Correlation	0.999	
Hypoth Mean Diff	0	
df	7	
t Stat	2.57	
P(T<=t) one-tail	0.0185	
t Critical one-tail	1.89	
P(T<=t) two-tail	0.0371	
t Critical two-tail	2.36	

4.1.4.2 Model behaviour at middle stress

The next several tables summarise model performance at the middle stress level, 1214 MPa (176 ksi). Table 14 shows the ECS values derived using the different material models in AFGROW. Table 15 is a summary of descriptive statistics for the ECS values arrived at by each model. Tables 16-18 are t-test comparison of the ECS values resulting from the application of each model. The t-test was performed on the means assuming a hypothesised mean difference of zero. The results of all the models were significantly different from each other at an alpha of 0.05, except between the modified LMTAS Mean and NASGRO.

Table 14. Comparison of ECS values (in microns) derived using Modified Forman, Modified LMTAS Mean, and the NASGRO material models for D6ac steel at 1214 MPa (176 ksi).

Specimen ID	Fatigue Life	ECS Forman	ECS LMTAS Mean	ECS NASGRO
D6CF	45 507	9.25	5.75	1.13
D6CG	29 513	16.00	9.00	3.95
D6CH	22 960	22.00	12.00	7.75
D6CI2	21 629	24.00	12.75	9.00
D6CJ2	18 700	28.75	15.25	13.25
D6CK2	44 183	9.38	5.78	1.13
D6CL	34 019	13.40	7.50	2.38
EM55CB	33 789	13.60	7.75	2.54
EL1CK	34 622	12.50	7.49	2.41
EM56BB	9954	68.70	38.10	55.88
EK7AL	15 954	35.00	18.29	18.80
EM56CK	18 955	27.90	14.48	12.19
Average	27 482	23.37	12.84	10.87
Standard Dev	11 225	16.53	8.92	15.26

Table 15. Descriptive statistics of the ECS values derived for each material model, 1214 MPa (176 ksi).

	ECS Forman	ECS LMTAS Mean	ECS NASGRO
Mean	23.37	12.84	10.87
Median	19.00	10.50	5.85
Std Dev	16.53	8.92	15.26
Range	59.45	32.35	54.76
Minimum	9.25	5.75	1.13
Maximum	68.70	38.10	55.88
Count	12	12	12

Table 16. Results of t-test for difference in means of the ECS values derived from the Modified Forman and the Modified LMTAS Mean material models at 1214 MPa (176 ksi). Means were significantly different at $\alpha = 0.05$.

	ECS Forman	ECS LMTAS Mean
Mean	23.37	12.84
Variance	273.12	79.54
Observations	12	12
Pearson Correlation	0.998	
Hypoth Mean Diff	0	
df	11	
t Stat	4.77	
P(T<=t) one-tail	0.0003	
t Critical one-tail	1.80	
P(T<=t) two-tail	0.0006	
t Critical two-tail	2.20	

Table 17. Results of t-test for difference in means of the ECS values derived from the Modified Forman and the NASGRO material models at 1214 MPa (176 ksi). Means were significantly different at $\alpha = 0.05$.

	ECS Forman	ECS NASGRO
Mean	23.37	10.87
Variance	273.12	232.75
Observations	12	12
Pearson Correlation	0.987	
Hypoth Mean Diff	0	
df	11	
t Stat	15.15	
P(T<=t) one-tail	5.116E-09	
t Critical one-tail	1.80	
P(T<=t) two-tail	1.023E-08	
t Critical two-tail	2.20	

Table 18. Results of t-test for difference in means of the ECS values derived from the Modified LMTAS Mean and the NASGRO material models at 1214 MPa (176 ksi). Means were not significantly different at α = 0.05.

	ECS LMTAS Mean	ECS NASGRO
Mean	12.84	10.87
Variance	79.54	232.75
Observations	12	12
Pearson Correlation	0.994	
Hypoth Mean Diff	0	
df	11	
t Stat	1.06	
P(T<=t) one-tail	0.1557	
t Critical one-tail	1.80	
P(T<=t) two-tail	0.3113	
t Critical two-tail	2.20	

4.1.4.3 Model behaviour at low stress

The next several tables summarise model performance at the middle stress level, 1144 MPa (166 ksi). Table 19 shows the ECS values derived using the different material models in AFGROW. Table 20 is a summary of descriptive statistics for the ECS values arrived at by each model. Tables 21-23 are t-test comparison of the ECS values resulting from the application of each model. The t-test was performed on the means assuming a hypothesised mean difference of zero. The results of all the models were significantly different from each other at an alpha of 0.05.

Table 19. Comparison of ECS values (in microns) derived using Modified Forman, Modified LMTAS Mean, and the NASGRO material models for D6ac steel at 1144 MPa (166 ksi).

Specimen ID	Fatigue Life	ECS Forman	ECS LMTAS Mean	ECS NASGRO
D6DC	58 910	8.73	5.63	0.85
D6DG	56 313	9.25	5.90	0.98
D6DJ	26 421	24.00	13.05	8.00
D6DK	76 254	6.13	4.28	0.35
D6DL	50 672	10.13	6.33	1.20
EM56BC	64 000	7.63	5.08	0.61
EK10AL	23 969	26.67	14.22	10.16
EK15AM	33 953	16.76	9.65	3.81
EM56BF	36 410	15.50	8.89	3.30
EM55BG	14 846	50.80	25.40	33.02
Average	44 175	17.56	9.84	6.23
Standard Dev	19 937	13.61	6.43	9.99

Table 20. Descriptive statistics of the ECS values derived for each material model, 1144 MPa (166 ksi).

	ECS Forman	ECS LMTAS Mean	ECS NASGRO
Mean	17.56	9.84	6.23
Median	12.81	7.61	2.25
Std Dev	13.61	6.43	9.99
Range	44.68	21.13	32.67
Minimum	6.13	4.28	0.35
Maximum	50.80	25.40	33.02
Count	10	10	10

Table 21. Results of t-test for difference in means of the ECS values derived from the Modified Forman and the Modified LMTAS Mean material models at 1144 MPa (166 ksi). Means were significantly different at α = 0.05.

	ECS Forman	ECS LMTAS Mean
Mean	17.56	9.84
Variance	185.12	41.32
Observations	10	10
Pearson Correlation	1.000	
Hypoth Mean Diff	0	
df	9	
t Stat	3.40	
P(T<=t) one-tail	0.0039	
t Critical one-tail	1.83	
P(T<=t) two-tail	0.0079	
t Critical two-tail	2.26	

Table 22. Results of t-test for difference in means of the ECS values derived from the Modified Forman and the NASGRO material models at 1144 MPa (166 ksi). Means were significantly different at α = 0.05.

	ECS Forman	ECS NASGRO
Mean	17.56	6.23
Variance	185.12	99.86
Observations	10	10
Pearson Correlation	0.978	
Hypoth Mean Diff	0	
df	9	
t Stat	8.24	
P(T<=t) one-tail	8.730E-06	
t Critical one-tail	1.83	
P(T<=t) two-tail	1.746E-05	
t Critical two-tail	2.26	

Table 23. *Results of t-test for difference in means of the ECS values derived from the Modified LMTAS Mean and the NASGRO material models at 1144 MPa (166 ksi). Means were significantly different at α = 0.05.*

	ECS LMTAS Mean	ECS NASGRO
Mean	9.84	6.23
Variance	41.32	99.86
Observations	10	10
Pearson Correlation	0.975	
Hypoth Mean Diff	0	
df	9	
t Stat	2.86	
P(T<=t) one-tail	0.0094	
t Critical one-tail	1.83	
P(T<=t) two-tail	0.0187	
t Critical two-tail	2.26	

4.1.5 Concluding remarks — material model selection

To summarise all these tables and discussions on material models, it is clearly important which model is selected for analyses, as it has a significant impact on the resulting ECS values.

If distributions are generated for one model, and pit feature *vs.* ECS curves (see coming discussions) are constructed based on that information, then that material model must be used for future life predictions. By changing material models from the one used to develop the ECS distributions, subsequent life predictions could be wildly conservative or, worse yet, unconservative.

The reasons for this can be seen directly from Figure 15 (shown earlier), where the crack growth curves for the three different material models are plotted at R = 0.1. The relative ECS values for a given life practically can be determined by examining the graph and having knowledge of the approximate starting stress intensity for the analysis. For instance, at low stress intensities, the NASGRO equation clearly has much faster crack growth rates, and as such, ECS values relating to this regime of K should be much smaller. This is indeed the case, as can be seen for any of specimens that had longer lives in the various stress levels. The smaller ECS produced by NASGRO in these conditions compensates for the faster crack growth in this model relative to the Modified Forman and Modified LMTAS Mean models at the lower starting stress intensity.

Similarly, the NASGRO equation produced larger ECS values in specimens with very short lives and high apparent starting K. Again, examination of Figure 15 shows that the NASGRO equation has slower crack growth behaviour at higher K, and this manifests itself as large ECS values in certain cases.

With this said, it was easy to expect that the Modified Forman would generally produce the largest ECS values since it has the slowest crack growth rates at the low stress intensities where most of the analyses started. The Modified LMTAS Mean model was expected to produce ECS values between the Modified Forman and NASGRO, and this was in fact the case.

It is important to point out (again) that once an ECS distribution is developed, it is necessary to continue using that material model for subsequent life predictions based on that ECS distribution. The life predictions presented later (Section 5) were accomplished using the Modified Forman model. Although this material model does not seem to describe the test data the best, it is what Lockheed, DSTO, and the RAAF all use to conduct DADTA on the F-111 D6ac structures. Thus, it was determined that the ECS *vs.* pit feature relationships would be most useful if developed for that material model.

Since current practice dictated the choice of ECS implementation approach more than anything else, it may be easy to ask why all this model comparison was done at all. Perhaps the above discussion answered all that. Mixing ECS distributions developed using one material model will produce erroneous results if the material model is subsequently switched.

4.2 Fractographic examinations — crack growth

Fractography was completed on a handful of the low-K_t specimens to ensure that crack growth behaviour was reasonable compared to the different material models. One specimen at each stress level was selected.

4.2.1 Marker bands for crack growth

The specimens selected for crack growth curve determination were EM56CC (1351 MPa, 196 ksi), EL1CK (1214 MPa, 176 ksi), and EM56BF (1144 MPa, 166 ksi). The actual load spectra (although basically constant amplitude) are discussed in more detail in Appendix B. Basically, the spectra were comprised of a block of desired test loads followed by a block of 50 underloads followed by a block of 50 overloads. The general effect was to produce marks on the fracture surface at intervals that could be measured (da) over a known number of cycles (dN). As such, da/dN, or crack growth rate, was measured directly from the fracture surface. Since the crack geometry was always of the thumbnail surface crack variety, known stress intensity solutions could be used to pair da/dN with ΔK. Figure 16 shows a typical set of marker bands on the fatigue surface of a pitted specimen.
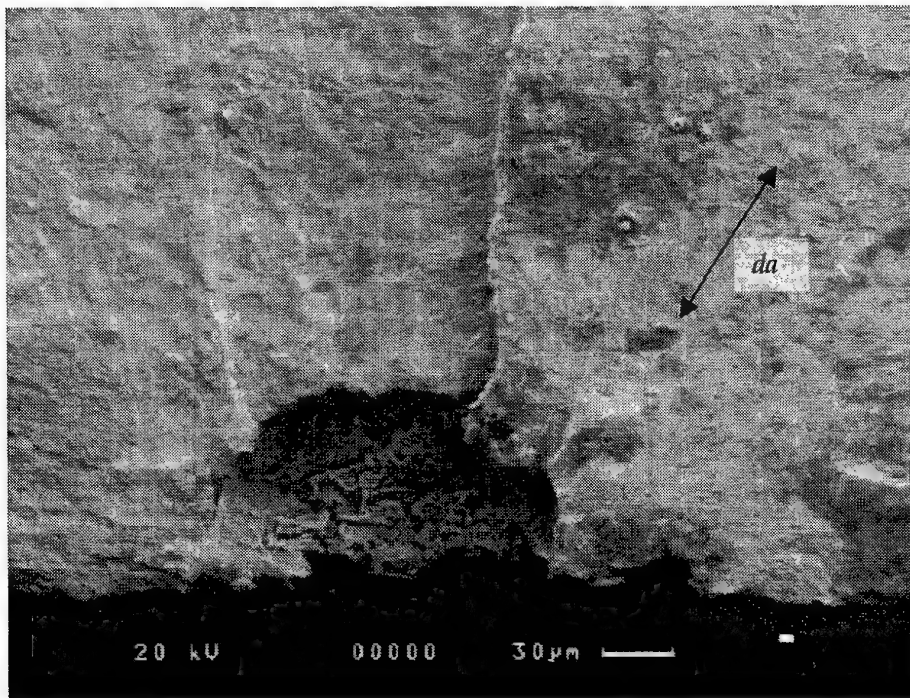
Figure 16. Marker bands on the fatigue surface of a pitted D6ac specimen.

4.2.2 Estimating crack length

Although estimating crack length from the fracture surface is straightforward and simple (provided one can locate the marker bands to begin with), there are a number of ways to look at the data. Three ways were investigated in this project. Two methods are straightforward and involve physical features of the specimen and marker bands.

Method 1) Treat the crack origin at the pit wall as the zero point, and measure the locations of the marker bands from that zero (distance 'a' in Figure 17).

Method 2) Treat the geometric centre of the pit as the crack origin, and measure the locations of the marker bands from that zero (distance 'b' in Figure 17).

The third method for determining crack length is more obscure but tied to the ECS concept around which this report is centred.

Method 3) For each of these specimens, an ECS was determined analytically using the Modified Forman crack growth model. This ECS is then used as the starting crack size, and the distance of the marker bands from the pit wall are then added to the ECS to make the crack growth curve. This adjusts the crack size to be in line with the computer model for its growth behaviour. In essence, since the ECS values are usually smaller

49

than the physical pit (since a crack is more severe than a pit), using the ECS as the starting crack size lowers the apparent stress intensity of the crack at short lengths. This is perhaps better explained graphically with the next few Tables and Figures.

Figure 18 shows a schematic of the ECS as used in conjunction with marker bands to generate a crack growth curve. In this figure, the radius denoted by 'b' is the pit radius, and the radius denoted by 'c' is that of the smaller ECS. Where in reality, marker bands are found emanating beyond radius 'b', the locations of the bands are instead added to the ECS value to make the final crack growth curve (see comparisons in Figure 19 and tabular data in Table 24). These lengths are in turn used to calculate the stress intensity as shown in Figure 20.
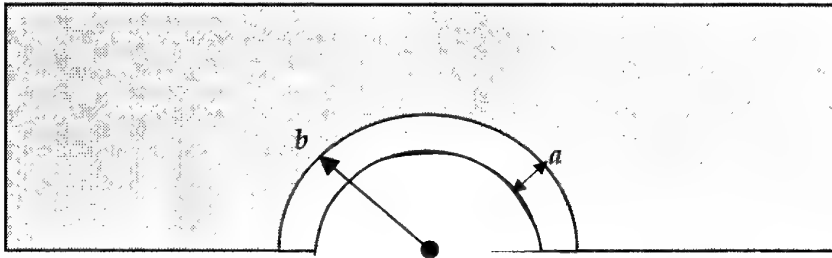

Figure 17. Different references for crack length measurement; distance "a" corresponds to Method 1, from pit wall to crack tip; distance "b" corresponds to Method 2, from pit centre to crack tip.
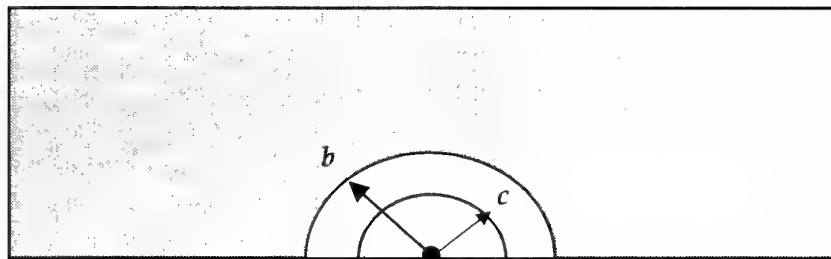
Figure 18. Schematic showing distance "b" measurement based on pit radius (Method 2) and distance "c" measurement based on ECS radius (Method 3).

50

Table 24. *Crack depth and load block data for specimen EL1CK (based on pit wall, pit centre, and ECS centre).*

Load Blocks	Crack Depth from Pit Wall (mm)	Crack Depth from Pit Centre (mm)	Crack Depth Based on ECS Centre (mm)
0	0	0.0382	0.0125
1	0.0013	0.0395	0.0138
2	0.0031	0.0413	0.0156
3	0.0054	0.0436	0.0179
4	0.0082	0.0464	0.0207
5	0.0108	0.0490	0.0233
6	0.0147	0.0529	0.0272
7	0.0173	0.0555	0.0298
8	0.0231	0.0613	0.0356
9	0.0292	0.0674	0.0417
10	0.0351	0.0733	0.0476
11	0.0416	0.0798	0.0541
12	0.0537	0.0919	0.0662
13	0.0605	0.0987	0.073
14	0.0744	0.1126	0.0869
15	0.0825	0.1207	0.095
16	0.0908	0.1290	0.1033
17	0.1045	0.1427	0.117
18	0.1280	0.1662	0.1405
19	0.1426	0.1808	0.1551
20	0.1590	0.1972	0.1715
21	0.1756	0.2138	0.1881
22	0.1910	0.2292	0.2035
23	0.2270	0.2652	0.2395
24	0.2515	0.2897	0.264
25	0.2803	0.3185	0.2928
26	0.3322	0.3704	0.3447
27	0.3724	0.4106	0.3849
28	0.4190	0.4572	0.4315
29	0.4948	0.5330	0.5073
30	0.6274	0.6656	0.6399
31	0.7211	0.7593	0.7336
32	1.0680	1.1062	1.0805
33	1.6646	1.7028	1.6771
34	2.9500	2.9882	2.9625
34.662	6.1030	6.1410	6.1155

Figure 19. Crack growth curves for EL1CK showing data based on measurement from pit wall, pit centre, and ECS centre.

Figure 20. Shift in ΔK values when ECS is used as starting crack size rather than pit radius. Notice how stress intensity markedly shifts at low values but eventually converges at higher values.
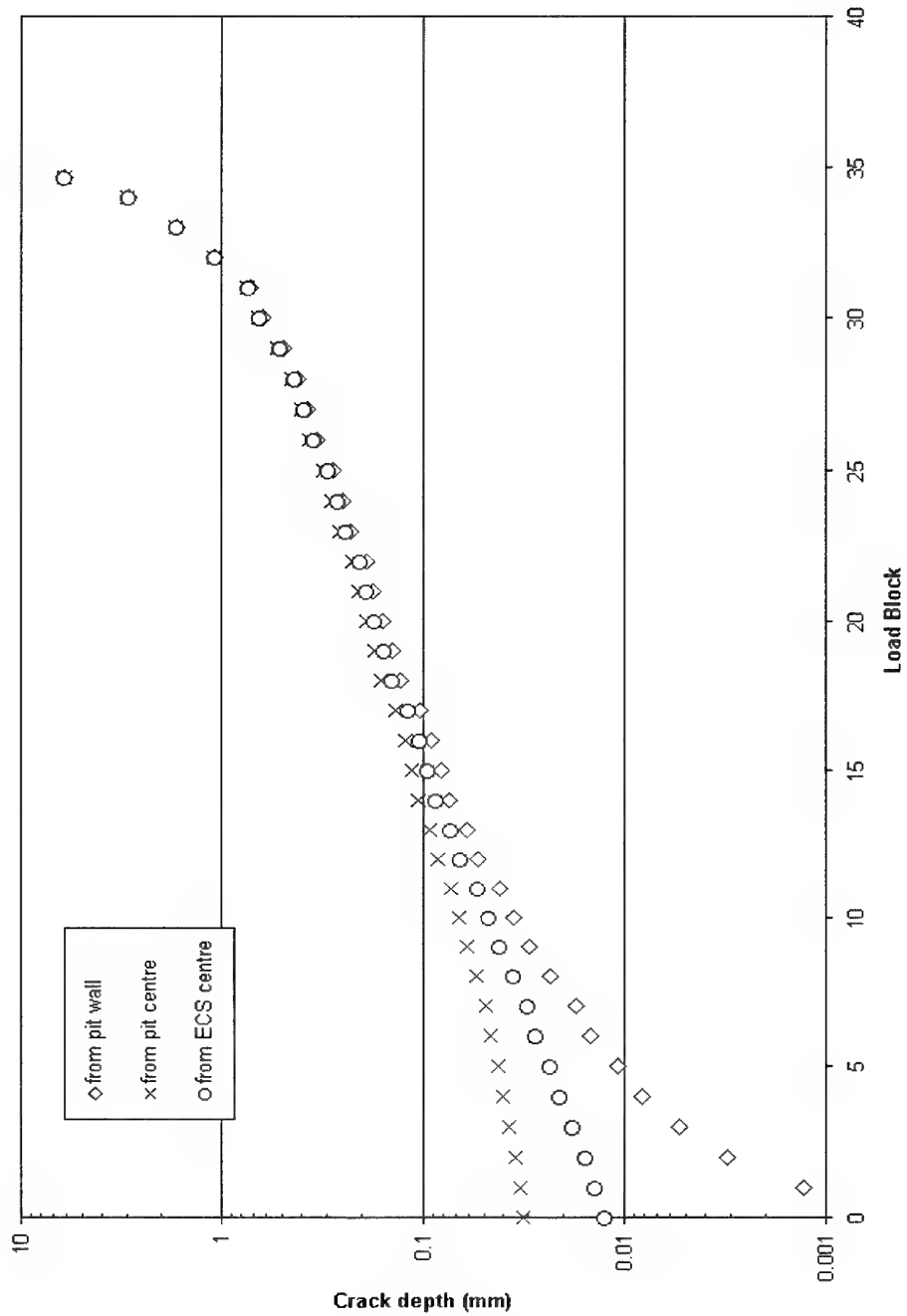
4.2.2.1 Crack growth curve for high stress specimen EM56CC

Specimen EM56CC was tested at 1351 MPa (196 ksi) maximum stress and had a total life of 9586 cycles. Each marker block consisted of 400 constant amplitude cycles and 50 underloads followed by 50 overloads, for a total of 500 cycles per block. Therefore, if every block marked the fracture surface, which would happen if a) cracking started almost immediately after the application of load and b) the marks could be resolved in the microscope, one would expect to find every marker band. All but five of the expected 19 bands were located. Where the bands were missing became obvious as the crack growth plot was constructed. The tabular data and crack growth curve for this specimen are shown in Table 25 and Figure 21.

Table 25. Crack depth and load block data for specimen EM56CC.

Load Blocks	Crack Depth from Pit Wall (mm)	Crack Depth from Pit Centre (mm)	Crack Depth Based on ECS Centre (mm)
0	0	0.0652	0.0398
1	0.0020	0.0672	0.0418
2	0.0106	0.0758	0.0504
3	0.0244	0.0896	0.0642
4	0.0538	0.1190	0.0936
5	0.0752	0.1404	0.115
6	-	-	-
7	0.1263	0.1915	0.1661
8	-	-	-
9	0.2129	0.2781	0.2527
10	0.2735	0.3387	0.3133
11	0.3138	0.3790	0.3536
12	-	-	-
13	-	-	-
14	0.5330	0.5982	0.5728
15	-	-	-
16	0.7007	0.7659	0.7405
17	0.8457	0.9109	0.8855
18	1.4077	1.4729	1.4475
19	2.7568	2.822	2.7966

Figure 21. Crack growth curves for EM56CC showing data based on measurement from pit wall, pit centre, and ECS centre.

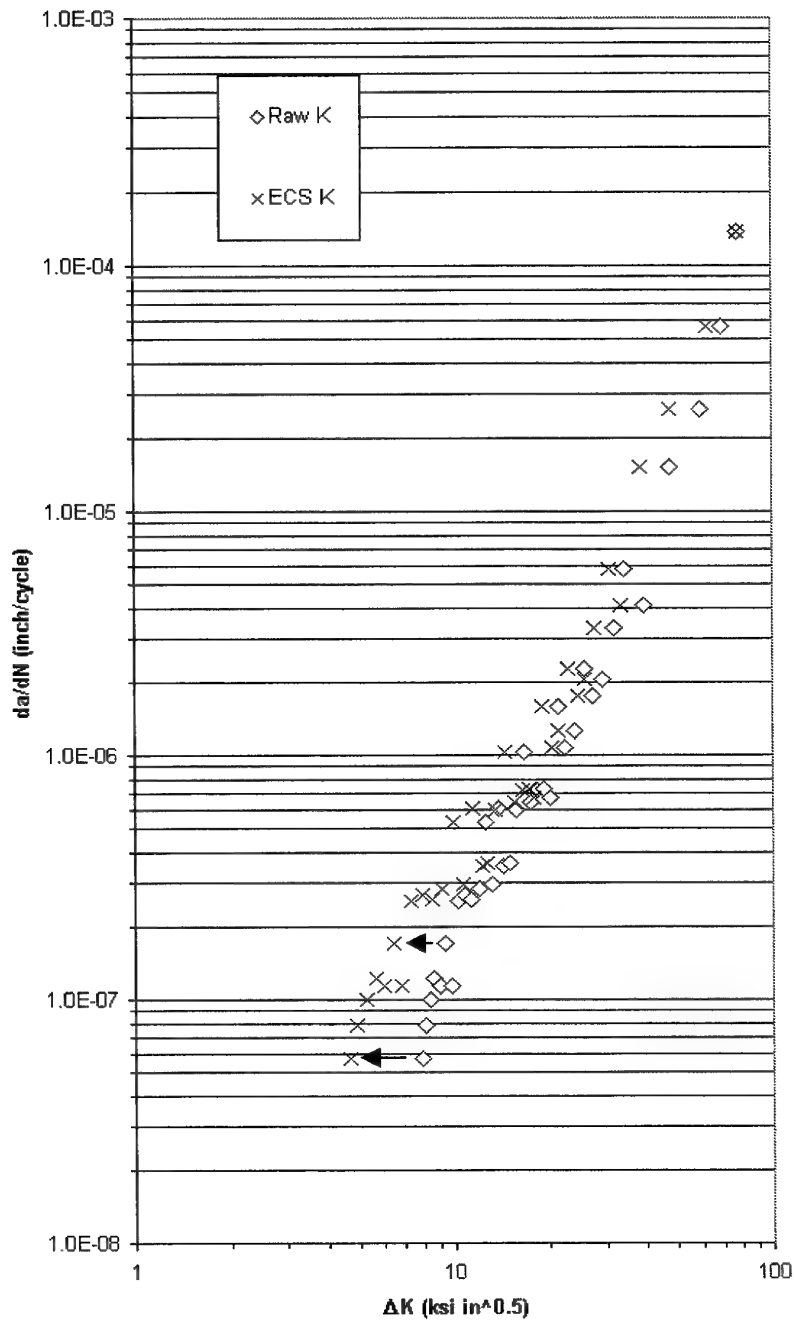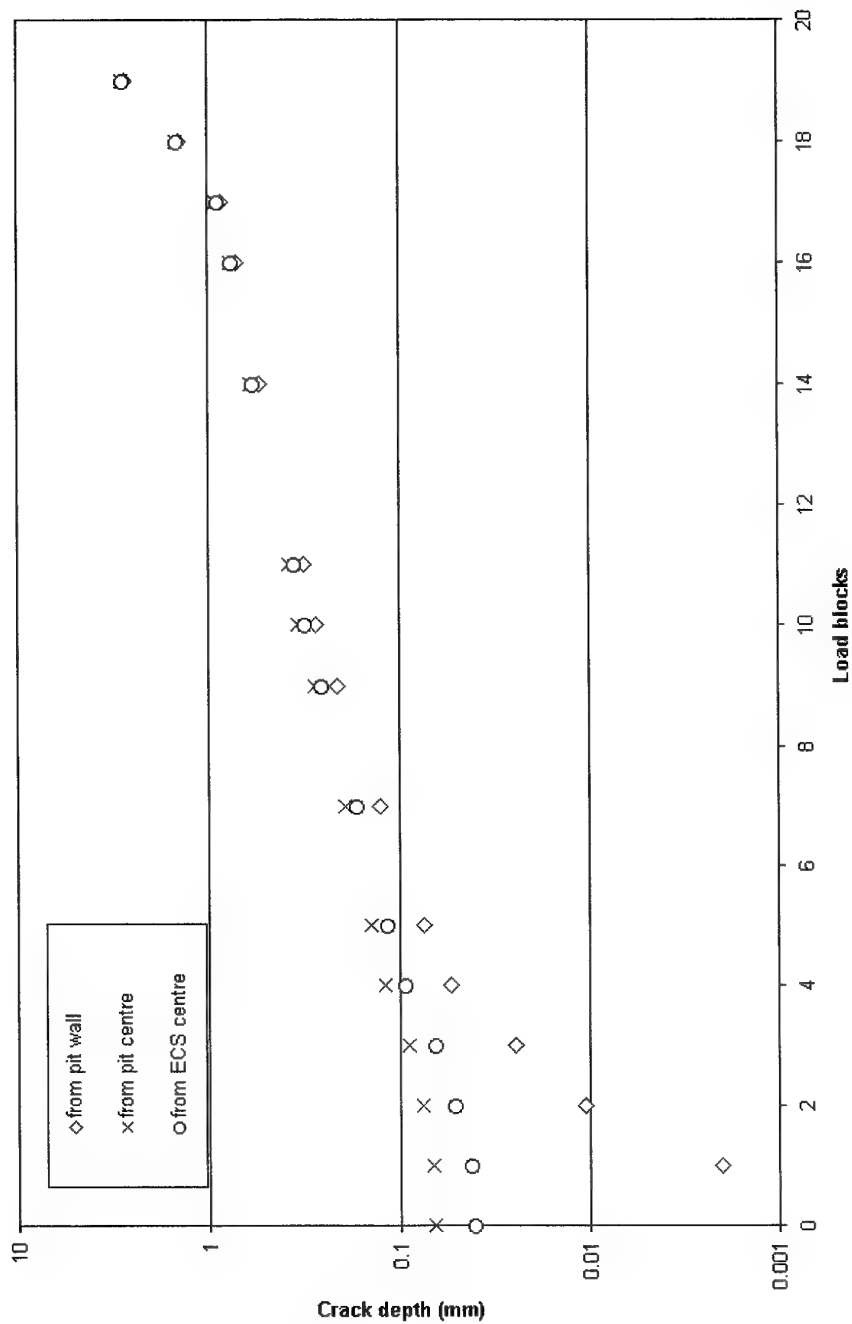### 4.2.2.2 Crack growth curve for middle stress specimen EL1CK

Specimen EL1CK was tested at 1214 MPa (176 ksi) maximum stress and had a total life of 34 622 cycles. Each marker block consisted of 900 constant amplitude cycles and 50 underloads followed by 50 overloads, for a total of 1000 cycles per block. Therefore, if every block marked the fracture surface, which would happen if a) cracking started almost immediately after the application of load and b) the marks could be resolved in the microscope, one would expect to find every marker band. This was the case, as 34 bands were located on the fracture surface using a light microscope.

The faintest bands at the shortest crack lengths were found using differential interference contrast in conjunction with a 100x lens and 10x eyepieces for total magnification of 1000x. At longer crack lengths, the bands could be easily resolved using lower magnification and bright field illumination. The crack growth curve and tabular data for this specimen were shown earlier in section 4.2.2 (Figure 19 and Table 24), so they will not be repeated here.

4.2.2.3 Crack growth curve for low stress specimen EM56BF

Specimen EM56BF was tested at 1144 MPa (166 ksi) maximum stress and had a total life of 36 410 cycles. Each marker block consisted of 1900 constant amplitude cycles and 50 underloads followed by 50 overloads, for a total of 2000 cycles per block. All but five of the expected 18 bands were located. Where the bands were missing became obvious as the crack growth plot was constructed. The tabular data and crack growth curve for this specimen are shown in Table 26 and Figure 22.

4.2.3 Calculating stress intensity

In the previous three sections (4.2.1.1-4.2.1.3), crack growth curves were developed for three different specimens at the various stress levels. However, before these data can be used to compare with other material models, they need to be converted into crack growth rate v stress intensity data, or $da/dN\ v\ \Delta K$.

In all the modelling efforts in this program, the cracks were assumed to be semi-circular surface cracks. Fractographic evidence showed this to be a reasonable assumption, since the ratio of a/c never seemed to vary much from 1.0. When using crack growth models for developing the ECS values in AFGROW, the program was allowed to vary a/c from 1.0 when calculating stress intensity, but in order to calculate stress intensity from fractographic data, a/c was fixed at 1.0.

Table 26. Crack depth and load block data for specimen EM56BF.

Load Blocks	Crack Depth from Pit Wall (mm)	Crack Depth from Pit Centre (mm)	Crack Depth Based on ECS Centre (mm)
0	0	0.0652	0.0398
1	0.0020	0.0672	0.0418
2	0.0106	0.0758	0.0504
3	0.0244	0.0896	0.0642
4	0.0538	0.1190	0.0936
5	0.0752	0.1404	0.115
6	-	-	-
7	0.1263	0.1915	0.1661
8	-	-	-
9	0.2129	0.2781	0.2527
10	0.2735	0.3387	0.3133
11	0.3138	0.3790	0.3536
12	-	-	-
13	-	-	-
14	0.5330	0.5982	0.5728
15	-	-	-
16	0.7007	0.7659	0.7405
17	0.8457	0.9109	0.8855
18	1.4077	1.4729	1.4475

The equations were those of Newman and Raju (1986), and these are the same solutions used by AFGROW. For a detailed discussion, please read the paper referenced above, as it presents the general solution for a semi-elliptical surface crack under both remote tension and bending. For the purposes of this report, the equations have been simplified to eliminate bending.

From Newman and Raju:

$$K = S_t (\pi a / Q)^{1/2} F_s (a/c, a/t, c/b, \phi) \tag{11}$$

where S_t is the remote tension, Q is the shape factor, and F_s is a function that accounts for crack shape (a/c), crack size (a/t), finite width (c/b), and angular location (ϕ). See figure 23 for the definitions of a, c, t, b, and ϕ.

$$F_s = [M_1 + M_2 (a/t)^2 + M_3 (a/t)^4] g f_\phi f_w \tag{12}$$

and for $a/c \leq 1$;

$$Q = 1 + 1.464 (a/c)^{1.65} \tag{13}$$
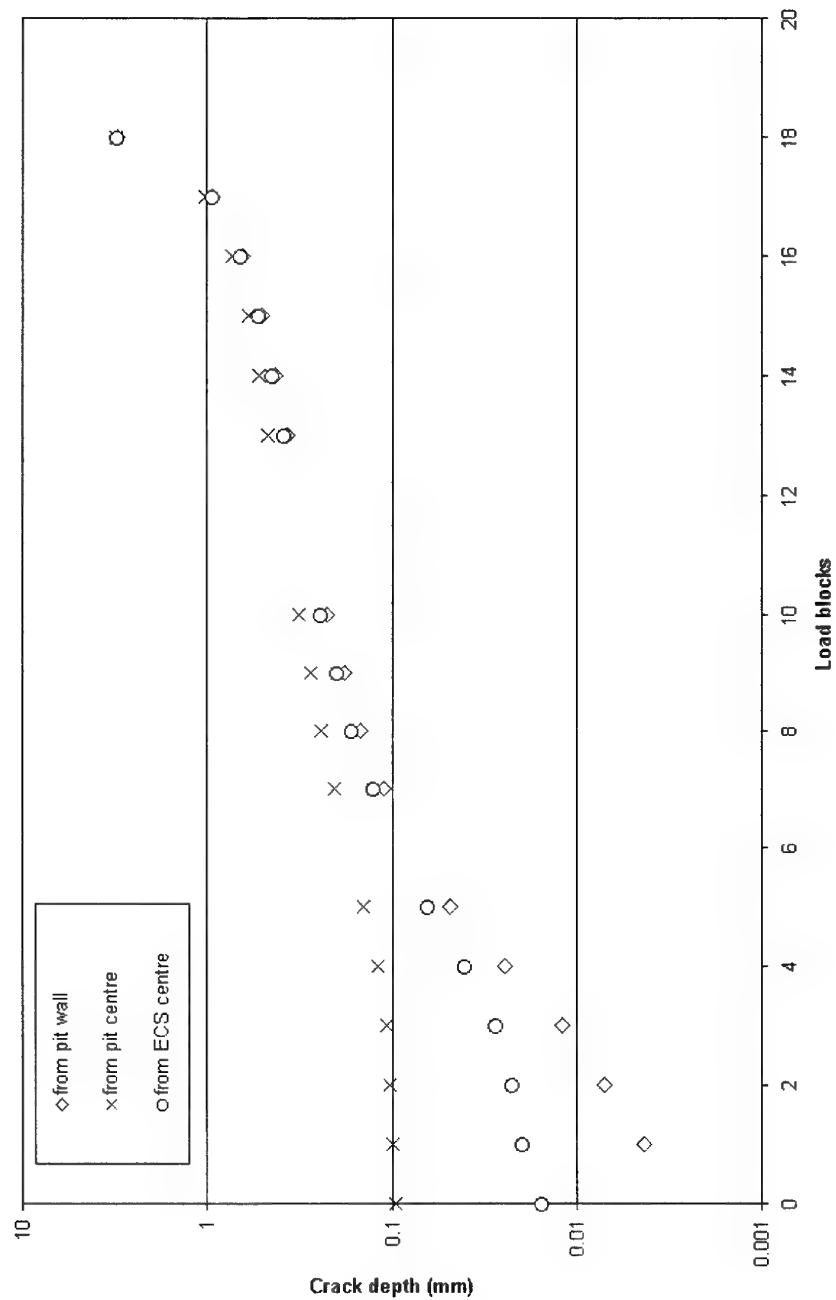
Figure 22. Crack growth curves for EM56BF showing data based on measurement from pit wall, pit centre, and ECS centre.

$$M_1 = 1.13 - 0.09a/c \tag{14}$$

$$M_2 = -0.54 + \frac{0.89}{0.2 + a/c} \tag{15}$$

$$M_3 = 0.5 - \frac{1}{0.65 + a/c} + 14(1 - a/c)^{24} \tag{16}$$

$$g = 1 + [0.1 = 0.35(a/t)^2](1 - \sin\phi)^2 \tag{17}$$

and where f_ϕ is given by Eq. 18, and f_w, the finite width correction, is given by Eq. 19.

$$f_\phi = [(a/c)^2 \cos^2\phi + \sin^2\phi]^{1/4} \tag{18}$$

$$f_w = \left[\sec\frac{(\pi c}{2b}\sqrt{\frac{a}{t}}\right]^{1/2} \tag{19}$$
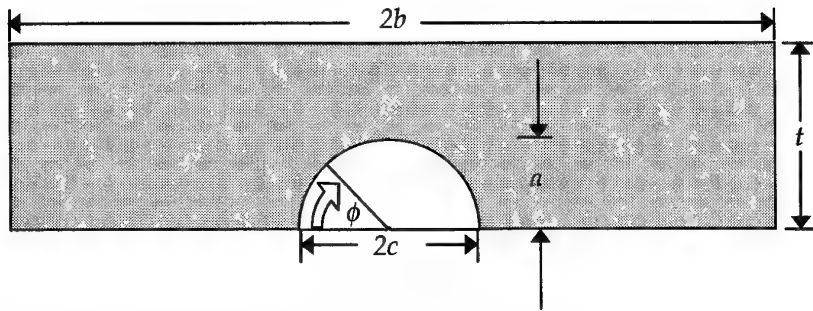
Figure 23. Newman-Raju surface crack configuration.

4.2.4 Comparison with other curve fit models

Crack growth rate vs. stress intensity was calculated using the marker bands data in conjunction with the Newman-Raju stress intensity solution. The data are shown in comparison with the work of Feddersen et al. (1972) in Figure 24. The marker band data seem to fall a factor of three lower in the intermediate stress intensities (11-33 MPa√m, 10-30 ksi√in), but the Feddersen data shows this much scatter at higher stress intensities, and the Feddersen data is sparse in the region in question. The marker band data matches quite well at low and high ΔK values. Figure 25 shows this same marker data compared to the different material models.
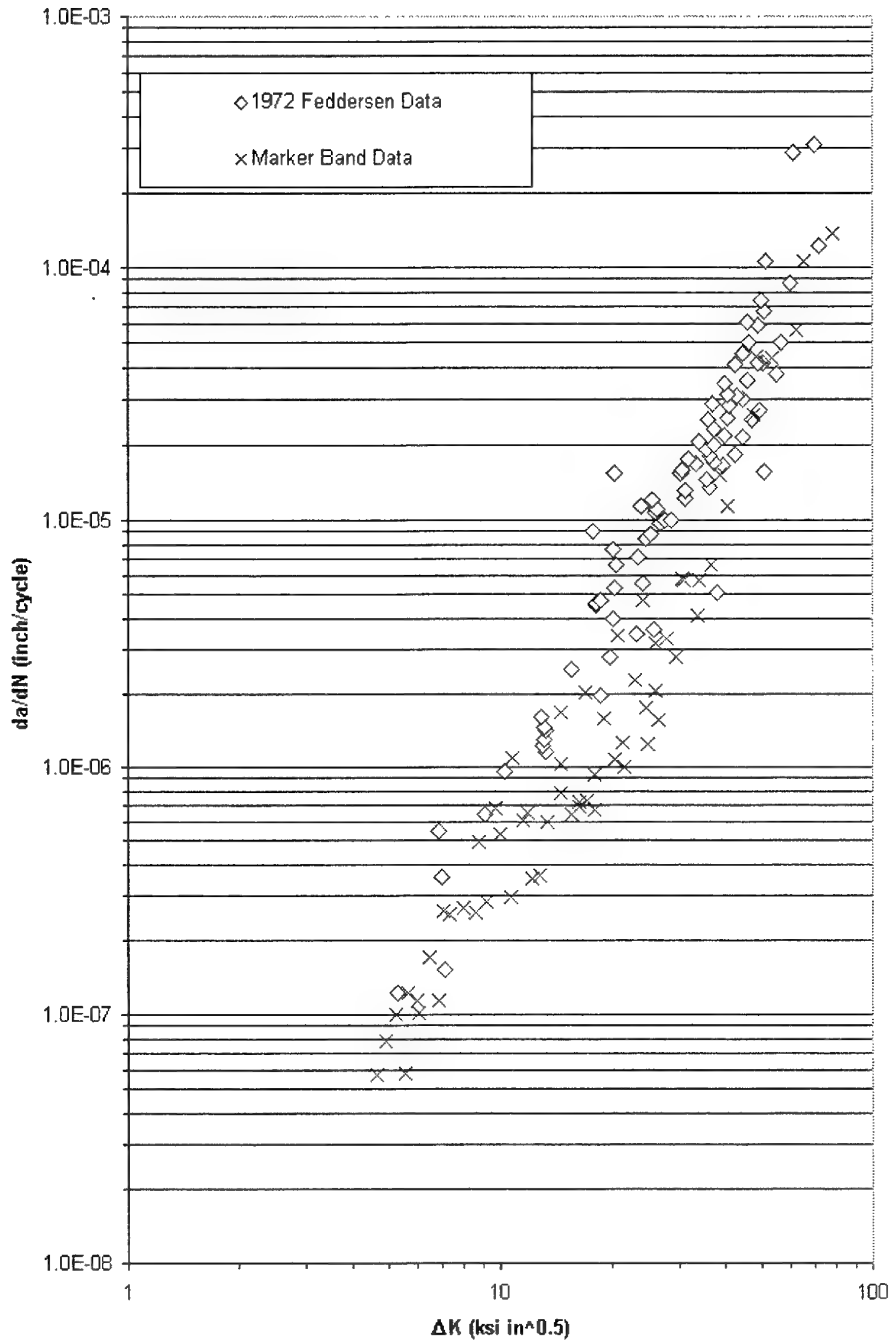
Figure 24. Feddersen data from 1972 F-111 DADTA study compared with marker band data. Dry/lab air, R = 0.1, 220-240 ksi heat treat.
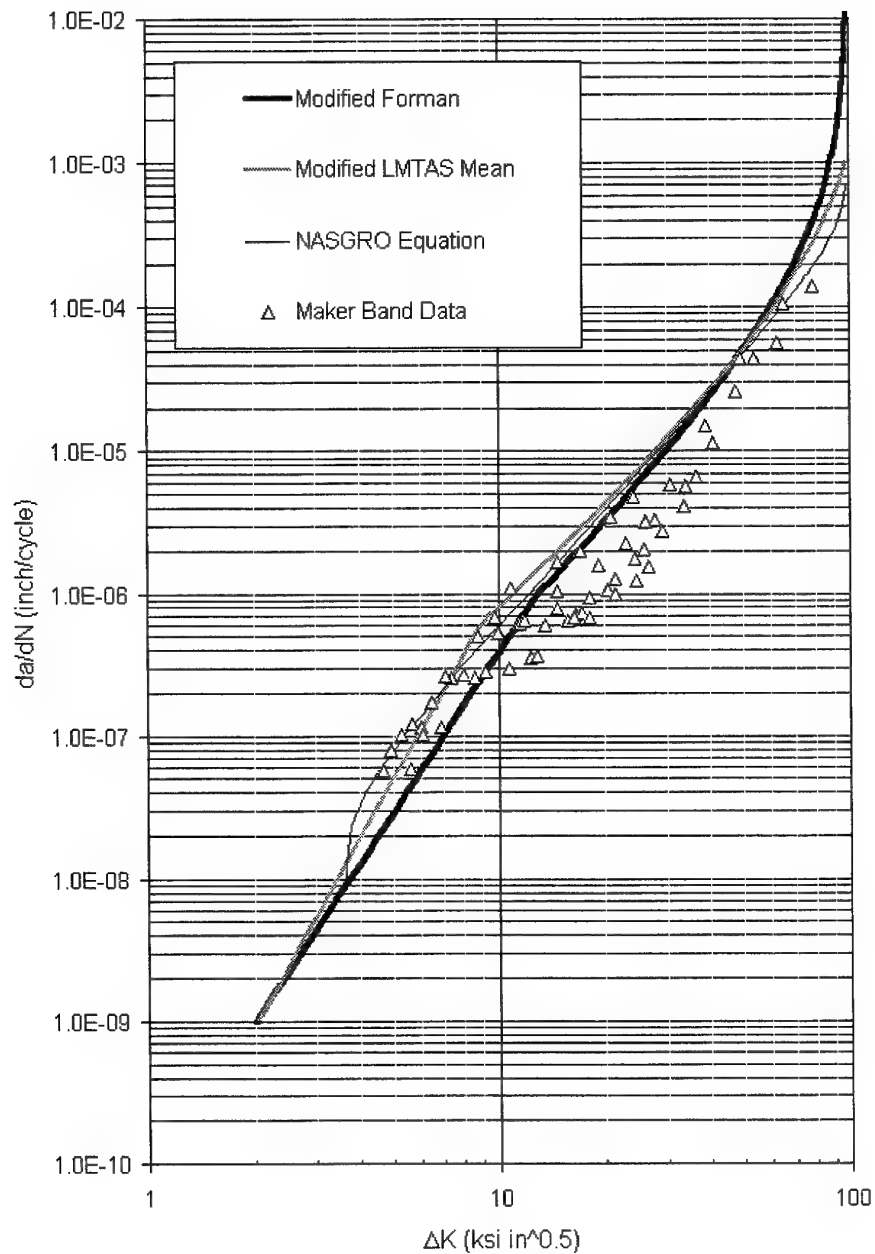
Figure 25. Modified Forman, Modified LMTAS Mean, and NASGRO material models compared with data derived from low-K$_t$ marker bands at R = 0.1.

4.3 Modelling of low-k_t results

After examining all the material models, it was determined that the Modified Forman curve fit was adequate for this program, as the behaviour of the laboratory specimens was not radically different from that basic material model. Admittedly, the Modified Forman model is not the best (as admitted by Lockheed) [Ball and Doerfler 1996], but it is what engineers have used for the F-111 DADTA throughout its history. As such, it is best if the ECS values and pit size correlations are based on that material model.

4.3.1 AFGROW settings and Forman model

In the AFGROW crack growth computer code, a number of options are available to ensure the model is as close as possible to representing the actual component being tested. Options exist for material model, crack geometry, stress distribution (tension and bending) load spectra, crack retardation models (load interaction), stress state (plane stress *vs.* plane strain)

The Forman material model was presented in Section 4.1.1 as equations 1-3. The AFGROW computer code [Harter 2000] can make use of the Forman equation and has menus available to directly input the material parameters. It allows for the fact that material behaviour often requires different segments in the equation based on stress intensity. The Forman model for D6ac as determined by General Dynamics all those years ago has two segments. The key parameters for the material model are:

Segment 1 ($\Delta K \leq 13$ ksi $\sqrt{\text{in}}$):

- C = 7.71E-09
- m = 3.655

Segment 2 (13 ksi $\sqrt{\text{in}} < \Delta K \leq K_c$):

- C = 1.46E-07
- m = 2.497

Both segments:

- K_c = 110 ksi $\sqrt{\text{in}}$
- ΔK_{th} = 2 ksi $\sqrt{\text{in}}$
- K_{Ic} = 67.5 ksi $\sqrt{\text{in}}$
- E = 210 GPa (30 000 ksi)
- σ_{ys} = 1310 MPa (190 ksi)

Other AFGROW parameters important to the modelling are:

Crack and component geometry:

- standard centre semi-elliptic surface flaw
- W = 44.45mm
- t = 6.35 mm
- crack aspect ratio (a/c) not kept constant
- tension load ratio = 1 (bending and bearing = 0)

Stress state:

- determine stress state automatically

Spectrum:

- stress multiplication factor (SMF) = 1 if spectrum used is in terms of stress, or SMF = desired applied stress is normalised.
- residual stress/strength requirement was not used.

Retardation model:

- closure model
- opening load ratio (@ R = 0) = 0.235
- determine initial opening load ratio from first load in spectrum
- note--these tests were mostly constant amplitude, but since they contained marker bands in some specimens, load interaction was used. Typically, the marker bands only affected total life by about 0.7%, so the use of retardation was for completeness.

Beta corrections:

- none were used

Residual stresses:

- not used

The above information should allow anyone to recreate the ECS values as reported in the next section. The version of AFGROW used during this program was 4.00.11.8 and was released on 24 April 2000. In future versions of the software, changes in the coding (for example, load interaction models or K solutions) could certainly alter the results if other things, such as material model, remain the same.

4.3.2 ECS back-calculated from actual fatigue lives

Table 27 is a summary of ECS values (in microns) as back-calculated from the fatigue lives of the laboratory results. The model set-up discussed in the previous section was run with the appropriate stress and spectrum (allowing for presence of and variations

in marker bands), and the initial crack size (ECS) was iterated until the life predicted by the simulation converged on the actual live by 2.5% or less. In most cases, predicted lives converged on the experimental results well within one percent. With these data, then, the next step was to see if the ECS values correlated with an aspect of the physical corrosion damage. This has to be possible if the ECS concept is to work for damage detected in the future and be of practical use to F-111 fleet managers. The next section discusses this process.

Table 27. ECS back-calculated from fatigue lives and Modified Forman model.

Stress Level (MPa)	Specimen ID	Fatigue Life	Calculated Life	ECS (μm) Modified Forman
1351	D6BF	12 394	12 404	30.75
	D6BG	13 764	13 449	27.50
	D6BH	12 368	12 316	31.00
	D6BJ3	11 913	11 768	31.25
	EM56CC	9586	9550	39.87
	EK14AL	5956	5889	96.50
	EM56CA	5196	5162	119.40
	EL1CL	5933	5889	96.50
1214	D6CF	45 507	45 694	9.25
	D6CG	29 513	29 557	16.00
	D6CH	22 960	23 077	22.00
	D6CI2	21 629	21 611	24.00
	D6CJ2	18 700	18 853	28.75
	D6CK2	44 183	44 032	9.38
	D6CL	34 019	33 980	13.40
	EM55CB	33 789	33 736	13.60
	EL1CK	34 622	34 829	12.50
	EM56BB	9954	9950	68.70
	EK7AL	15 954	15 870	35.00
	EM56CK	18 955	18 884	27.90
1144	D6DC	58 910	59 041	8.73
	D6DG	56 313	56 346	9.25
	D6DJ	26 421	26 532	24.00
	D6DK	76 254	76 258	6.13
	D6DL	50 672	50 888	10.13
	EM56BC	64 000	64 480	7.63
	EK10AL	23 969	23 805	26.67
	EK15AM	33 953	34 199	16.76
	EM56BF	36 410	36 359	15.50
	EM55BG	14 846	14 836	50.80

4.4 Fractographic examinations – pit features

One of the most important factors in the ECS concept is the ability to correlate real, physical damage features (Figures 26-28) with the fatigue lives of laboratory specimens. In this way, ECS values can be derived from damage detected in service when it comes time to apply the concept to an aircraft component. In this case, the damage is pitting, and several aspects of corrosion pits are available for investigation, although some features lend themselves to realistic measurement more than others do. The pit features measured in D6ac were:

- pit depth (a),

- pit width ($2c$),

- aspect ratio (a/c),

- pit area (or volume assuming planform stays constant in 3D space), and

- pit tip radius.

Some simplifying assumptions were required to effectively correlate pit features with fatigue life, and thus ECS. As a rule, most fractures in a specimen originated from many corrosion pits, and the challenge was to decide which pit was responsible for first cracking. Fortunately, if several cracks were present on a fracture plane, it was rather obvious which crack was longest before it linked with others, but that longest crack may also have had several pit origins. In these cases, the most central pit, which happened to be the deepest in most cases, was taken to be the primary crack-starter.

As is typical of fatigue, higher stresses generate more cracks. In this program, the specimens tested at 1351 MPa (196 ksi) often contained as many as 13 separate crack origins on the fracture plane. On the contrary, cracking usually emanated from just one pit at the lower stress of 1144 MPa (166 ksi).

In the coming discussions and tables, the critical pit features reported for each specimen belong to the pit believed to be responsible for the first crack.

A number of things became obvious very quickly when attempting to correlate pit features to fatigue life. First, pit tip radius performed poorly, followed closely by pit area (volume), and, not surprisingly, pit width. As was hoped, one of the more promising correlations came from correlating ECS (hence life) with pit depth. A fair amount of discussion is reserved for this in upcoming sections, and it is given particular attention because pit depth is the feature that stands the greatest chance of being measured accurately. Although depth worked reasonably well, correlation was further improved by combining measured pit features into a new metric; this will be discussed shortly.
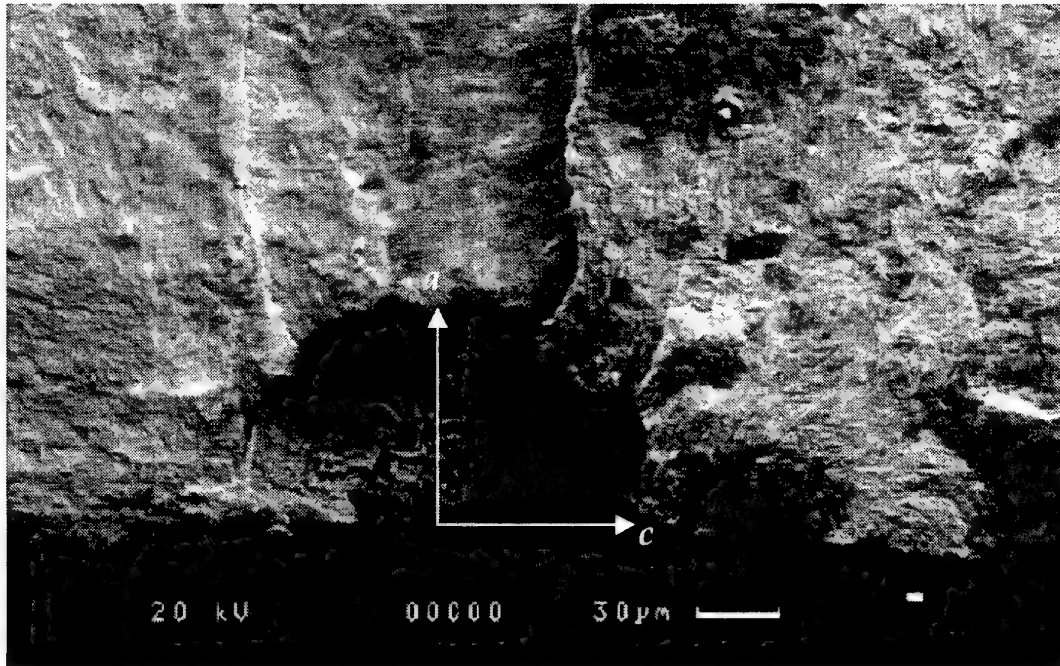
Figure 26. Nearly perfect hemispherical pit with aspect ratio, a/c =1.
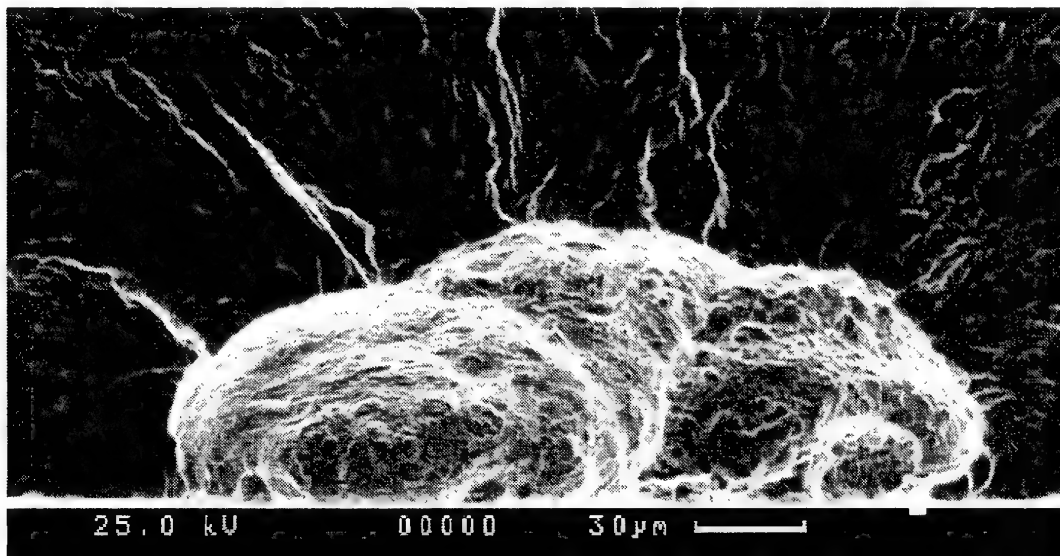
Figure 27. This shows a cluster of pits that have joined to produce, in effect, one large pit of very low aspect ratio, in this case a/c = 0.69.
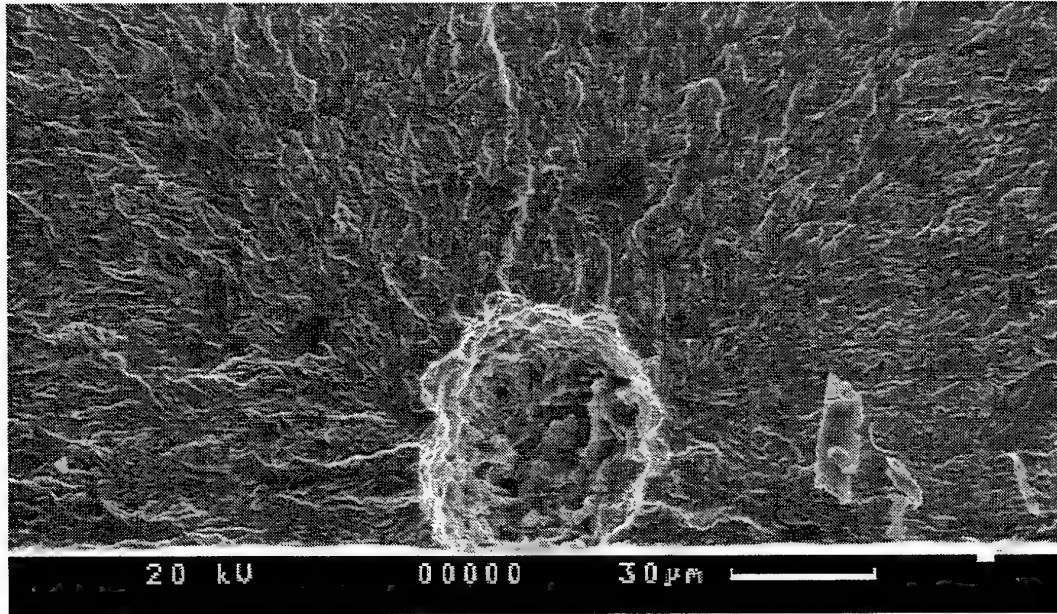
Figure 28. Some of the pits seem to have grown as a complete sphere under the surface, which gives rise to a high aspect ratio, in this case a/c = 2.23.

4.5 Correlation of pit features with ECS

The most important aspect of the ECS development process is the correlation of ECS with real pit features, so ECS values can be determined for damage that is detected in the future. As discussed earlier, several different features were investigated and correlated with ECS. Two stood out as having promise (Table 28), namely: pit depth and pit depth multiplied with pit aspect ratio (depth/over half the maximum width).

Table 29 show the Pearson correlation matrix, as determined using Systat statistical software. The matrix was built for the basic features needed to look at depth *vs.* ECS and depth*aspect ratio *vs.* ECS. These features are: depth, width, aspect ratio, and depth*aspect ratio. Table 29 assumes no outliers, although there were a couple, and these are filtered out based on the studentised residual. The revised correlations are shown in Table 30. Figures 29 and 30 show the pit depth *vs.* ECS and pit depth*aspect ratio *vs.* ECS, respectively. Curve fits are added to the data in these figures (with and without outliers) in following sections.

Table 28. Critical pit parameters (bold) that correlate well with fatigue life in D6ac steel.

Specimen ID	Fatigue Life	Depth (a) microns	Width (2c) microns	Aspect Ratio (a/c)	Product Depth * Aspect
D6BF	12 394	30.4	39.6	1.54	46.7
D6BG	13 764	48.4	100.1	0.97	46.8
D6BH	12 368	42.5	36.8	2.31	98.2
D6BJ3	11 913	65	90.3	1.44	93.6
EM56CC	9586	80.4	153.9	1.04	84.0
EK14AL	5956	87.2	110.5	1.58	137.6
EM56CA	5196	94.4	258.2	0.73	69.0
EL1CL	5933	87.9	198.5	0.89	77.9
D6CF	45 507	30.8	43.1	1.43	44.0
D6CG	29 513	43.2	43.2	2.00	86.4
D6CH	22 960	47.1	96.1	0.98	46.2
D6CI2	21 629	56.4	130.3	0.87	48.8
D6CJ2	18 700	55.9	85.1	1.31	73.4
D6CK2	44 183	30.3	44.2	1.37	41.5
D6CL	34 019	38.6	74.7	1.03	39.9
EM55CB	33 789	31.6	46.8	1.35	42.7
EL1CK	34 622	34	64.3	1.06	36.0
EM56BB	9954	66	75	1.76	116.2
EK7AL	15 954	87.5	226.8	0.77	67.5
EM56CK	18 955	105	398	0.53	55.4
D6DC	58 910	23.7	32.2	1.47	34.9
D6DG	56 313	43.8	59.5	1.47	64.5
D6DJ	26 421	70.4	164.1	0.86	60.4
D6DK	76 254	34.5	73	0.95	32.6
D6DL	50 672	41	71.5	1.15	47.0
EM56BC	64 000	42.9	152	0.56	24.2
EK10AL	23 969	61.3	88.9	1.38	84.5
EK15AM	33 953	69.1	213	0.65	44.8
EM56BF	36 410	88.5	223.3	0.79	70.2
EM55BG	14 846	102.3	177.3	1.15	118.1
		Average Aspect Ratio		1.18	
		Standard Deviation		0.42	

Table 29. Pearson correlation matrix for all data not excluding outliers. Note that Depth vs. ECS and Depth*A.R. vs. ECS give the highest correlations. A.R. stands for aspect ratio.

	Depth	Width	A.R.	Depth*A.R.	ECS
Depth	1				
Width	0.848	1			
A.R.	-0.455	-0.747	1		
Depth*A.R.	0.568	0.086	0.425	1	
ECS	**0.592**	0.342	-0.13	**0.599**	1

Table 30. Pearson correlation matrix for data excluding outliers. *For the case of Depth vs. ECS, the outlier was specimen EM56CA. **For the case of Depth*A.R. vs. ECS, the outliers were specimens EM56CA (again) and EL1CL. These specimens were both tested at high stress. Correlations improve considerably.

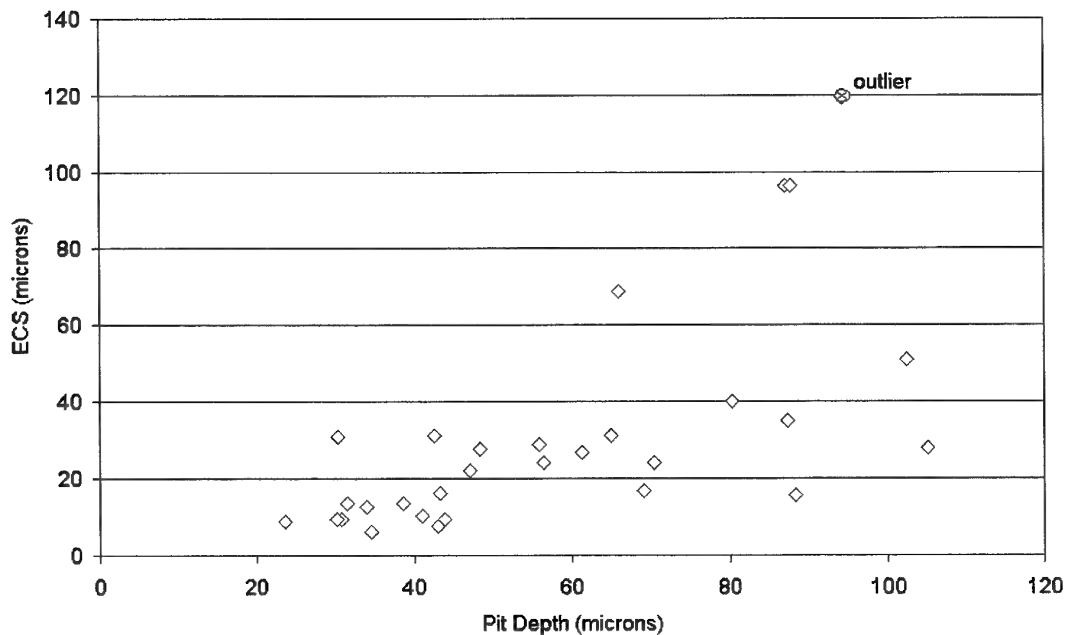|	Depth	Depth*A.R.	ECS
Depth	1		
Depth*A.R.	0.189	1	
ECS	**0.700**	**0.828**	1

Figure 29. ECS vs. Pit Depth, all data, outlier labelled.
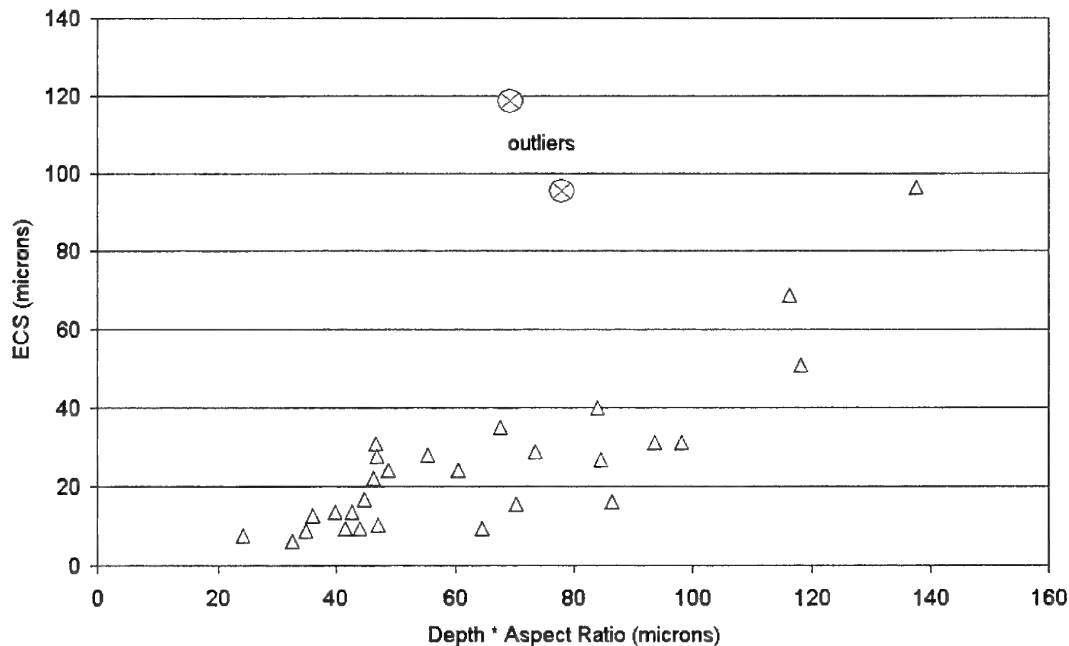
*Figure 30. ECS vs. Pit Depth*Aspect Ratio, all data, outliers labelled.*

4.5.1 ECS *vs.* pit depth

Being able to correlate ECS with pit depth is desirable, as depth is the most intuitive pit feature that influences life and is one that stands a chance of being measured, unlike pit tip radius, for instance. If a reliable method of measuring pit depth in a structure can be developed or found, then determining the ECS from that information is simple. Of course, errors in depth measurement could lead to significant errors in ECS, which then causes significant errors in fatigue life prediction. However, the aim of this report is not to develop techniques for NDI of pits, although different techniques were tried as part of the research process. The method simply demonstrates that if pit features can be measured accurately, then reasonable life estimates can be achieved.

4.5.1.1 All data

In Figure 31, all the calculated ECS values from the successful constant amplitude tests, as well as the calculated ECS values from the four pitted constant amplitude high-kt specimens, are plotted against pit depth. This approach gave a reasonable correlation with ECS values. If all data are included, the correlation coefficient is 0.592. An exponential function ($ECS = Ae^{-\alpha(\text{pit depth})}$) best described these data. Figure 31 shows the mean the 95% confidence upper and lower bounds, and the 99.95% confidence upper and lower bounds. One of the points (representing specimen EM56CA) was considered an outlier by the Studentised Residual statistical method.

Figure 31. ECS vs. Pit Depth, all data with curve fit and confidence bands.

4.5.1.2 Excluding outlier

In order to further increase the correlation coefficient and tighten the confidence bands, the statistical outlier (specimen EM56CA) described in the previous section was excluded from the data set. A new mean curve was plotted, and new confidence bands were fitted. These revamped data are shown in Figure 32 with the 95% and 99.95% confidence bounds. Correlation improved to 0.700, but the scatter is still excessive.

4.5.2 ECS vs. pit depth * aspect ratio

The other correlation that was tried stemmed from viewing corrosion pitting as a notch. In other words, the depth of the pit is not the only important factor with regards to influencing life. The aspect ratio of the pit should also play a role if it is considered, for instance, that a 90-micron deep pit that is very narrow would cause a higher stress concentration than a 90-micron deep pit that is very wide. Aspect ratio, as defined in this program, is the ratio of depth (a) over half surface length (c) (see Figure 26). If the pit is very narrow relative to its depth, then the aspect ratio will be greater than one. Similarly, if the pit is wide relative to depth, the aspect ratio will be less than one. Multiplying the aspect ratio by depth produces a weighted metric. This correlation technique worked very well.
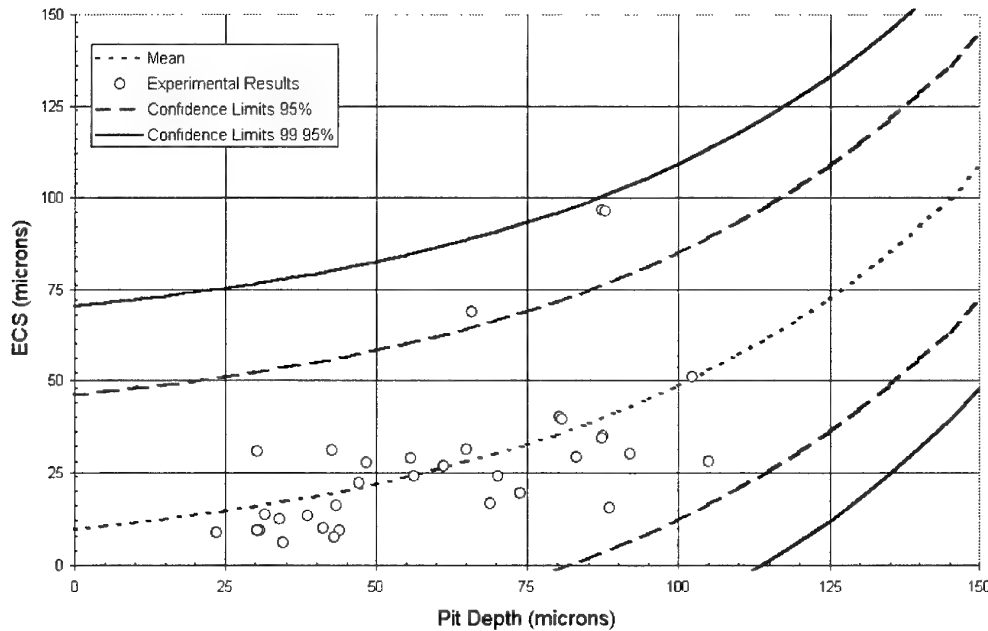
Figure 32. ECS vs. Pit Depth, excluding outlier with curve fit and confidence bands.

Increased correlation has its benefits in that it decreases the spread in predicted fatigue lives when considering the upper and lower confidence bounds on the mean.

4.5.2.1 All data

In Figure 33, all the calculated ECS values from the successful constant amplitude tests, as well as the calculated ECS values from the four pitted constant amplitude high-k_t specimens, are plotted against the product of pit depth and aspect ratio. This combination of features gave the strongest correlation with ECS values, and if all data are included, the correlation coefficient is 0.599.

Again, an exponential function best described this data. Figure 33 shows the mean, the 95% confidence upper and lower bounds, and the 99.95% confidence upper and lower bounds. Two of the points (representing specimens EM56CA and EL1CL) were considered outliers by the Studentised Residual statistical method.
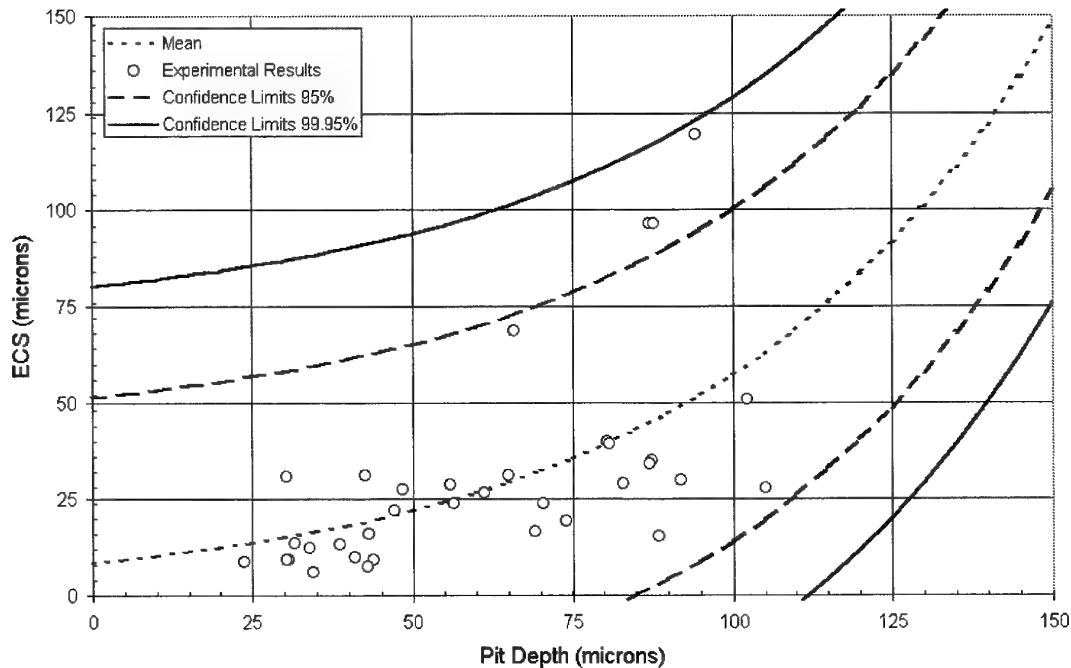
4.5.2.2 Excluding outliers

In order to further increase the correlation coefficient and tighten the confidence bands, the statistical outliers described in the previous section were excluded from the data set. A new mean curve was plotted, and new confidence bands were fitted. These data are shown in Figure 34 with the 95% and 99.95% confidence bounds. Correlation improved drastically, increasing from 0.599 to 0.828.

Figure 33. ECS vs. Depth*Aspect Ratio, all data and showing mean curve and confidence bands.

Figure 34. ECS vs. Pit Depth*Aspect Ratio, excluding outliers and showing revised mean curve and confidence bands. Notice how much tighter these bounds are compared to the other three charts (Figures 31-33).

4.6 Summary of ECS development

The ECS development process is the heart of this research effort. In this section, several material models were investigated to describe the behaviour of the low-k_t laboratory coupons. These materi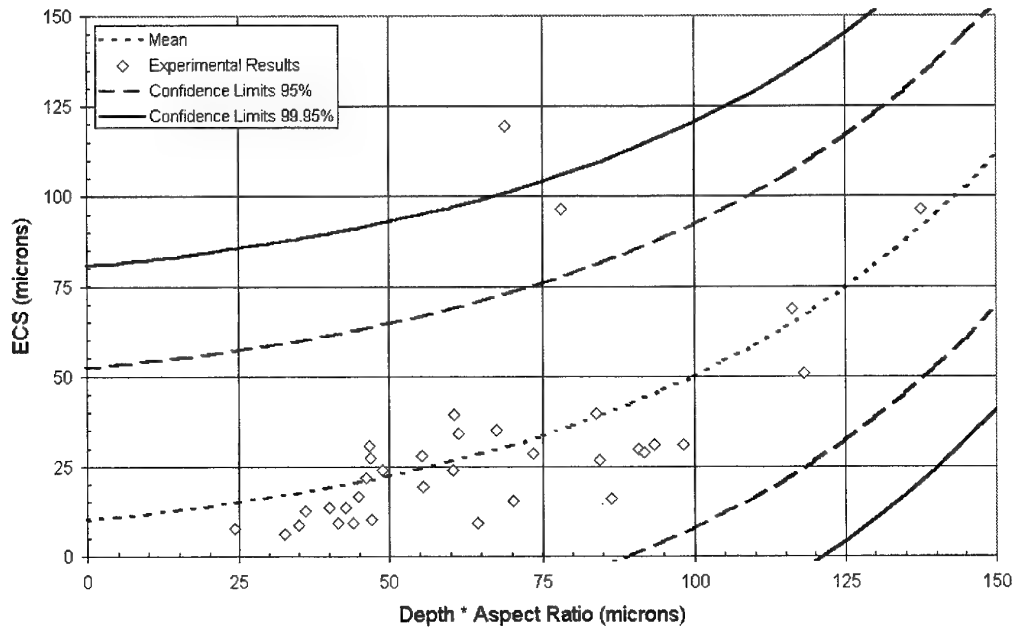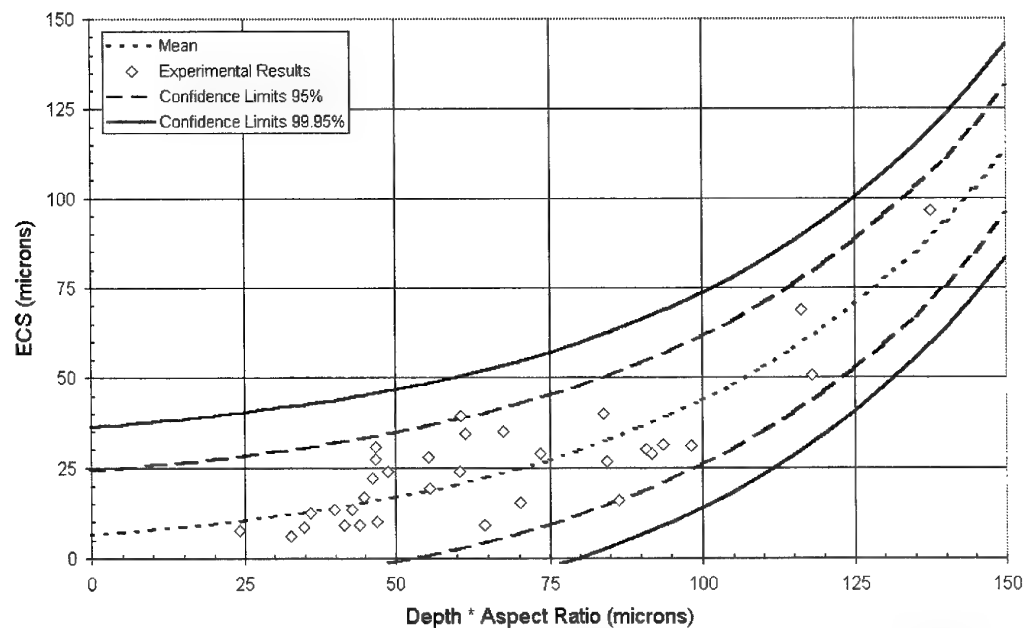al models were used to generate ranges of equivalent crack size values for each specimen tested. The material models were then compared to actual crack growth data (using marker bands) from the low-k_t coupons. Finally, once a material model was selected, correlations were sought between the ECS values generated by that material model and the pit features that caused fracture in the low-k_t coupons. The significant findings follow.

- Three different material models were investigated to see which was best for the purposes of ECS development.

- The three models were the original Forman curve fit used by LMTAS for DADTA management of the F-111, a mean-curve fit of the same data used to develop the Forman fit, and a NASGRO data set as found in the USAF fracture code, AFGROW.

- Values for ECS were developed for all of the low-k_t coupons using each of these material models. In some cases, the models yielded very different results, especially at low K values where the NASGRO model in particular had a very fast crack growth rate, thus small ECS values.

- Marker bands were placed in many of the specimens using a minor load spectrum. A marker band specimen was investigated for each of the three stress levels. From this, crack growth curves and da/dN vs ΔK (using Newman-Raju surface crack solutions to derive ΔK) curves were developed for the actual laboratory coupons. These laboratory developed curves were compared against the three crack growth models.

- From this, the Forman curve fit was selected, as it matched the low K crack growth data quite well. Also, the Forman curve fit was originally used by LMTAS in F-111 management.

- *Any future ECS-based life predictions must use the model from which the ECS distribution was developed.* By using the Forman curve fit, the same material model can be used for the original DADTA work as well as any new work based on the corrosion pitting.

- As would be expected, since ECS was back-calculated from fatigue life, the ECS distribution correlated strongly with fatigue life, even across the different stress levels.

- To make a useful life prediction tool, a feature of corrosion pits needed to be found that also correlated strongly with life. If this could be done, then the pit feature should also correlate strongly with ECS.

- Several pit features were studies to try to determine correlations with fatigue life. The strongest correlation was provided by the product of depth times aspect ratio, where aspect ratio is defined as depth over half width (a/c). This had a much stronger correlation than just pit depth. By using the product of depth and aspect ratio, the pits were treated as notches of varying severity where a very deep but narrow pit had a higher effective k_t than a pit of equal depth but wide cross section.

- Once the best correlation of pit feature with fatigue life was found, the feature was plotted *vs.* ECS. The subsequent relationship was fitted with a mean curve and 95% and 99.95% confidence bands.

- All subsequent validation (see next section) was done using the mean curve for best estimates of life prediction along with the upper 99.95% confidence bound for more conservative estimates.

5. Predictive Capability--the High-k_t Experiments

The intent of this testing program is to apply the results of the constant amplitude ECS study to a representative piece of F-111 structure. This section discusses the following elements of the predictive capability sought using the ECS method.

- Design and execution of a blind testing program using high-Kt specimens under both constant amplitude and spectrum loading.

- Life prediction of these specimen tests using a linear elastic crack growth code (AFGROW) for the elastic cases.

- Presentation of the results and discussions as to their significance.

5.1 The specimens

The desire to test the ECS concept on a more complex specimen led to selection of a well-tested and analysed specimen from earlier test programs. The FFVH 13 specimens (Figure 35) designed by Kowal and Heller (1999) were used for this portion of the experimental program.

Figure 36 shows the approximate location of FFVH 13 in the F-111 wing pivot fitting. Figure 37 shows the specific geometry of the oblong hole in the FFVH 13 coupon. The design of the hole is meant to reproduce the stress concentration and stress gradient associated with the FFVH 13 at the critical locations. Use of this specimen design was desirable because it has been extensively validated with finite element analysis and experimental microgrid plastic strain analysis [Kowal and Heller 1999].

5.2 Test conditions

The high-k_t fatigue tests were conducted at 10Hz, in laboratory air, using a 250 kN Instron load frame. Marker band spectra were used for the constant amplitude test, whereas the spectrum load was self-marking (all spectra are discussed in Appendix 2). The spectrum load was not run at a constant 10 Hz, instead 10 Hz was an average. The actual frequency varied heavily depending on the amount of load excursion during an individual cycle. In other words, small load excursions (ΔP) led to higher frequencies, and very large ΔP values led to very slow frequencies. Also, a Kodak Megaplus 1.4i black and white digital camera was used as a backup to monitor cracking and was focused on the maximum stress location in the specimen, which also contained corrosion pits. Stress levels are discussed in the next section.
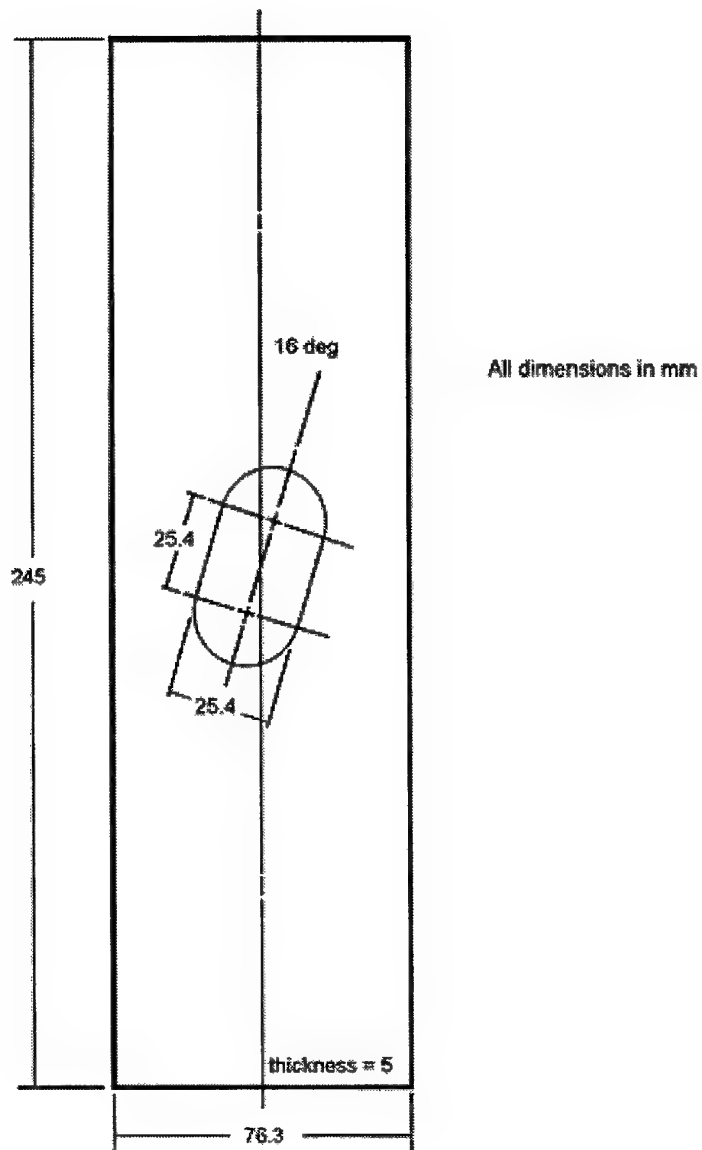
Figure 35. Geometry of FFVH 13 representative coupon (after Kowal and Heller 1999). Note: some of the specimens were surface ground and were 3.8 mm thick as opposed to the 5 mm shown in the figure. These specimens were leftovers from an old program, and it was simply necessary to use what was available.
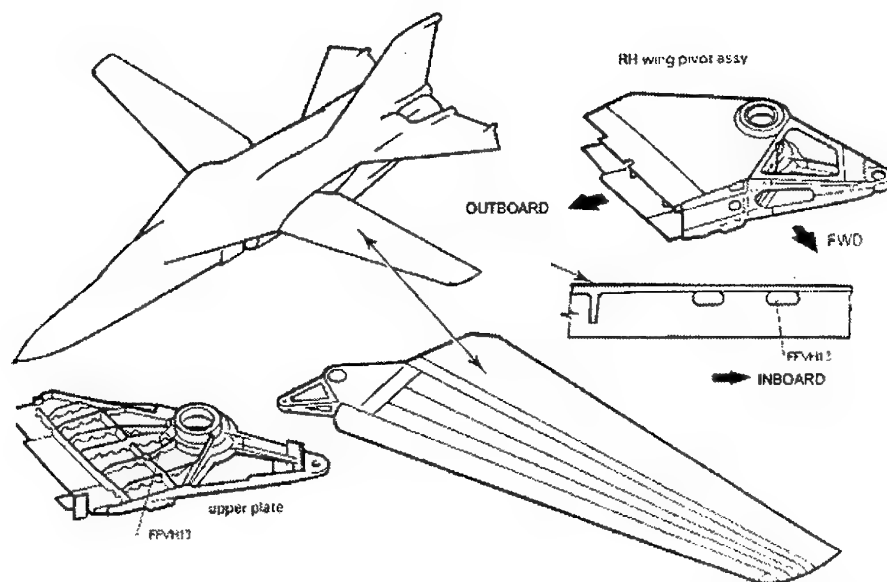
Figure 36. Diagram of components showing FFVH 13 location (after Kowal and Heller 1999).

5.3 Test matrix

The high-k_t test matrix was divided into two portions, constant amplitude and spectrum. Twenty specimens were available for testing, and they were left overs from an old test program. Therefore, specimen numbers were limited.

In both the constant amplitude and spectrum portions, a baseline was established using uncorroded specimens. After the baseline specimens were tested and analysed, corrosion pits were introduced in the remaining specimens.

5.3.1 Constant Amplitude

Only eight specimens were available for this portion of the testing. The purpose of these tests was to see if fatigue results would match those from the low-k_t experiments within reason. However, only one test was available per condition because of limited specimen numbers. Four different stress levels were selected, including two largely elastic, and two clearly elastic-plastic cases. Each stress level contained an unpitted and a pitted specimen. This was done to construct a crude stress-life curve and to determine a knockdown factor associated with the pitting. Peak stresses in the constant amplitude matrix were:
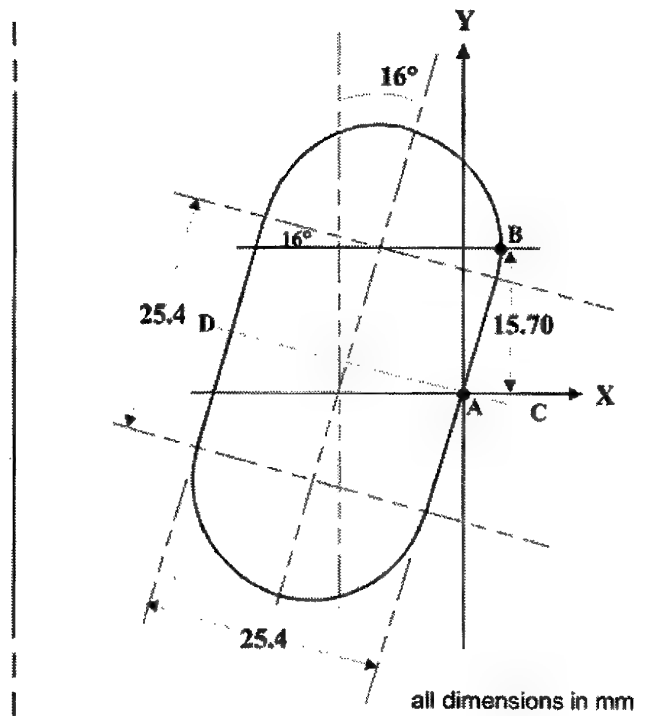
Figure 37. Detail of oblong hole in FFVH13 coupon showing maximum stress location (B) (after Kowal and Heller 1999).

- 896 MPa (130 ksi), below the cyclic proportional limit—completely elastic,

- 1144 MPa (166 ksi), one of the stress levels from the low-k_t program,

- 1310 MPa (190 ksi), just on the verge of monotonic yield,

- 1386 MPa (201 ksi), well developed plasticity at the max-stress location.

The remote stresses (as reported in Table 31) were arrived at by dividing the desired peak stress by the k_t of 4.0 assumed for the specimen. Pit depths were all targeted at 90 microns, whereas real maximum pit depths ended up varying between 74 and 95 microns for the different specimens.

The constant amplitude matrix was not really such, as it used marker bands so crack growth curves could be made post mortem if need be. The marker blocks were the same as those used in the constant amplitude, low-k_t test program described in Section

3. Appendix B contains all the details of the various marker spectra, as they varied slightly with maximum stress.

Table 31. FFVH 13 representative coupon test matrix. Remote stresses are multiplied by 4 to get the peak stress for the tests at the high-K_t location.

Specimen Number	Remote CA Max Stress (MPa)	Remote CA Min Stress (MPa)	Peak Remote Spectrum Stress (MPa)	Predicted Pit Depth (microns)
FP82AD	224	22.4	-	-
FP85AG	286	28.6	-	-
FP87AF	327.5	32.8	-	-
FP78AK	346.5	34.7	-	-
FP82AC	224	22.4	-	90
FP81AD	224	22.4	-	90
FP85AD	286	28.6	-	90
FP85AF	327.5	32.8	-	90
FP78AE	346.5	34.7		90
FP82AD*	-	-	224	-
FP82AJ	-	-	327.5	-
FP85AK	-	-	224	60
EM47AG1B	-	-	224	60
FP78AL	-	-	327.5	60
EM49AA2B	-	-	327.5	60
FP78AD	-	-	224	90
EM49AA1B	-	-	224	90
FP81AB	-	-	327.5	90
EM47AF2B	-	-	327.5	90
EM50AF2A	-	-	327.5	130
EM47AF2A	-	-	327.5	-

5.3.2 Spectrum loading

The true spectrum tests used a filtered DADTA 2B spectrum for DADTA Item 86 (DI86), which is FFVH 58 in the WPF lower plate. Spectrum details are explained in Appendix B, so they are not discussed here in detail. Two different peak stresses were selected based on the information obtained from the eight constant amplitude high-k_t specimens tested earlier. The two peak stresses were 896 MPa (130 ksi) and 1310 MPa (190 ksi), as can be seen in Table 31. Three different pit sizes were targeted to see how well the ECS vs. pit feature curves worked at different points. It would have been desirable to have a larger variety of stresses to thoroughly test the model, but the resources simply were not available. As it were, several pits sizes ended up being used simply by the nature of the specimen design. This will be discussed later.

Even though these specimens are called FFVH 13 representative coupons, it is important to note that the stress spectrum used for these tests was not representative of the actual stress environment at FFVH 13. The stresses at that location are compression dominated since FFVH 13 is in the upper plate of WPF; however, it was desired to have a tension-dominated spectrum for the high-k_t program, so a spectrum for a lower plate feature (FFVH 58) was selected. Again, the coupon was chosen because it has been subjected to rigorous analysis in the past, and the spectrum for FFVH 58 has been the subject of many analyses in recent years.

5.4 Experimental results — constant amplitude

The constant amplitude experiments demonstrated the knockdown factors associated with corrosion pitting in D6ac steel. Also, since some of the stress levels were the same as with the low-k_t tests from earlier, similar fatigue lives would be expected in the high-k_t cases.

Unfortunately, not many specimens were available, so these results are cursory at best. They do however illustrate a point.

Table 32 shows the fatigue lives for the different specimens along with the size of the pits they contained, if applicable. For the uncorroded specimens, the lowest stress specimen did not fail after four million cycles, so the test was stopped. For the higher stress cases (166-201 ksi, 1144-1386 MPa), the corrosion pits significantly reduced the fatigue life over the uncorroded cases. Average knockdown in life was by a factor of four.

Figure 38 shows the fatigue behaviour of all the specimens with a comparison between the uncorroded and pitted specimens.

Table 32. Table of constant amplitude fatigue lives for high-kt specimens.

Specimen Number	Remote CA Max Stress (MPa)	Max Stress at Kt (MPa)	Fatigue Life (Cycles to Failure)	Actual Max Pit Depth (microns)	Pit Metric (Depth * Aspect Ratio) (microns)
FP82AD	224	896	4 000 000 (runout)	-	-
FP85AG	286	1144	83 515	-	-
FP87AF	327.5	1310	54 180	-	-
FP78AK	346.5	1386	31 955	-	-
FP82AC	224	896	48 137	83	92
FP81AD	224	896	64 253	74	56
FP85AD	286	1144	19 784	92	91
FP85AF	327.5	1310	11 510	87	61
FP78AE	346.5	1386	8950	81	61
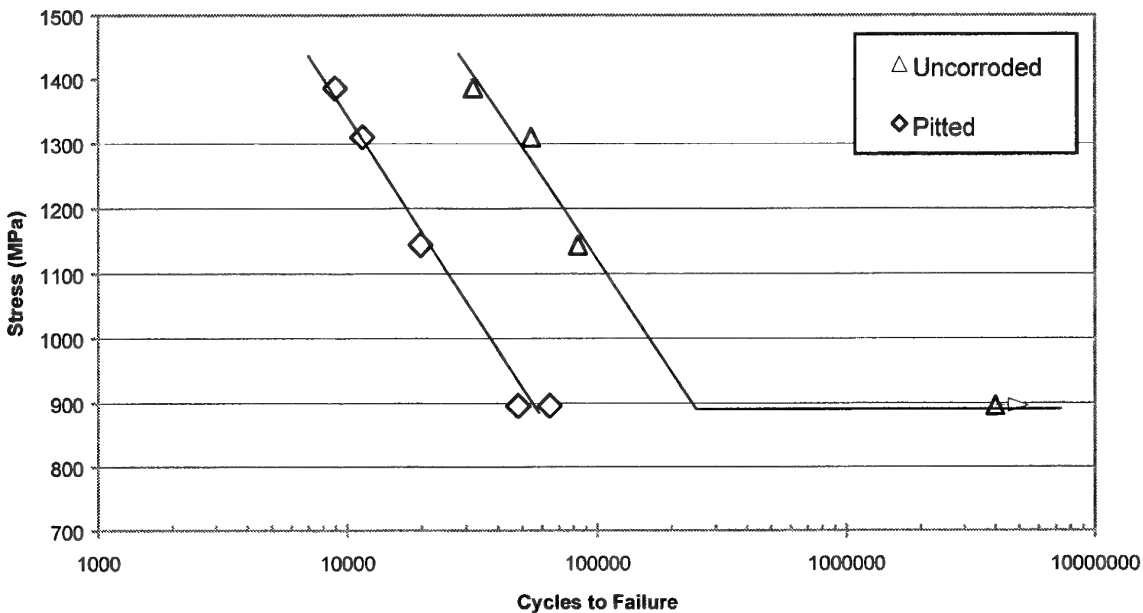
Figure 38. Stress vs. cycles to failure for constant amplitude high-k_t specimens, corroded and uncorroded. Uncorroded specimen at lowest stress reached runout of 4 000 000 cycles.

For further comparison, Figure 39 shows how the how the fatigue lives of the high-k_t specimens matched well with those of the low-k_t fatigue specimens. Next to low-k_t data points, the minimum and maximum pit metrics as shown corresponding with the maximum and minimum fatigue lives, respectively. The high-k_t information is superimposed on these data to show the relative lives and pit metrics. It is important to note that the pit metrics for the high-k_t specimens were quite large (near the upper bound of the pit metrics found in the low-k_t specimens), so it was expected that the fatigue lives of the high-k_t specimens would be on the low end of the range defined by the low-k_t experiments.

5.5 Experimental results — variable amplitude

The variable amplitude experiments using the FFVH13 coupons were again few in number because of limited specimen availability, but unlike the constant amplitude experiments, maximum stress levels were limited to two to increase the replicates.
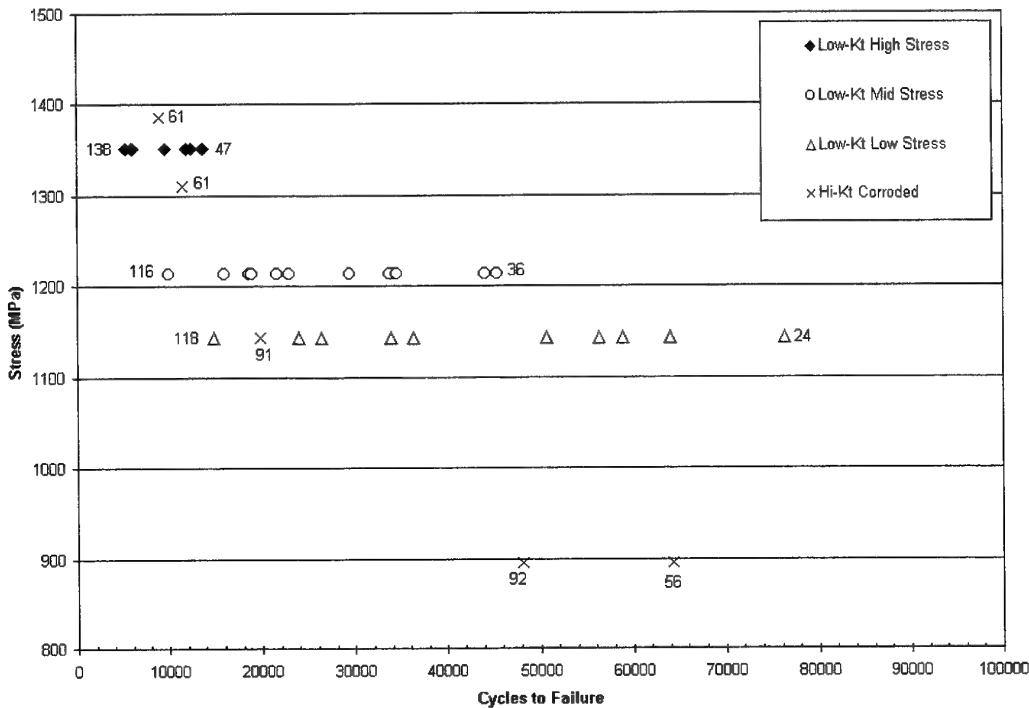
Figure 39. Comparison of low-k_t and high-k_t constant amplitude fatigue data.

A total of eleven specimens were tested in this phase of the program. Two of the specimens were uncorroded, and the other nine contained pits.

Table 31 (earlier) listed the predicted pit sizes, for the appropriate specimens. Similarly, Table 33 shows the actual maximum pit depth and metric for the specimens in the location of the fracture plane. This brings up an important difference between the low-k_t and the high-k_t experiments, as will be discussed.

In the low-k_t experiments, every pit saw the same stress since the pitting was in a flat plate. As such, it was typically the largest pit that caused fracture, so it was easily characterised during fractography. Therefore, Figure 8 from much earlier (section 2.3.4) showed excellent agreement between predicted and actual pit sizes that caused failure.

However, the stress gradient in these FFVH13 specimens was quite pronounced, so the stress one millimetre from the peak location was reduced by five percent. The significance of this is that it was not possible to place a pit of 'predicted' depth exactly on the location of peak stress. In fact, in many cases, the deepest pit (closest to the predicted size) was quite far away from the zone of peak stress.

83

*Table 33. Table of constant amplitude fatigue lives for high-k_t specimens. *Specimen FP82AD was reused to conserve on specimens. FP82AD was the low stress, uncorroded specimen for the constant amplitude high-k_t experiment. It survived 4 000 000 constant amplitude cycles at 896 MPa without failure. Subsequently, it was cycled for 160 000 spectrum hours before being considered a runout. **Specimen FP82AJ failed in the grip after some 80 000 hours. Considered runout. ***See text in this section for explanation of long fatigue life for specimen EM49AA2B.*

Specimen Number	Remote CA max Stress (MPa)	Max Stress at K_t (MPa)	Fatigue Life (DADTA 2B Spectrum Hours)	Actual Max Pit Depth (microns)	Pit Metric (Depth * Aspect Ratio) (microns)
FP82AD*	224	896	160 000	-	-
FP82AJ	327.5	1310	80 000**	-	-
FP85AK	224	896	47 624	55	71
EM47AG1B	224	896	89 404	76	95
FP78AD	224	896	47 184	67	100
EM49AA1B	224	896	62 055	97	98
FP78AL	327.5	1310	13 805	40	36
EM49AA2B	327.5	1310	74 164***	60	68
FP81AB	327.5	1310	12 850	58	49
EM47AF2B	327.5	1310	10 195	67	86
EM50AF2A	327.5	1310	15 367	86	124

Therefore, the pits that caused failure were often much smaller and of a variety of sizes other than the maximum. With this in mind, the fact that three "predicted maximum pit sizes" were used for the high-k_t variable amplitude tests really means little. One pit size could have been targeted and still yielded eight different pit sizes in the plane of maximum stress. Figure 40 shows the wide variation between target pit sizes for the specimen and the largest pits that actually occurred in the zone of maximum stress, the fracture plane.

Figure 41 shows the results from Table 33 in graphical form. Notice the tight grouping of fatigue lives at the highest stress of 1310 MPa. This is typical fatigue behaviour. Also expected was the greater variability in fatigue lives at the lower stress level. At the high stress, lives ranged from 10 195 to 15 367 simulated flight hours (SFH). One of the other specimens that was supposedly tested at a high stress (EM49AA2B) had an uncharacteristically long fatigue life of 74 164 hours. Thus, this specimen was given special attention.

All of the fatigue tests in this program were conducted under the scrutiny of a digital camera to record late stages of crack growth. To investigate the long life of EM49AA2B, the digital images were examined to see if the crack occurred in an odd location. Indeed it did occur in an odd location which happened to be far removed from the zone of peak stress. This is shown in Figure 42a-b. In part a, pits were present in the plane of peak stress, and the crack occurred at that location.
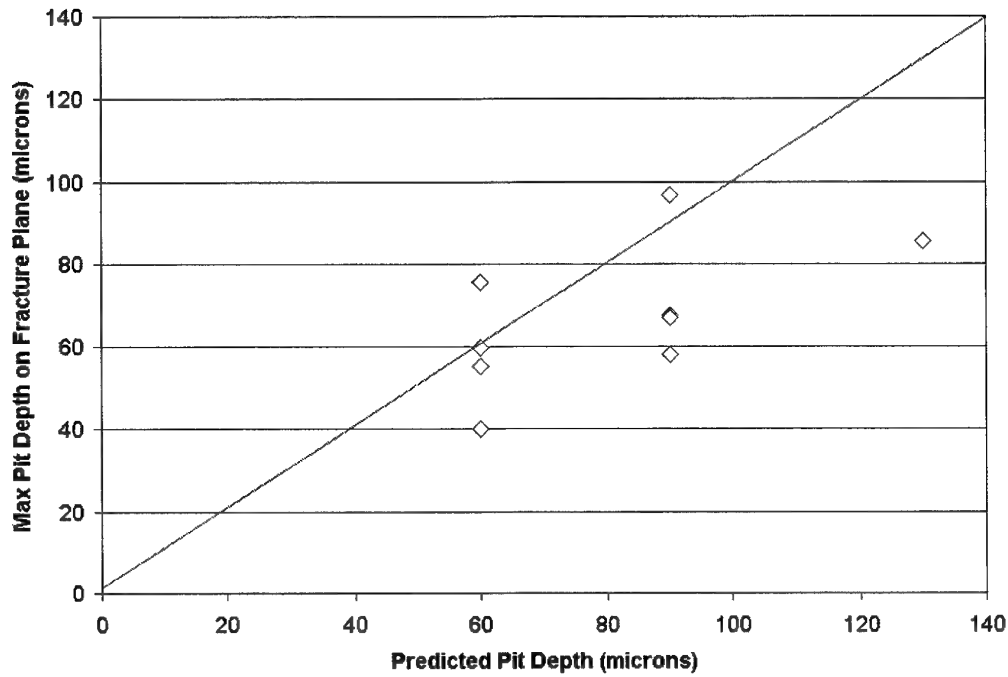
Figure 40. Maximum pit depth along fracture plane vs. predicted pit depth for high-k$_t$ coupons.
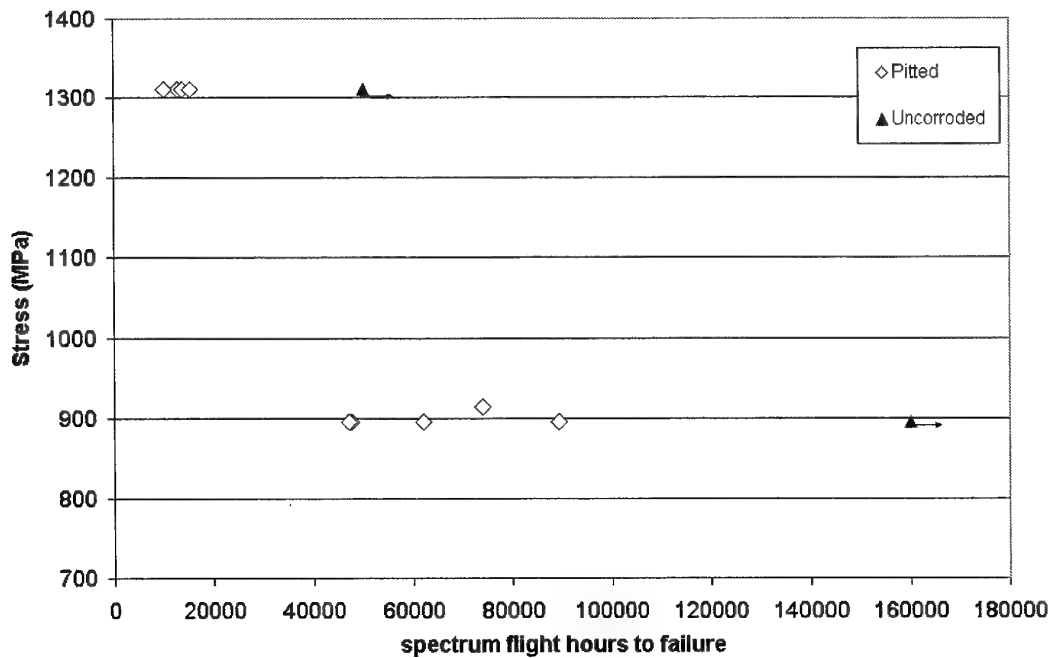
Figure 41. Results of high-k$_t$ FFVH13 fatigue tests.

In Figure 42b, no pit was present in the zone of peak stress. For that matter, the corrosion area on this specimen was unusually small and only resulted in one pit. This pit was far removed from the zone of peak stress, but the pit was still significant enough to cause cracking, even in the area of reduced stress. In this situation, the crack formed some five to six millimetres away from the zone of peak stress. In the location where the crack formed the stress was actually 65-70 percent of the peak (1310 MPa), or 851-917 MPa. This fact puts the life of specimen EM49AA2B (74 164 SFH) firmly in line with those of the low stress (896 MPa) experiments, which had lives ranging from 47 184 SFH to 89 404 SFH. This particular specimen has been shown at 915 MPa on all data charts to show it as being different from the specimens tested at the 896 MPa stress level.
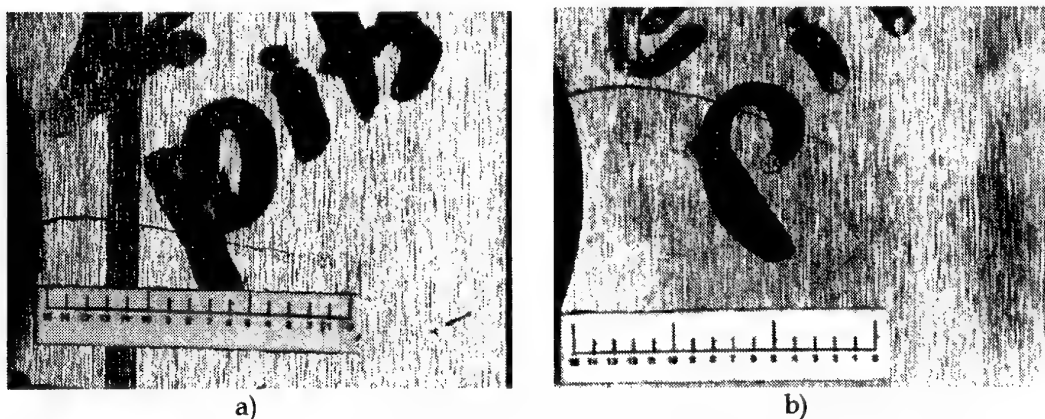
Figure 42. Crack camera image of a) specimen EM47AF2B with cracking in the high-k_t location, and b) specimen EM49AA2B with cracking much higher up the radius of the cut-out.

It was not possible to get a clear indication of the knockdown factor caused by corrosion pits in the spectrum tests. Only two unpitted specimens were tested, and one of those had previously undergone 4 000 000 million constant amplitude cycles at 896 MPa. In the spectrum tests, as discussed in Appendix B, the peak stress occurred once every 500 spectrum hours. In Figure 41, which showed the experimental results for the spectrum tests, the high stress test was shown as runout at 80 000 SFH, when in actuality the specimen failed in the grips near this value. At the low stress, 160 000 SFH was called runout. Either way, these show that the highly polished, undamaged form of the FFVH profile is extremely durable. It also shows that the material is not very damage tolerant, since the introduction of pits severely degraded the life.

5.6 FFVH13 high-k_t life predictions

Now that the fatigue results have been presented, this portion of the report will show life predictions for these tests based on Equivalent Crack Size distribution developed in Section 4 for this material/pitting combination. Figure 43, which also was shown in Section 4, is repeated here (as Figure 34) to show where the ECS values relate to the pit

metrics measured for each of the FFVH13 specimens. The predictions for the constant amplitude experiments and the spectrum experiments are treated seperately.
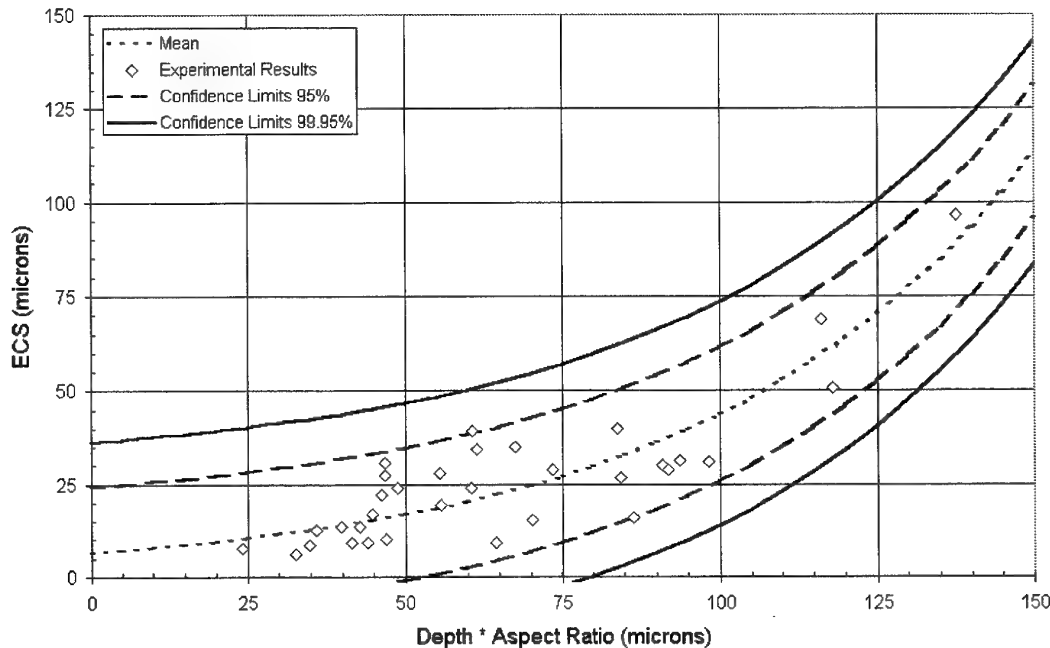
*Figure 43. ECS vs. pit metric (depth*aspect ratio) relationship used for all fatigue life predictions (repeat of Figure 34).*

Before getting to the actual results, however, the following AFGROW modelling parameters are summarised so that these predictions can be repeated or examined at a later date if so desired.

A similar summary was provided for the original ECS development experiments in Section 4.3.1. Much of this has stayed the same, such as the material model. The main thing that has changed is the component and crack geometry, since the FFVH13 specimen used for ECS validation is different from the simple flat plate originally used during ECS development. But for completeness, everything is summarised here.

In the AFGROW crack growth computer code, a number of options are available to ensure the model is as close as possible to representing the actual component being tested. Options exist for material model, crack geometry, stress distribution (tension and bending) load spectra, crack retardation models (load interaction), stress state (plane stress *vs.* plane strain)

The Forman material model was presented in Section 4.1.1 as equations 1-3. The AFGROW computer code [Harter 2001] makes use of the Forman equation easy and has menus available to directly input the material parameters. It allows for the fact that material behaviour often requires different segments in the equation based on stress intensity. The Forman model for D6ac as determined by General Dynamics all those years ago has two segments. The key parameters for the material model are:

Segment 1 ($\Delta K \leq 13$ ksi $\sqrt{in}$):

- C = 7.71E-09
- m = 3.655

Segment 2 (13 ksi $\sqrt{in} < \Delta K \leq K_c$):

- C = 1.46E-07
- m = 2.497

Both segments:

- K_c = 110 ksi $\sqrt{in}$
- ΔK_{th} = 2 ksi $\sqrt{in}$
- K_{Ic} = 67.5 ksi $\sqrt{in}$
- E = 210 GPa (30 000 ksi)
- σ_{ys} = 1310 MPa (190 ksi)

Other parameters important to the modelling are:

Crack and component geometry:
- single surface crack at hole
- W = 3 inch (76.2mm)
- t = 0.15 inch (3.81mm)
- hole diameter = 1.00 inch (25.4mm)
- crack aspect ratio (a/c) not kept constant
- tension load ratio = 1 (bending and bearing = 0)

Stress state:

- determine stress state automatically

Spectrum:

- stress multiplication factor (SMF) = 1 if spectrum used is in terms of stress, or SMF = desired applied stress is normalised.
- residual stress/strength requirement was used. Specimen always required to carry peak spectrum stress.

Retardation model:

- closure model
- opening load ratio (@ R = 0) = 0.235
- determine initial opening load ratio from first load in spectrum

Beta corrections:

- none were used

Residual stresses:

- not used

The above information should allow anyone to recreate the fatigue life predictions reported in the following sections. The version of AFGROW used for this phase changed from the version used during ECS development. The new version was 4.00004.12.10 and was released on 1 June 2001.

In this AFGROW model, a generalisation had to be made to account for the inability to model the exact stress distribution of the FFVH13 coupon. As pointed out earlier, the approximate stress concentration of the FFVH13 coupon was a factor of 4. However, a finite plate with a hole was used in the AFGROW model, which has a k_t of approximately 3.18. Thus, when doing predictions, it was necessarily to artificially raise the applied stress by a factor of 1.26 (4/3.18) to get the appropriate stress at the location of the crack.

Although this approximation is not as precise as desired, it was deemed adequate for this demonstration. When this program moves into the next phase, in which the technique is validated using the ADAMSYS computer code (or METLIFE), provisions exist to put in the correct stress distribution, and this will be done at that time.

5.6.1 Life predictions—constant amplitude

The ECS distribution developed in Section 4 provided good fatigue life predictions for the constant amplitude experiments using the FFVH13 coupons. For the predictions, the mean and upper 99.95% confidence limit curves in Figure 43 were used. The mean represents our best guess of the fatigue life, where the upper 99.95% confidence strives to capture deviations from the mean by as far as three standard deviations. This takes into account scatter in fatigue crack growth rates and provides a buffer that may be necessary due to inaccuracies in measuring corrosion damage in the field.

The lower 99.95% confidence limit curve was shown in Figure 43 but never used for practical purposes. The mean represents the best guess of the fatigue life, and no

engineer would use the lower confidence limit, which provides a life estimate longer than the mean, as that would likely be unconservative. Furthermore, the lower confidence limit is not useful below pit metrics of 50 microns.

So, for all the predictions shown in the following graphs and tables, only the predictions based on the mean and upper 99.95% confidence limit are shown. Table 34 summarises the fatigue life of each specimen, its pit metric, the associated mean and upper limit ECS values for that pit metric, and the life predictions resulting from those ECS values. Figure 44 shows these results graphically.

Table 35 shows the accuracy of the predictions relative to the actual fatigue life. The accuracy is represented as a percentage. A positive percentage means that the model over-predicted the fatigue life, and a negative percentage means that the model under-predicted the fatigue life. In a perfect world, the fatigue life would fall directly on the mean prediction, but as a rule, the actual life tended to fall between the mean and upper confidence limit predictions. This is considered more than adequate, since the obvious application of this technique would find us using the shorter life as derived from the upper confidence limit as a base for future inspections or other maintenance actions. In only one case (specimen FP78AE) did the upper confidence limit over-predict the fatigue life of the specimen, and here only by 1.6%.

The trend in the data suggests that at lower elastic stresses, the mean tends to do a better job predicting the fatigue life, and at higher stresses where peak stresses are at or above the yield point of the material, the upper confidence limit does a better job predicting the actual life. In the one case where the upper confidence limit over-predicted life, the peak stresses were about 11% above yield. This analysis should really be repeated as an elastic-plastic analysis using METLIFE, since it was only considered an elastic case in AFGROW.

Table 34. Table of ECS sizes and life predictions for constant amplitude FFVH13 coupons. ECS values in microns.

Specimen Number	Max Stress at Kt (MPa)	Pit Metric (Depth * Aspect Ratio) microns	ECS from mean curve	ECS from 99.95% curve	Fatigue Life Experiment SFH	Life predict mean ECS	Life predict 99% CL ECS
FP82AD	896	-	-	-	4E+6 (runout)	-	-
FP85AG	1144	-	-	-	83 515	-	-
FP87AF	1310	-	-	-	54 180	-	-
FP78AK	1386	-	-	-	31 955	-	-
FP82AC	896	92	37.5	67.4	48 137	48 066	31 227
FP81AD	896	56	18.7	48.6	64 253	81 733	39 555
FP85AD	1144	91	36.8	66.7	19 784	20 547	13 682
FP85AF	1310	61	20.8	50.6	11 510	19 736	10 728
FP78AE	1386	61	20.7	50.6	8950	16 474	9094
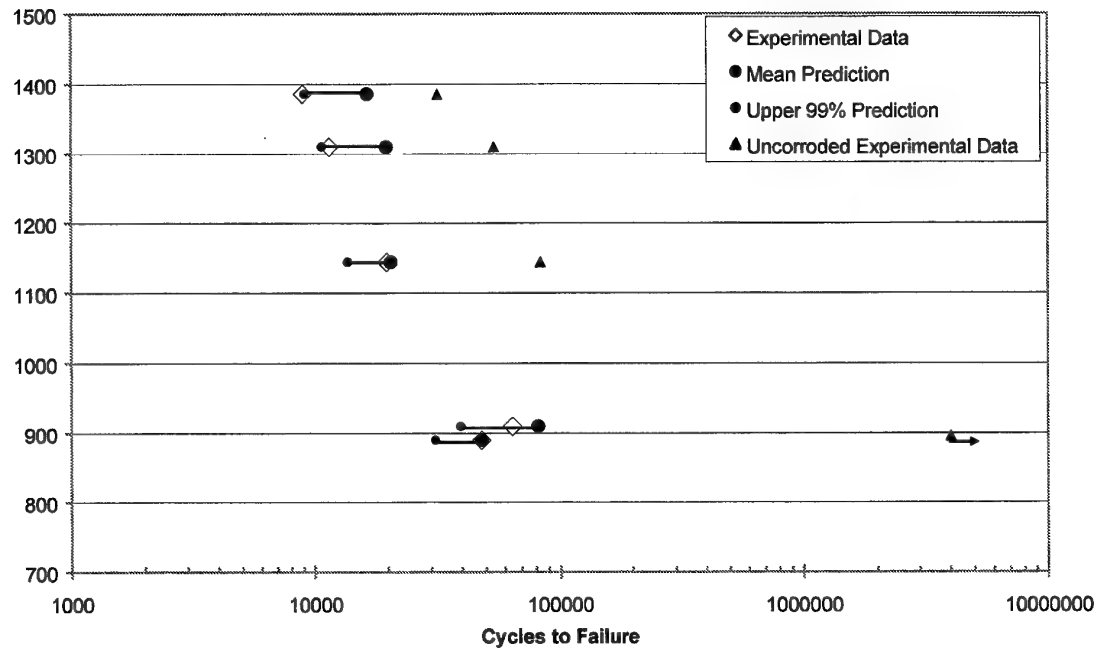
Figure 44. Graph showing fatigue life predictions and experimental results for FFVH13 constant amplitude experiments.

Table 35. Table of prediction accuracy for FFVH13 constant amplitude experiments.

Specimen Number	Max Stress at Kt (MPa)	Fatigue Life Experimental SFH	Life predict mean ECS	Life predict 99% CL ECS	% diff mean predict to actual life	% diff upp99 predict to actual life
FP82AD	896	4E+6 (runout)	-	-	-	-
FP85AG	1144	83 515	-	-	-	-
FP87AF	1310	54 180	-	-	-	-
FP78AK	1386	31 955	-	-	-	-
FP82AC	896	48 137	48 066	31 227	-0.2%	-35.1%
FP81AD	896	64 253	81 733	39 555	+27.2%	-38.3%
FP85AD	1144	19 784	20 547	13 682	+3.9%	-30.8%
FP85AF	1310	11 510	19 736	10 728	+71.5%	-6.8%
FP78AE	1386	8950	16 474	9094	+84.1%	*+1.6%*

5.6.2 Life predictions — spectrum loading

Before any life predictions could be conducted for the spectrum loading cases, the appropriate load interaction (crack retardation parameters) needed to be determined for the material. This has been done and is shown in Appendix C.

As with the constant amplitude life predictions, all the predictions for the spectrum loading experiments were based on the mean ECS curve and the upper 99.95% confidence limit curve from Figure 43.

The basic summary of ECS sizes and life predictions are given in Table 36. Likewise, these predictions are represented graphically in Figure 45.

The most descriptive way to look at the predictions, however, is to investigate the accuracy. As with the constant amplitude predictions, accuracy is described by the percent difference between the prediction and the actual life. The accuracy is summarised in Table 37, and the key points are discussed below.

As was indicated by the trend in the constant amplitude experiments, tests conducted at lower stress were better described by the predictions based on the mean ECS curve. On average, the mean predictions described the low stress tests within +11%. The +11% indicates that the mean ECS tended to over-predict the fatigue life in the low stress cases. The performance of the mean prediction in the high stress tests was +47%, which shows that the mean ECS over-predicted life by a much wider margin.

For the predictions based on the upper three sigma confidence interval, these ECS values tended to under-predict the fatigue life by a wide margin in the low stress cases. Performance under these conditions was -46%. For the high stress cases, the margin improved, where the predictions were within -24% of the mean.

There are two important things to notice. First, the mean ECS predictions were sometime greater than the actual life, and sometimes they were less than the actual life. The mean predictions are the least conservative from a fatigue perspective, but in many cases, they were still 'safe.' Second, the predictions based on the upper confidence limit were always conservative. In other words, no experimental fatigue lives were shorter than those predicted by the upper 99.95% confidence limit in the spectrum loading condition, either at the low stress or the high stress.

An increase in model fidelity could be (and should be) achieved by METLIFE in the high stress cases to account for any elastic-plastic effects.

Table 36. Table of ECS sizes and life predictions for spectrum FFVH13 coupons.

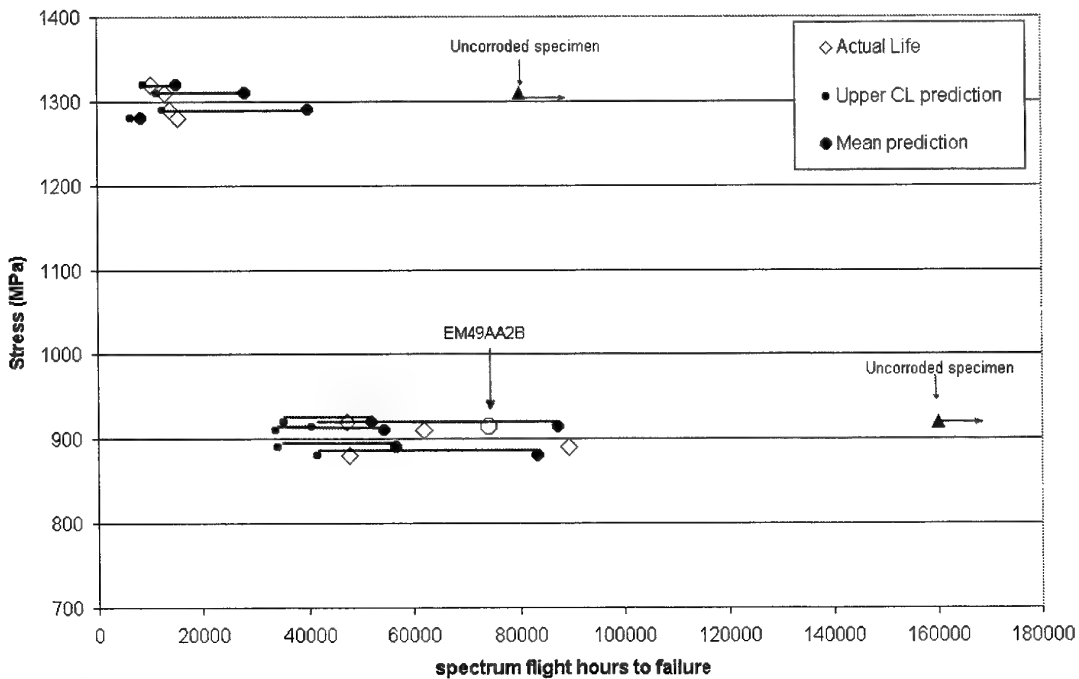| Specimen Number	Max Stress at Kt (MPa)	Pit Metric (Depth * Aspect Ratio)	ECS from mean	ECS from 99.95% CL	Fatigue Life (SFH)	Life predict mean ECS	Life predict 99.95% CL ECS
FP82AD	896	-	-	-	160 000	-	-
FP82AJ	1310	-	-	-	80 000	-	-
FP85AK	896	71	26.7	56.5	47 624	83 477	41 694
EM47AG1B	896	95	40	70	89 404	56 795	34 195
FP78AD	896	100	43.7	68.2	47 184	52 106	35 194
EM49AA1B	896	98	41.7	71.5	62 055	54 501	33 694
EM49AA2B	915	68	23.8	53.6	74 164	87 315	40 557
FP78AL	1310	36	12	42	13 805	40 083	12 489
FP81AB	1310	49	16.9	46.7	12 850	28 281	11 304
EM47AF2B	1310	86	33.4	63.1	10 195	15 255	8735
EM50AF2A	1310	124	70	100	15 367	8332	6291

Figure 45. Graph showing fatigue life predictions and experimental results for FFVH13 variable amplitude experiments.

Table 37. Table of prediction accuracy for the FFVH13 spectrum tests.

Specimen Number	Max Stress at Kt (MPa)	Fatigue Life (SFH)	Life predict mean ECS	Life predict 99% CL ECS	% diff mean predict to actual life	% diff upp99 predict to actual life
FP82AD*	896	160 000	-	-	-	-
FP82AJ	1310	80 000	-	-	-	-
FP85AK	896	47 624	83 477	41 694	+75.2%	-12.5%
EM47AG1B	896	89 404	56 795	34 195	-36.5%	-61.8%
FP78AD	896	47 184	52 106	35 194	+10.4%	-25.4%
EM49AA1B	896	62 055	54 501	33 694	-12.2%	-84.1%
EM49AA2B	915	74 164	87 315	40 557	+17.7%	-45.3%
FP78AL	1310	13 805	40 083	12 489	+65.6%	-9.5%
FP81AB	1310	12 850	28 281	11 304	+120.1%	-12.0%
EM47AF2B	1310	10 195	15 255	8735	+49.6%	-14.3%
EM50AF2A	1310	15 367	8332	6291	-45.8%	-59.1%

5.7 Life predictions — POD study specimens

The predictions for the FFVH13 specimens worked very well. Still, it was desirable to find other specimens where this technology could be applied. Another DSTO research project provided the necessary information.

A project by Hugo and Harding sought to develop a revised probability of detection (POD) threshold for the magnetic rubber non-destructive inspection method used for finding cracks in D6ac. This program provided a number of specimens that had been pitted and subject to an F-111 spectrum. A brief discussion of the experimental setup and a summary of ECS model performance are provided for these tests, which will be referred to as the POD specimens.

Three specimens were selected for model validation, including two specimens that were tested to failure (pilot specimens for spectrum tuning) and one specimen that was cycled just long enough to generate a small crack that would later be scrutinized by NDI technicians as part of the POD study.

5.7.1 Specimen description

The specimens used in the POD study were quite simple. Two types were used:

1) a plate with a hole.
2) a plate with a cutout meant to simulate a fuel venthole (similar to the FFVH 13 coupons).

The specimens selected for ECS application were of the first type: plate with a hole. The D6ac specimens were approximately 5.1 mm (0.2 inch) thick and 38.8 mm (1.53 inch) wide and contained a 9.5mm (3/8 inch) diameter hole.

5.7.2 Load spectrum

The load spectrum used in these experiments is described in detail in Appendix B.

This spectrum is essentially another filtered version of the DADTA2b sequence discussed in the previous section on the high-k_t specimens.

In addition to being heavily filtered to the point that it only had 18 742 turning points (vs. 52 403 in the previous iteration of the spectrum), the POD spectra was also clipped to take out all loads that were either negative or zero.

The peak load in the spectrum was 90 kN (19.8 kips), which translated to a peak remote stress of 446.8 MPa (64.8 ksi). At the high-k_t location of the hole, assuming a stress concentration of 3.18, this gave a max elastic stress in the specimen of 1420 MPa (206 ksi). As such, it is expected that the specimens saw some plasticity at the peak.

5.7.3 Pit characterisation

Three specimens were selected. Two of the specimens were completely fractured during fatigue testing, and the pits were easily characterised using the optical microscope. The third specimen was not cycled to failure, so the specimen was broken open to not only measure the pit morphology, but to record the final crack size and shape, too. Table 38 shows the details recorded for the three specimens. The pits were introduced to the specimens using the same protocol developed by Holden (1999) and later optimised by Mills and Loader (2000).

Table 38. Pit characterisation for POD specimens.

Specimen ID	Pit Depth (microns)	Pit Width (microns)	Pit Metric (Depth *Aspect Ratio) (microns)
POD 43B	19	31	23.5
POD 14	50	112	44.6
MRIPOD 33	27	72	19.4

5.7.4 Life prediction

Life predictions for the POD specimens, particularly POD43B and MRIPOD33 had the potential to be a severe test of the model, since the pit metrics were very small. This in

turn translated into smaller ECS values and a wide range in ECS between the mean and the upper 99.95% confidence limit. In particular, the span in ECS values crossed an area where the predictions were very sensitive. As was discussed in this report in Section 4 (and also discussed by Mills et al. [2001]), the crack growth model used is very sensitive at low ΔK, so when ECS values are low, small changes in those values can have a wide impact on predicted life. This is obvious in these cases, even with such a high stress. Of course, these were variable amplitude tests, and the highest stress only occurred once per 500 hours. Table 39 shows the ECS values and associated predicted lives for the three specimens. The table is preceded by a summary of the AFGROW input parameters. The spectrum file used is shown in Appendix B.

The key parameters for the material model are:

Segment 1 ($\Delta K \leq 13$ ksi $\sqrt{in}$):

- $C = 7.71E-09$
- $m = 3.655$

Segment 2 (13 ksi $\sqrt{in} < \Delta K \leq K_c$):

- $C = 1.46E-07$
- $m = 2.497$

Both segments:

- $K_c = 110$ ksi $\sqrt{in}$
- $\Delta K_{th} = 2$ ksi $\sqrt{in}$
- $K_{Ic} = 67.5$ ksi $\sqrt{in}$
- $E = 210$ GPa (30 000 ksi)
- $\sigma_{ys} = 1310$ MPa (190 ksi)

Other parameters important to the modelling are:

Crack and component geometry:
- single surface crack at hole
- $W = 1.53$ inch (38.8mm)
- $t = 0.2$ inch (5.1mm)
- hole diameter = 0.375 inch (9.5 mm)
- crack aspect ratio (a/c) not kept constant
- tension load ratio = 1 (bending and bearing = 0)

Stress state:

- determine stress state automatically

Spectrum:

- SMF = 64.877
- residual stress/strength requirement was used. Specimen always required to carry peak spectrum stress.

Retardation model:

- closure model
- opening load ratio (@ R = 0) = 0.235
- determine initial opening load ratio from first load in spectrum

Beta corrections:

- none were used

Residual stresses:

- not used

Run time:

- POD 43B and 14 were run until failure
- MRIPOD 33 was run until reaching a crack depth of 97 microns (0.004 inch)

These predictions used AFGROW version 4.00004.12.10 released on 1 June 2001.

The results of the predictions are shown in Table 39. Notice how long the life predictions are for the small ECS values associated with the mean ECS. Unfortunately, the pit sizes (in general) were below the size studied and considered important in the early phases of this program. Earlier studies did not consider pits below 30 microns in depth. As can be seen in Table 38, these pits were quite small and gave quite long lives even at the high stress.

Table 39. Table of ECS sizes and life predictions for spectrum POD coupons. *MRIPOD33 was cycled to failure. This fatigue life represents time to a crack that was 157 microns long by 97 microns deep. Life predictions are for a crack to 97 microns deep.

Specimen Number	Max Stress at Kt (MPa)	Pit Metric (Depth * Aspect Ratio)	ECS from mean	ECS from 99.95% CL	Fatigue Life (SFH)	Life predict mean ECS	Life predict 99.95% CL ECS
POD 43B	1420	23.5	10.2	40	67 000	119 695	28 950
POD 14	1420	44.6	15.5	45	23 500	73 350	26 401
MRIPOD 33	1420	19.4	9.6	36	47 000*	116 703	16 838

Table 40 shows the prediction accuracy for the POD tests. As was stated earlier, the small pit sizes led to small ECS values, which stretched the model. It would be easy to argue that the prediction window was so wide, how could we miss? This explains why these small pit sizes were avoided in the research program, but the POD specimens were simply as provided. They were pitted independently and thus provided an excellent opportunity to apply the model in unknown, uncontrolled conditions.

As can be seen in the table, the mean ECS tended to over-predict the life by an exceedingly wide margin. This was known to be the case from the earlier high stress tests using the FFVH13 coupons. If history held true, then we would expect the upper 99.95% confidence interval to do a better job predicting the life. This is in fact the case, although the predictions in the cases with small ECS values (POD 43B and MRIPOD 33) still give the actual life a wide berth. And in the case where the ECS values were in line with those studied throughout the program, the prediction was very close to the actual but slightly unconservative by about 12%. However, considering how damage tolerance is typically applied, this is not viewed as a big problem. This will be discussed in the concluding section of this chapter.

Table 40. Table of prediction accuracy for the POD spectrum tests.

Specimen Number	Max Stress at Kt (MPa)	Fatigue Life (SFH)	Life predict mean ECS	Life predict 99.95% CL ECS	% diff mean predict to actual life	% diff upp99 predict to actual life
POD 43B	1420	67 000	119 695	28 950	+78.6%	-56.8%
POD 14	1420	23 500	73 350	26 401	+212%	**+12.3%**
MRIPOD 33	1420	47 000*	116 703	16 838	+148%	-64.1%

5.8 DI36/CPLT coupons

When this research program was originally planned, the final demonstration of the ECS tool at the coupon level was to involve high-k_t coupons subjected to a largely compressive spectrum that reached plastic levels under the addition of the cold proof load test sequence.

The purpose was to see just how broadly the ECS concept could be applied. Early demonstrations showed that it worked well under elastic constant amplitude and spectrum conditions. However, some areas of the F-111 structure undergo plastic tension and compression loads. The plastic compression stresses present an interesting problem because, as shown by Cox (1985), these stresses result in a residual tension that can aid in crack propagation in a normally compressive stress field. The only crack growth code to date that can handle this scenario is METLIFE. These final experiments were designed to see if the ECS would work with METLIFE in elastic-plastic conditions.

The unavailability of METLIFE at the time the testing was completed, however, required that this report be finished without the addition of this analysis. However, the basics of the testing are given in this report so that the information can be placed into METLIFE in the future.

The load spectrum used in the testing was a DADTA 2b DI36 spectrum that repeated in 500 blocks. The CPLT sequence was repeated every four blocks, or 2000 hours. The spectrum is shown in Appendix B. The rest of the details of the testing are shown in Appendix D.

5.9 Conclusions from high-k_t program

The purpose of the high-k_t test program was to validate the ECS distribution derived from the low-k_t experimental program. The key points of the high-k_t program are as follows:

- A total of eight constant amplitude tests were conducted at four stress levels using FFVH13 coupons.

- The constant amplitude tests were designed to illustrate the knockdown in life associated with corrosion pitting.

- Four of the constant amplitude specimens had corrosion pits of various sizes.

- The fatigue lives of the high-k_t coupons were in line with those from the low-k_t program at similar stress levels. The relative severity of the corrosion pits seemed to influence the fatigue live predictably.

- The ECS values coupled with the AFGROW model did a reasonable job predicting the fatigue lives of the high-k_t constant amplitude specimens. In most every case, the mean ECS over-predicted the experimental fatigue life, and the upper 99.95% confidence limit ECS under-predicted the experimental fatigue life.

- In only one case was there an unconservative result, where the fatigue life was shorter than that predicted by the most conservative 99.95% confidence limit ECS. This case involved a specimen with high plasticity, and since the analysis was done using an linear elastic fracture mechanics code, the results should, in any case, be questioned. The result was unconservative by 1.6%.

- Eleven FFVH13 coupons were used to validate the ECS distribution under variable amplitude conditions.

- Two of the coupons did not contain pits and experienced runout.

- Nine of the coupons contained pits of varying sizes, and they were tested at two peak stress levels.

- Again the ECS values derived from the low-k_t program did a good job predicting the fatigue life for this more demanding series of experiments.

- As with the constant amplitude experiments, the mean ECS tended to over-predict the experimental fatigue life, although in some cases it under-predicted — a very conservative result.

- As with the constant amplitude experiments, the upper 99.95% confidence limit ECS tended to under-predict the experimental fatigue life. At the high stress levels, where the validity of AFGROW could be questioned, the experimental life was quite close to the predictions by the upper limit.

- Three specimens were selected from a probability of detection study by Hugo and Harding at DSTO/AMRL to check the validity of the ECS distribution in predicting the lives of material corroded outside our control. This trial showed that the model was heavily challenged by small corrosion sizes, since there is such a wide spread in the life predictions between the mean and upper 99.95% confidence limit ECS values.

- The sizes of corrosion damage in the specimens investigated in the POD specimens were much smaller than those used in the rest of this research project. In the one case where the corrosion was of the same magnitude, both the mean ECS (not surprisingly) and the upper 99.95% confidence limit ECS (surprisingly) over-predicted the experimental fatigue life.

- The upper 99.95% confidence limit ECS over-predicted the experimental fatigue life of the one POD coupon by +12.3%.

- This coupon was tested at a very high stress level, and in keeping with other observations where the model was unconservative, the validity of LEFM analysis in these cases is flagged as a probably source of error.

From these facts, the following three important observations can be made:

First, many of the tests were deliberately stressed to levels at or exceeding monotonic yield. This was because many of the problem areas in the F-111 structure are stressed beyond either compressive or tensile yield, particularly in the Cold Proof Load Test. As such, it was deemed important that the ECS distribution developed in this program be validated both in elastic stress cases as well as elastic−plastic cases. Unfortunately, the METLIFE computer code, which handles plasticity and stress/strain accumulation, was not ready at the time of these analyses, so the best thing available (the LEFM code, AFGROW) was used for all analyses. Still, the elastic-plastic cases need to be re-evaluated using METLIFE when that code is functioning fully to determine the validity of the ECS for those cases. For now, we can only say that it is fully conservative in elastic cases.

Second, because of limited specimen availability, we did not have much data at larger pit sizes. As shown in Appendix D, the largest of the corrosion damage generated in the laboratory matches well with that found in service. However, not many tests were done at these larger pit metric sizes. Therefore, we recommend expanding the original low-k_t tests to shore up the original ECS distribution and then apply revised prediction distributions to some more high-k_t coupons with similar large corrosion damage.

Third, further conservatism than that allowed by the upper 99.95% confidence limit would come from proper application of the ECS engineering tool. This tool should be viewed as giving the best estimate of the life of the structure when corrosion damage is detected. However, to keep with the traditional application of damage tolerance analysis, an inspection interval of at least half that would be applied in a fleet scenario. So, while the upper bound ECS produces some predictions that are very close indeed to the actual life, safety is gained by halving that life for an inspection interval.

6. ECS Sample Application

The previous chapters explain in detail how the Equivalent Crack Size distribution for corrosion pitting in D6ac steel was developed, and to a limited extent, its application was shown through the validation processes in Section 5. However, the best word to describe Section 5 is still validation, not application, as there was a fundamental difference between how the life predictions were made for the validation as compared to how they would be made in service. This difference is probably quite obvious, but it is spelled out here, nonetheless.

During the validation process, it was necessary to be meticulous with pit measurement to see if the ECS really applied under these new conditions of high-k_t and spectrum loading. The results were definitely favourable, but the path taken was not realistic from a maintenance point of view. In the laboratory, we had the luxury of knowing exactly which pit or pits caused the primary fatigue crack. Undeniable proof was permanently recorded on the two fractured pieces of metal pulled from the test machine. However, waiting until a crack is detected in an F-111 wing carry through box in order to say, "yes, we could have predicted that," is hardly useful.

For this approach to be of any maintenance benefit, this model needs to be applied to any pit detected in any D6ac structure long before cracks form. This hinges on several things:

- a reliable non-destructive method of determining pit size is needed.

- a solid knowledge of the stress distribution or at least the peak stress in the component is necessary.

- a solid knowledge of the stress spectrum experienced by a problem location is necessary.

To be absolutely thorough, one would have to comb over every pit, measure its size, determine the stress at the location of the pit, and conduct crack growth modelling using the stress spectrum for that location. This has been done in this section, although admittedly, there is one important difference. Here we were unable to apply a reliable non-destructive method for determining pit size since it was beyond the scope of this project. In this study, the pit metrics were determined using an optical microscope. Unfortunately, this is not a practical NDI technique when pits are found in a wing.

It is imperative that reliable NDI capable of measuring pits in D6ac be developed for this technique to applied liberally and effectively in the field or depot. Some techniques have been tried both at DSTO/AMRL and at NDTSL at RAAF Amberley, and success seems to be closely tied to the experience of those performing the work. Appendix G contains a discussion on such techniques.

In the following example of technology application, a number of steps are carefully illustrated in much more detail than would actually be needed to use this tool for maintenance decisions. The steps to be covered are:

- Determining pit locations in the component

- Determining location of the pits in relation to the stress distribution

- Determining the pit metrics for the pits (greater than 30 microns deep)

- Determining the ECS for each pit

- Conducting life predictions for each ECS at the appropriate stress

6.1 Low stress case

A number of figures are shown to help describe the pitting locations and corroded area of specimen FP78AD, which was selected for this demonstration.

Coupon number FP78AD was one of the specimens tested at the low stress of 896 MPa. It survived 47 184 hours of spectrum loading. It contained corrosion pits in one of the critical stress regions of the specimen, as indicated in Figure 46.

Similarly, specimen FP81AB, tested at 1310 MPa, was selected for another demonstration, although it was given only a cursory examination to show how quickly an life estimate could be arrived at if some basic (conservative) assumptions were made during analysis.

Specimen FP81AB is dealt with in Section 6.2, but the next several pages of detail are devoted to FP78AD.

The corroded surface of FP78AD is shown in Figure 47. Notice how a large number of pits are present above the fracture plane (bottom of the image). More pits were present on the portion of the specimen not shown (other half of the fracture), but they were few in number. A set of axes are shown on Figure 47 which are used in reference to all the subsequent graphs that show pit depths, pit metrics, ECS values, and fatigue lives.

Figures 48 and 49 are simply SEM micrographs of the pits intersecting the fatigue fracture surface in specimen FP78AD.
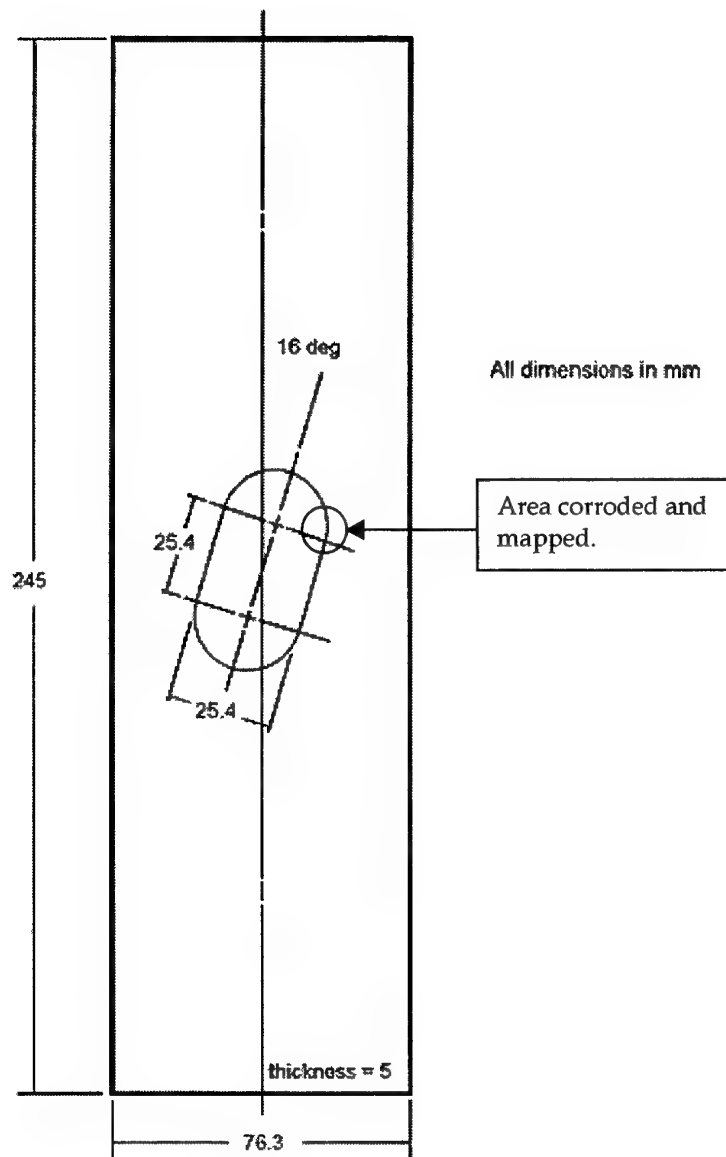
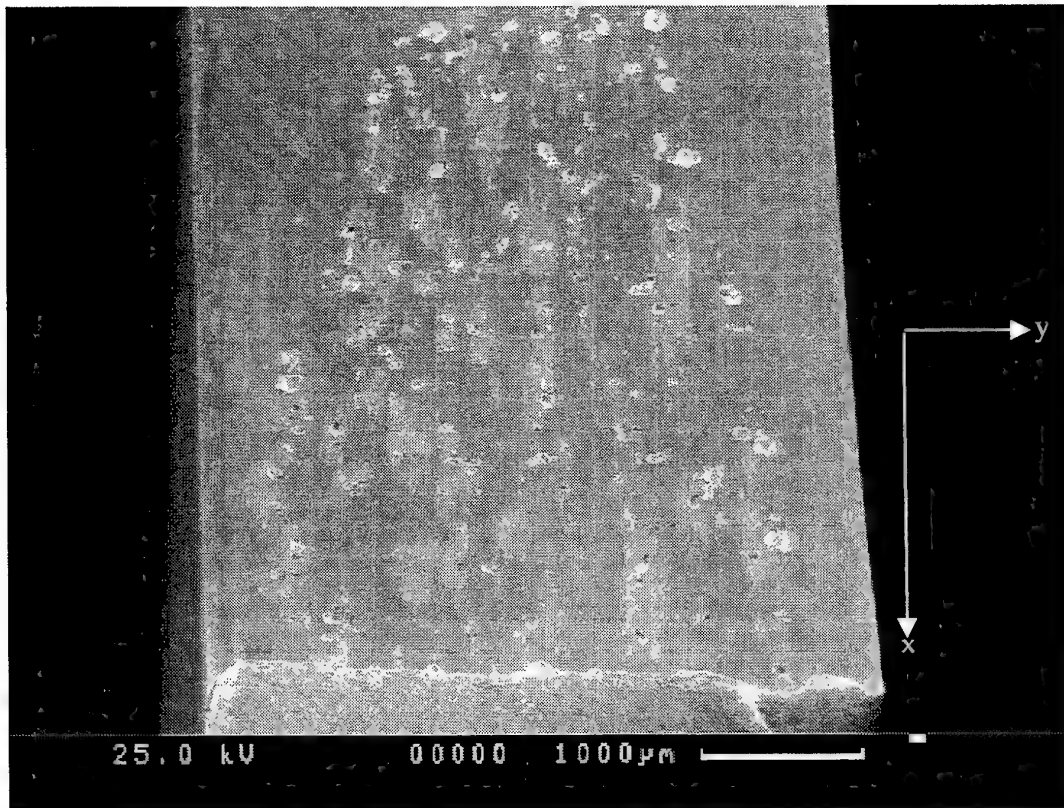Figure 46. Area corroded and mapped in FP78AD.

Figure 47. Pitting corrosion on radius of oval hole coupon. Fracture plane was in high stress location.
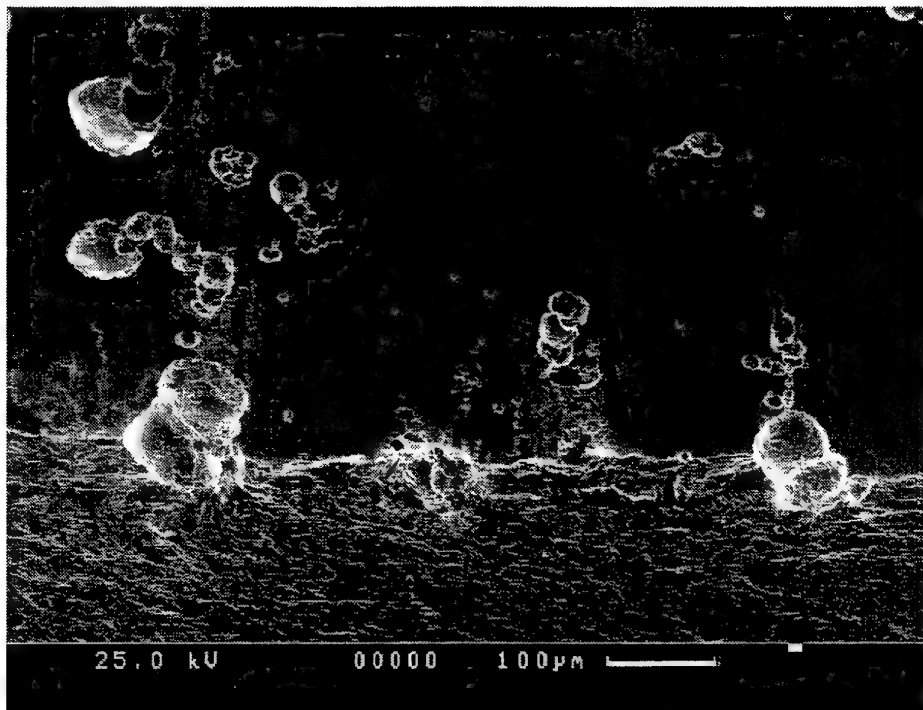
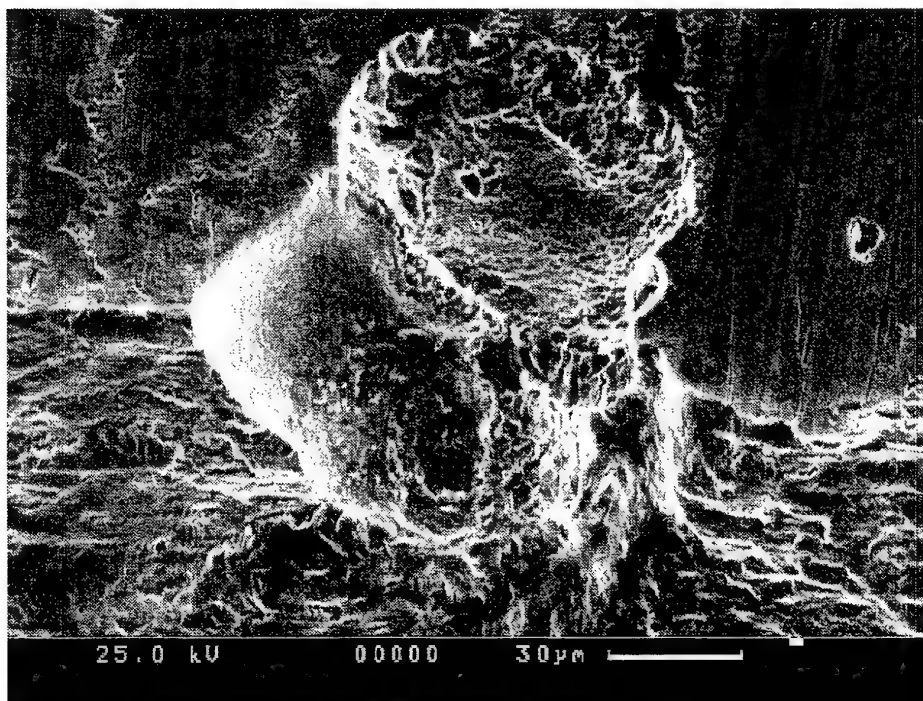*Figure 48. Collection of pits on specimen radius intersecting with fatigue fracture surface.*

Figure 49. Higher magnification view of pit/fatigue interaction.

6.1.1 Pit and stress distribution in hi-k$_t$ specimen FP78AD

The first step in demonstrating the ECS tool involved determining pit metrics for each pit in the specimen. Previous experience in the low-k$_t$ program showed that only pits over 30 microns in depth were a serious threat to this material at the stresses investigated. This allowed the search to be focused only on those pits greater than 30 microns deep in specimen FP78AD.

In this specimen, 57 pits met this criteria. This is a large number of pits, and it required a long time to sort through all this information. If it is any consolation, the review of fleet corrosion damage in the F-111 by Mills (summarised in Appendix E) seldom revealed more than a handful of pits in any one location. This occurred because of the differences in mechanisms driving pit formation in the laboratory *vs.* the field. Namely, in the laboratory pitting in the bare D6ac was driven electrochemically, and the pits formed at microstructurally favourable locations. In the field, pitting usually occurs at areas of local breakdown in the protective cadmium plating. In general, this seems to lead to fewer pits.

Focusing on the 57 pits found in this example specimen, Figure 50 is a map of not only the corrosion pit locations, but it is colour and size coded to indicate what is essentially a histogram of the pit depth at each location. All subsequent figures will use similar convention, and all the figures contain other information, as listed here:

- The primary x axis represents the specimen front face.

- The plane of maximum stress of this specimen travels in the y direction and intersects the x axis at zero. It is represented by a dotted line.

- The primary x and y axes provide coordinate positions relative to the plane of maximum stress (x) and front face of the specimen (y).

- The back face of the specimen is represented by the dotted line at y = 3.8mm.

- The secondary y axis represents the normalised stress. The peak of one is at x = 0. The solid line represents the general shape and magnitude of the stress distribution ranging from 6 mm above the peak location (-x) and 2 mm below (+x), which captures the range where pits were present on the face of the cutout.

In Figure 50, notice that two of the three deepest pits (red circles) are far removed from the location of maximum stress.

Most of the pits near the plane of maximum stress were relatively shallow relative to the target pit depth of 90 microns. However, one of the pits reached 68 microns, as

indicated by the yellow circle on the dotted line. This pit was one of seven in the second-deepest histogram category.

An interesting thing to note is that while the plane of maximum stress tended to have shallower pits (especially when you consider that deeper pits were nearby in very high stress zones), it also had the most pits along any one line. This plane intersected five pits and came very close to a sixth. This illustrates an aspect of the model that is not addressed anywhere. All the life predictions were made based on one crack from one pit. The model does not consider multiple pits generating multiple cracks. This will be discussed more in concluding sections of this report.

6.1.2 Pit metric distribution for FP78AD

In the previous step, the pits were 'screened' and mapped to determine the locations of those over 30 microns deep. In this step, the pits were described in the terms of the 'metric' that has been used throughout the ECS development in this report, namely: depth * aspect ratio. This has been coined 'pit metric,' and Figure 51 shows the map of the pit locations. Each data point is colour coded in histogram fashion to show the relative magnitudes of the pit metrics.

The most interesting thing to note is that five pits made it into the most severe category (100-130 microns) in the pit metric plot, but only two of these pits were in the most severe category according to depth (see Figure 51). It is also important to note that one of the pits with the most severe pit metric is on the maximum stress plane. The other pits in the most severe category were far removed from the zone of maximum stress and were not a factor.

6.1.3 ECS distribution from 99.95% confidence interval

Between Figure 50 (pit depth map), and Figure 51 (pit metric map), many changes are obvious, because the deepest pits do not necessarily generate the largest metrics. However, once the pit metrics are generated, it follows that the pit with the largest metric will also have the largest ECS. Figure 52 is the ECS map for FP78AD as determined from the 99.95% confidence interval of the ECS *vs.* pit metric relationship shown in Sections 4.5.2.2 and 5.6.

The values at which the histograms are divided influence the appearance of the plots, but notice how the five largest ECS values correspond with the five largest pit metrics from Figures 51. The two largest ECS values were away from the highest stress.
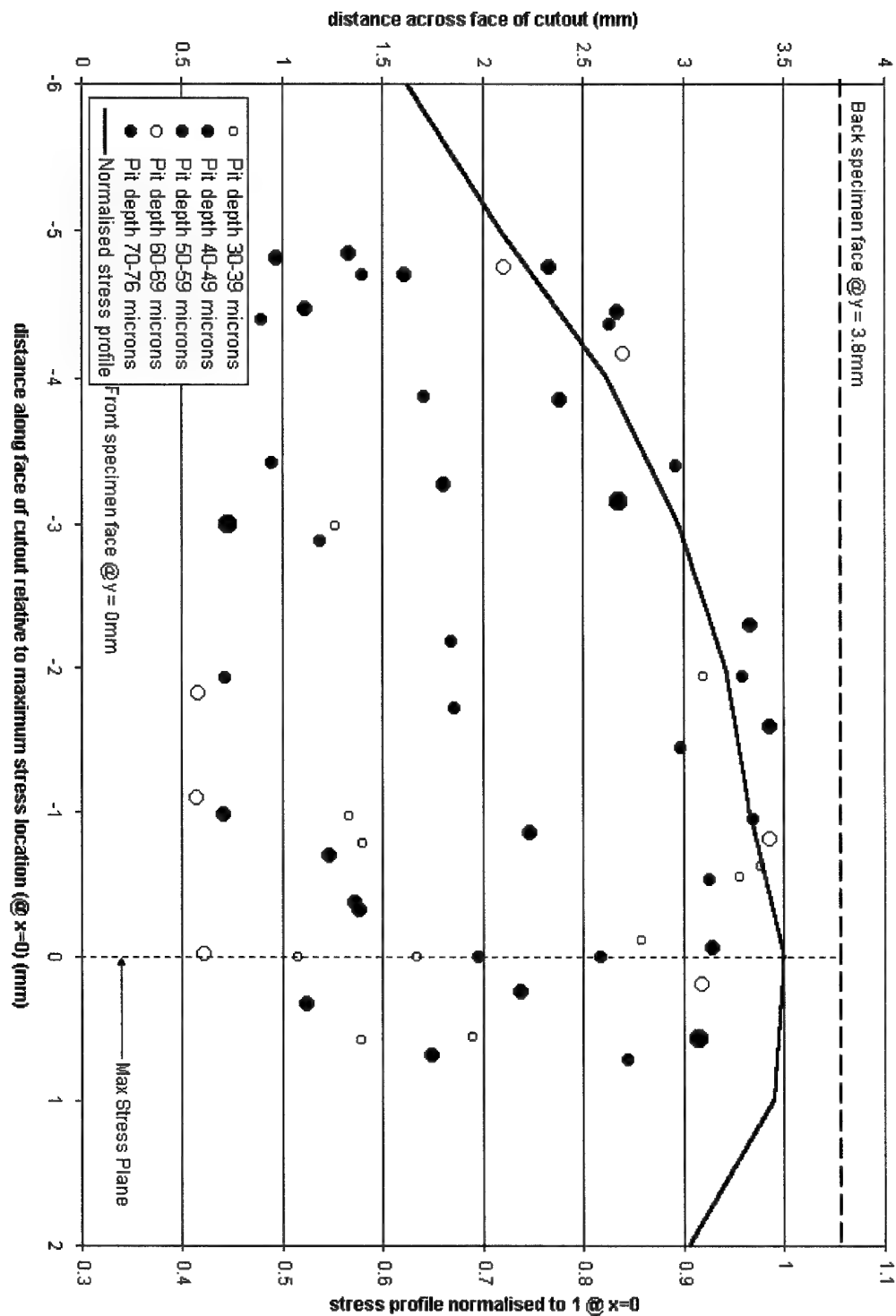
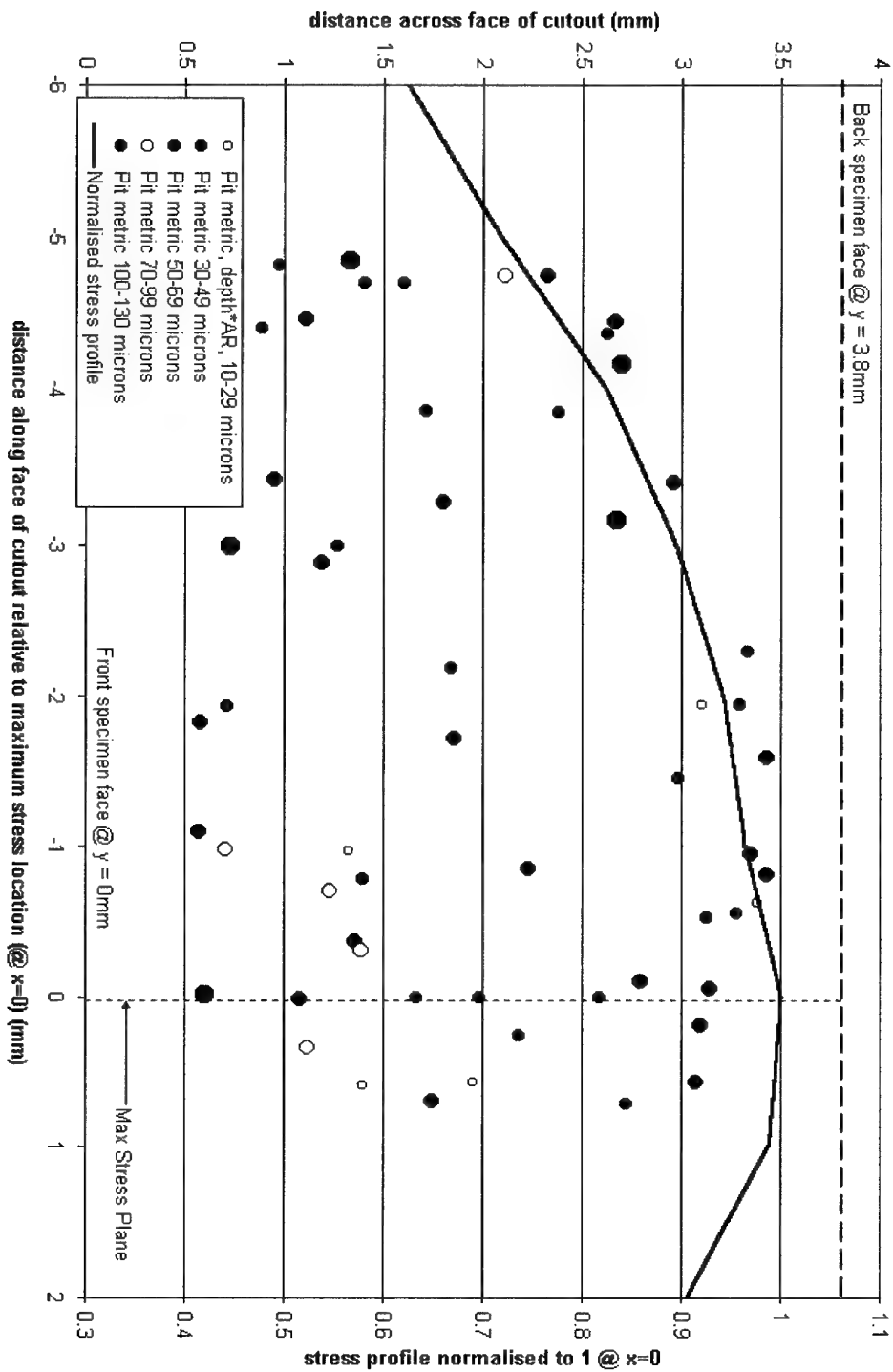*Figure 50. Pit locations and sizes in specimen FP78AD.*

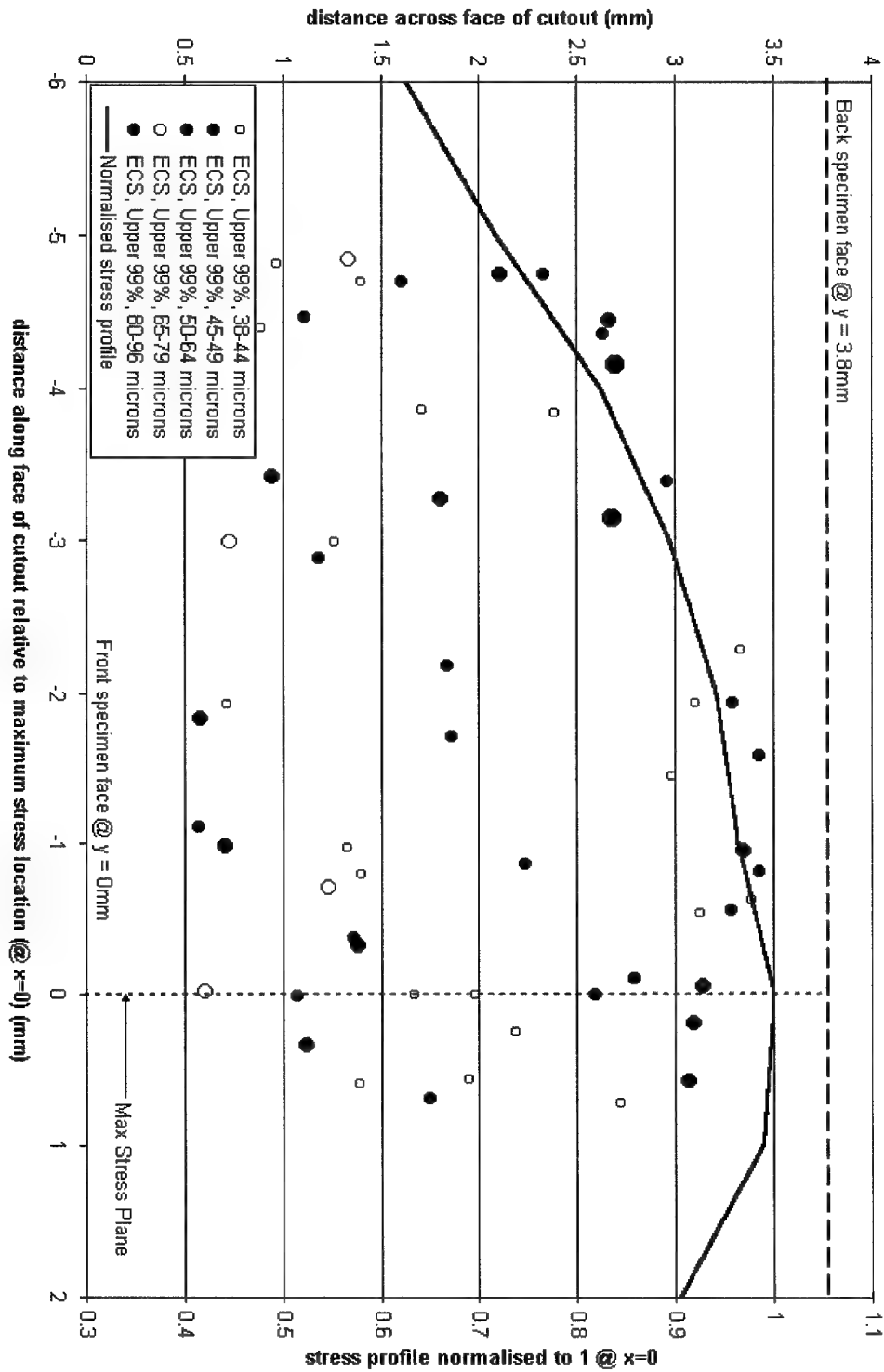*Figure 51. Pit metric distribution in specimen FP78AD.*

Figure 52. ECS sizes by pit location on FP78AD (based on upper 99.95% confidence band).

6.1.4 ECS distribution from mean curve

Figure 53 shows the ECS distribution for FP78AD from the mean curve. In this case, the largest ECS values were for pits well away from the plane of maximum stress. But still, a moderately large ECS was near this region, and its presence in the location of highest stress dictated that it was the most critical life limiter.

In general, the ECS values for the mean curve were much smaller, ranging from 8-76 microns for all pits measured. For the upper 99.95% confidence limit curve, the ECS values ranged from 38-96 microns. For the mean curves, only nine of the pits had ECS values larger than 30 microns.

6.1.5 Predicted lives based on upper 99.95% confidence interval

The final step in the life prediction process is to input the ECS values into AFGROW as starter cracks and apply the load spectrum at the appropriate level of stress (recall that the pits in this example are scattered across an 8mm x 3mm area that has a steep stress gradient).

The first batch of predictions is based on the upper 99.95% confidence interval of the ECS distribution. These are the largest ECS values and thus give the most conservative results. In reality, two different approaches could be applied here.

1. Each pit could be evaluated at its exact stress, and then the 57 crack growth predictions could be perused to see which resulted in the lowest life.

2. To add even more conservatism, the largest ECS in the entire specimen could be evaluated as if it were in the zone of maximum stress. Doing this requires only one crack growth prediction for the entire specimen. This second approach is discussed in Section 6.1.7.

In Figures 54 and 55, we see the results of the first approach. Fifty-seven crack growth models have been run, and they results are presented as crack growth curves (Figure 54) and a colour-coded histogram map (Figure 55). Four pits resulted in short life predictions. These four are shown in red in Figure 55; one of these pits was the largest pit that intersected the actual fracture. The ECS combined with the high stress at this location resulted in a predicted life of approximately 31 000 hours. The specimen failed at 47 184 hours. The level of conservatism afforded by using the upper 99.95% ECS curve is a 34% under-prediction of fatigue life.

Also shown on Figure 55 is the location of other cracks in the sample. Several pits near the zone of maximum stress cracked to some degree, varying from 18 microns in length to 1 mm.
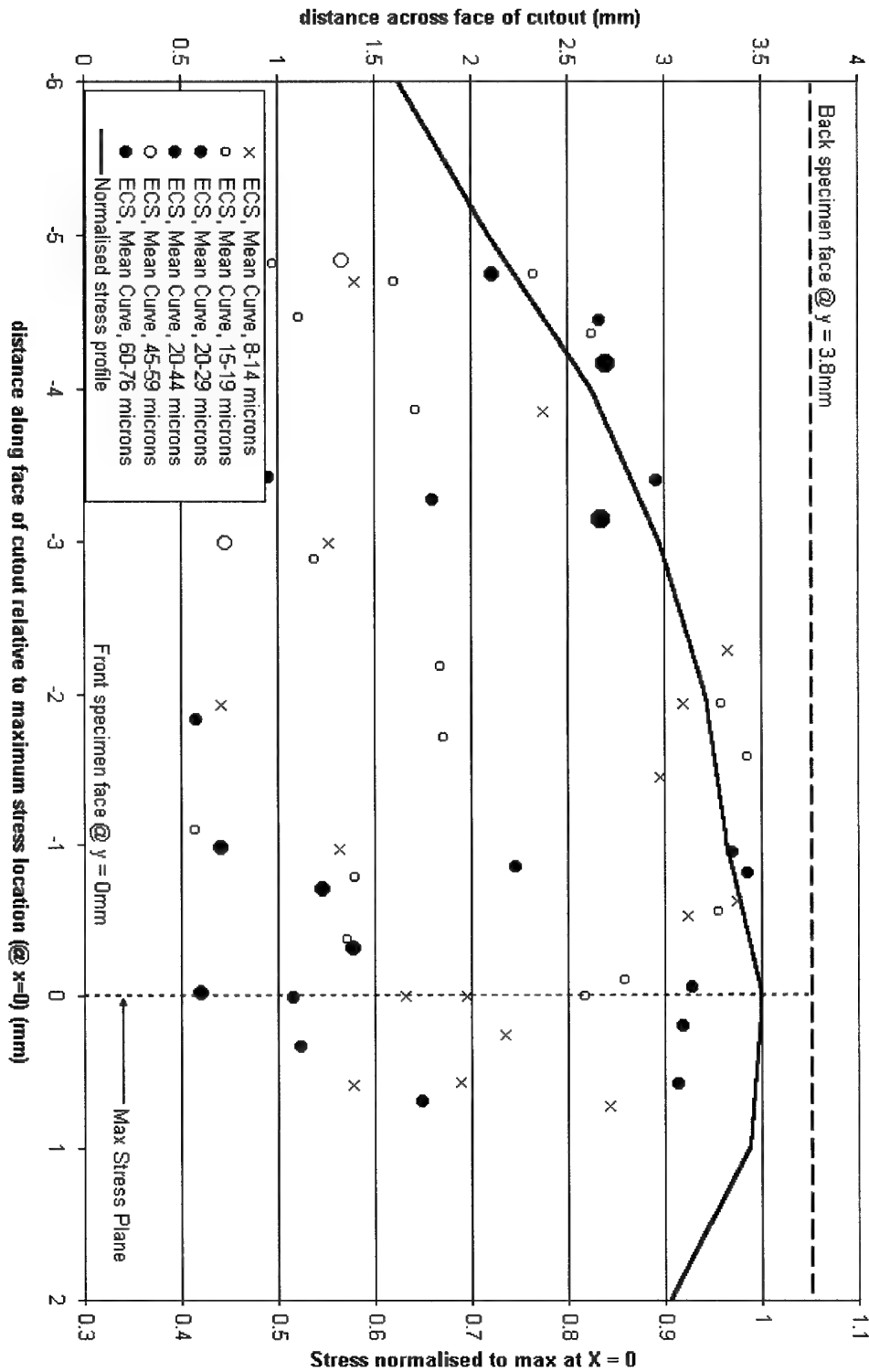
Figure 53. ECS sizes by pit location on FP78AD (based on mean curve).
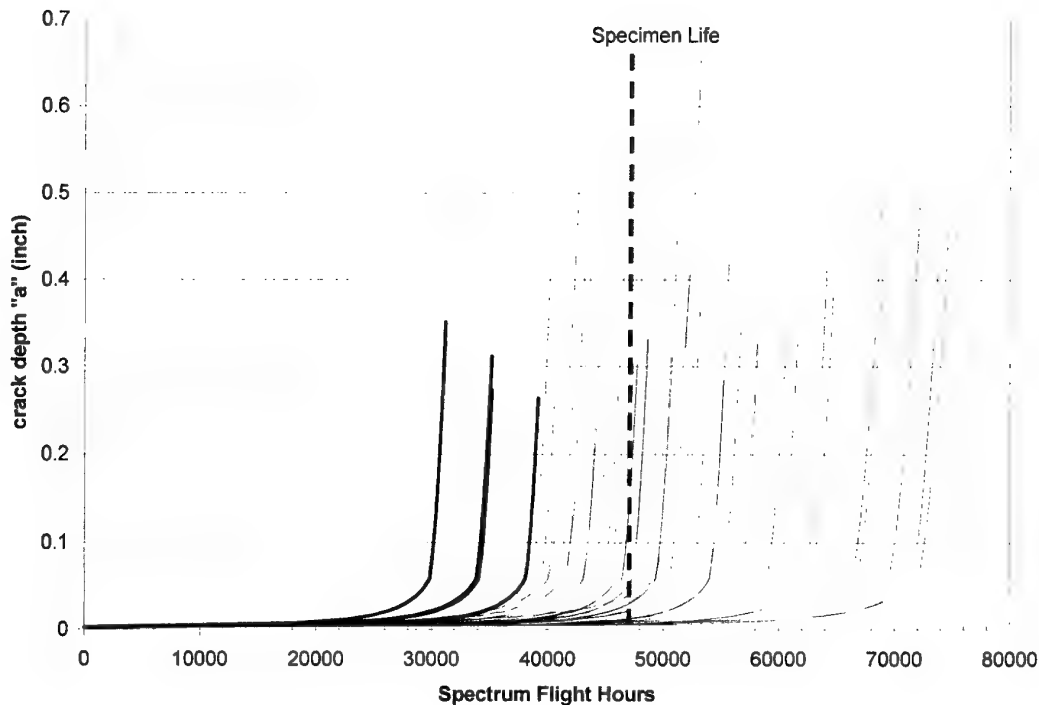
Figure 54. Crack growth predictions for every pit in FP78AD based on the ECS values from the upper 99.95% confidence limit. Life predictions greater than 80 000 hours not shown.

6.1.6 Predicted lives based on mean curve

In Figures 56 and 57, we see the techniques used for the upper 99.95% curve applied to the mean curve. Only models for which life was less than 80 000 flight hours have been shown as crack growth curves in Figure 56. Only six pits gave this result. Figure 57 is and a colour-coded histogram map showing the relative life predictions for all the pits. Here, all the pits whose lives were over 80 000 hours are marked with 'x.' The ECS combined of the largest pit on the fracture plane, coupled with the high stress at this location, resulted in a predicted life of approximately 47 194 hours. The specimen failed at 47 184 hours — a very close prediction indeed.

6.1.7 Final result for low stress case

Figure 58 shows the result of taking the 'short cut' of applying the highest stress in the specimen to the largest ECS in the specimen. Recall in this case that the largest ECS of any of the pits was in a location that was only seeing 80% of the maximum stress. However, if the largest ECS is analysed at the highest stress, then one can clearly see the extra conservatism.
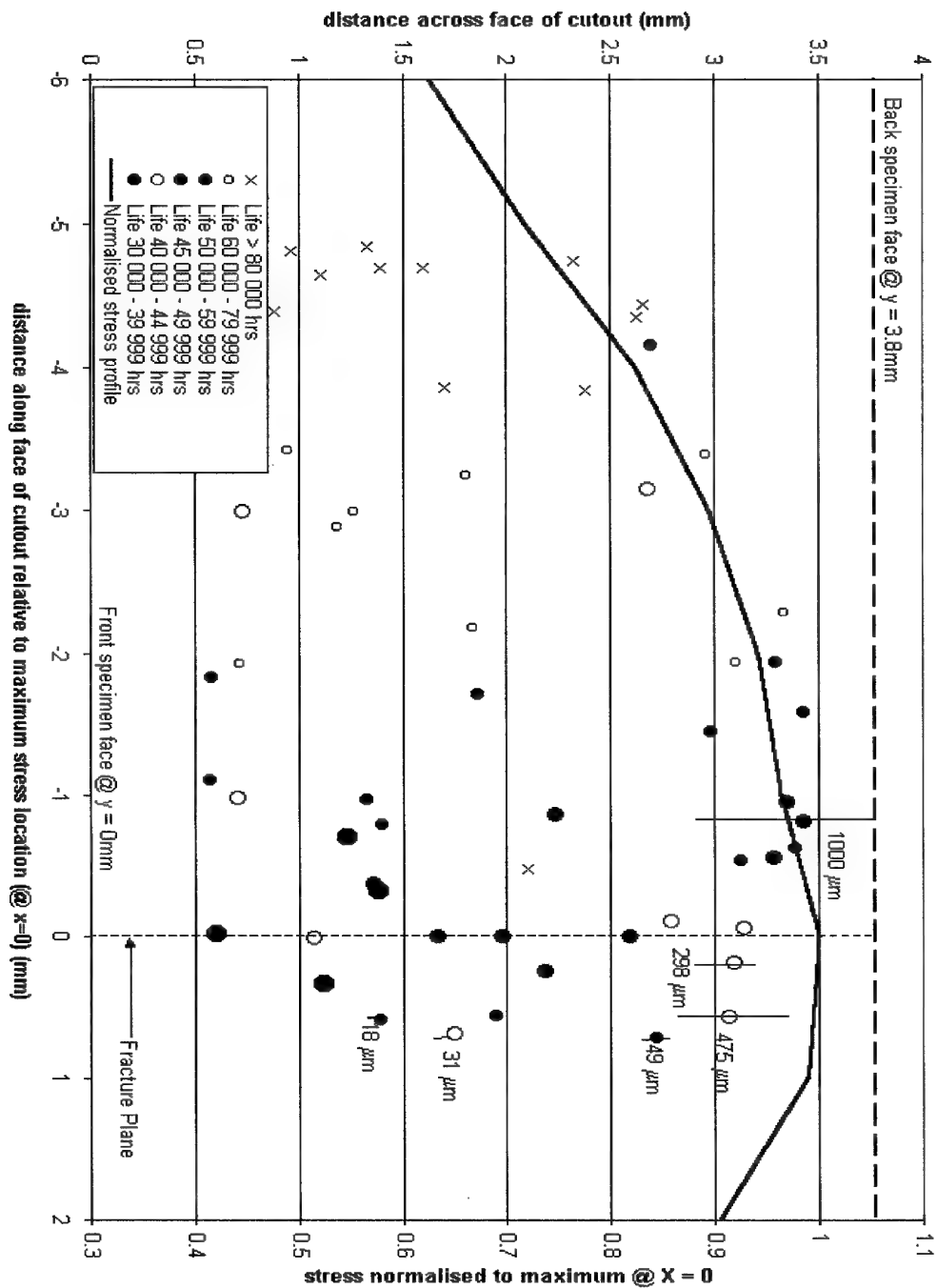
Figure 55. Distribution of predicted lives based on pit location (upper 99.95% confidence band).
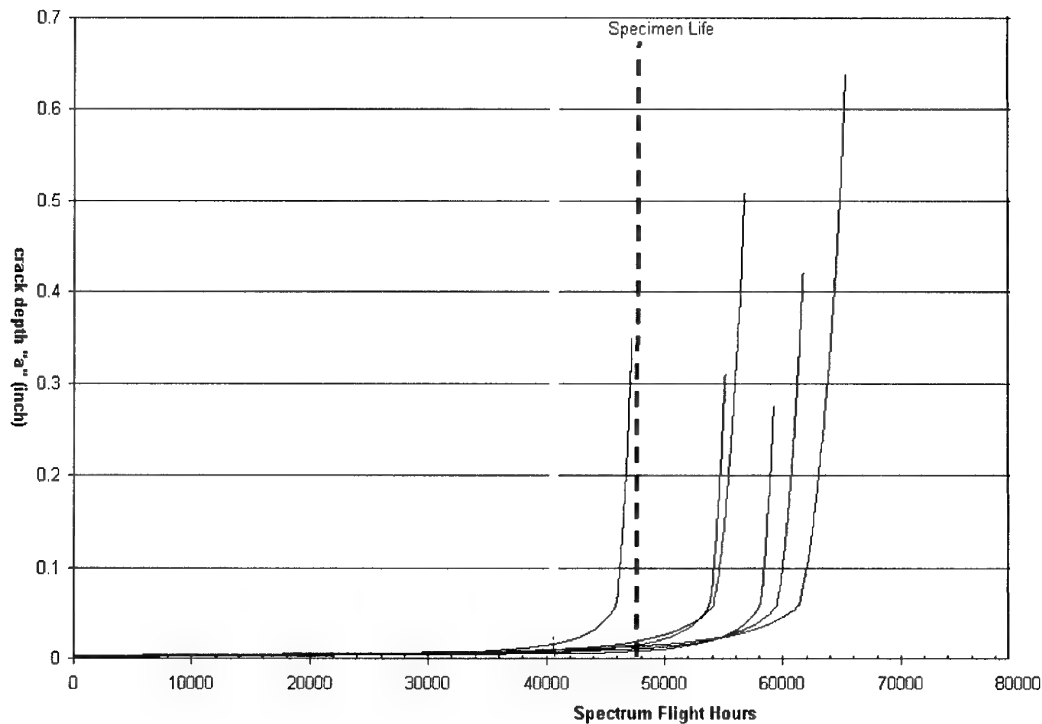
Figure 56. Crack growth curves for the handful of pits that generated a remaining life less than 80 000 spectrum flight hours. Predictions based on mean ECS curve.

In Figure 58, both the maximum ECS from the 99.95% upper bound and the mean were used to calculate fatigue lives based on the maximum spectrum stress of 130 ksi. Plotted for comparison are the predictions of the 'best guess' — the actual pits that caused fracture at the maximum stress location. For the mean curve, the 'best guess' prediction was 47 194 hours, and the prediction based on the biggest ECS analysed at the peak stress was 28 000 hours. In this case, treating the largest ECS as if it were in the worst possible stress location reduced the predicted life by almost 20 000 hours. This new result under-predicts the actual life by almost 41%.

For the upper 99.95% confidence limit, the 'best guess' prediction was around 31 000 hours. Now, with the largest ECS reanalysed in the zone of maximum stress, the prediction falls to around 22 000 hours. This new result under-predicts the actual life by over 53%.

Appendix F is a compilation of all the data collected on the 57 pits in this specimen, and it is also a summary of the modelling results for each pit.
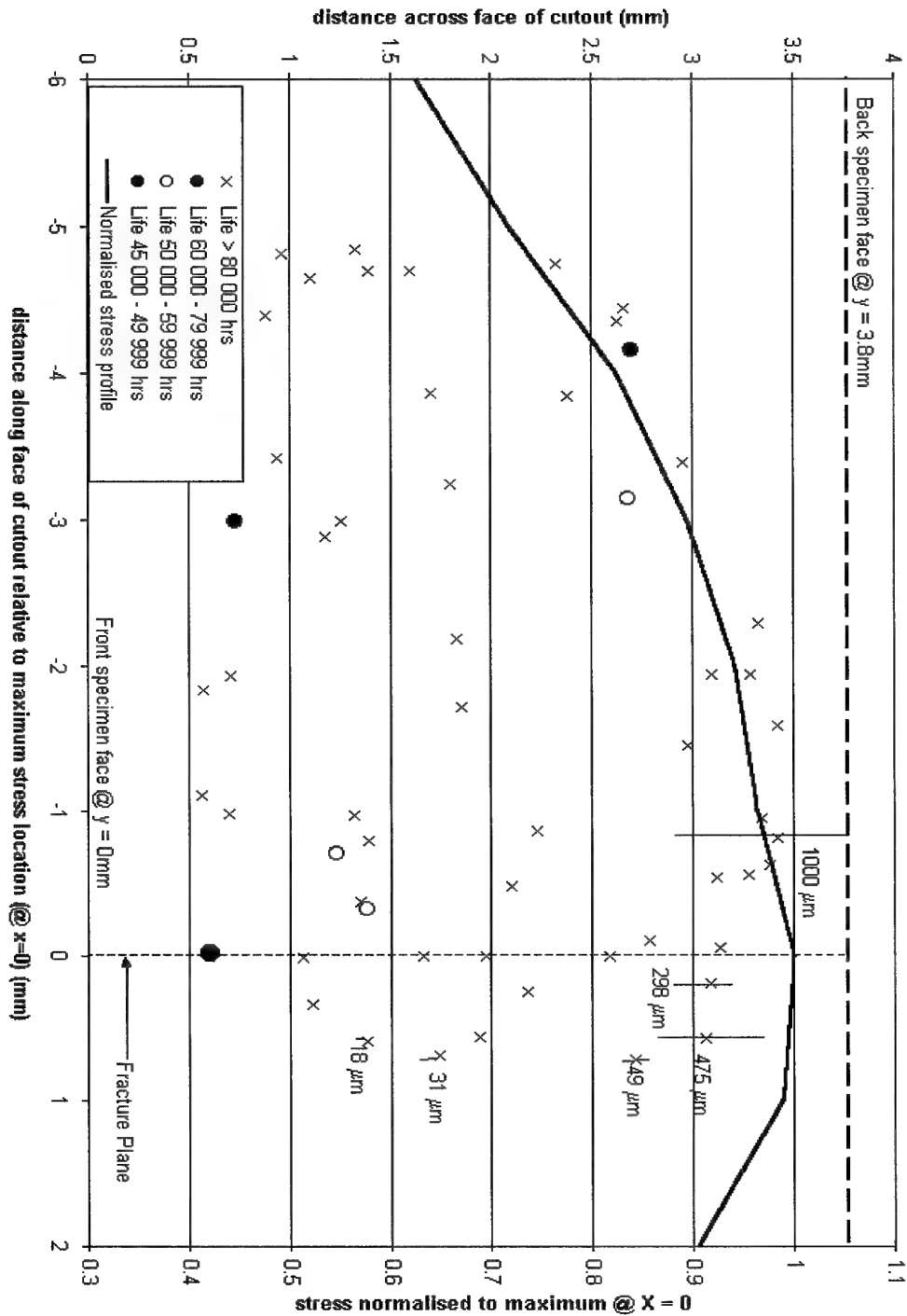
Figure 57. Life prediction plot based on pit location and ECS mean curve.

117
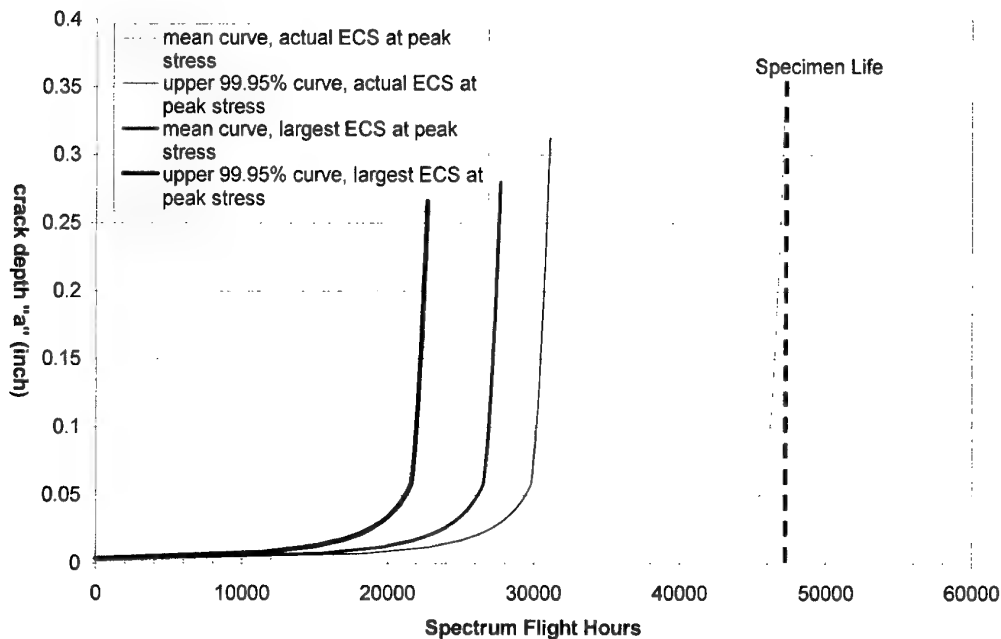
Figure 58. Final predictions for specimen FP78AD.

6.2 Sample for high stress case

A more typical case was evaluated at high stress (1310 MPa, 190 ksi) to provide a second example of this technique. All the data are summarised in the following two tables (41 and 42).

The specimen used was FP81AB. Table 41 gives details of pit size and location as well as stress information. Table 42 shows the results of the modelling effort.
This case was more typical of the level of effort that would be required in the field as only two pits in the specimen were of significant depth (greater than 30 microns). In the previous example, there were 57 such pits.

Table 41. Pit and ECS details for the specimen FP81AB.

Pit number	Distance from max stress (mm)	Normalised Stress	Pit Depth (microns)	Pit Metric (depth * aspect ratio)	ECS mean curve	ECS upper 99.95% curve
1	0	1.0	58	49	16.9	46.7
2	3.5	0.87	63	55	19	49.5

As can be seen in Table 41, the two significant pits in this specimen are of very similar size and severity, with Pit 2 having the slightly larger ECS value. However, Pit 2 is at a location that is seeing only 87% of the maximum stress on the specimen. The effect of the location on life is quite clear in Table 42.

Table 42. Life predictions for the two pit locations in FP81AB.

Pit number	Normalised Stress	Actual life (SFH)	Life based on mean ECS	Life based on ECS upper 99.95%
1	1.0	12 850	28 281	11 304
2	0.87	12 850	44 103	18 275

Finally, the 'short cut' approach was taken wherein the larger Pit 2 was translocated to the zone of maximum stress. The new life predictions for these cases (upper 99.95% confidence limit and mean curve, respectively) are 10 795 hours and 25 404 hours. By translocating the second pit to the zone of maximum stress, even more conservatism is offered in the predictions from the upper 99.95% confidence limit. In this case, the revised calculation under-predicted the actual life by 16%.

6.3 Potential impact of SCC on fatigue lives

One of the concerns in applying this technology is the possibility that stress corrosion cracking may be present in the same location as the pitting. In at least one case in the RAAF, intergranular cracking was detected at the origin of a pitting-induced crack. This could well have been the result of stress corrosion cracking or hydrogen embrittlement. Whatever the mechanism, the problem is that the zone of intergranular cracking was a 'mere' 40 microns in length. 'Mere' is in quotes because 40 microns is tremendous in terms of the Equivalent Crack Size concept. Furthermore, that size of damage is well below any non-destructive inspection threshold. Even if a pit was easily detected, the state of the material at the base of the pit could not be readily assessed.

A demonstration of the magnitude of the impact 40 microns of intergranular attack could have on fatigue life predictions is given by adding 40 microns to the ECS determined for a pit. Using the previous example of specimen FP81AB, where the upper 99.95% confidence limits ECS was 46.7 microns, it suddenly becomes 86.7 microns. Where once the life prediction was 11 307 hours, it now drops to 6680 hours.

Similarly, with the other example specimen, low stress specimen FP78AD, where the upper 99.95% ECS of the critical pit was 68.2 microns, the new ECS becomes 108.2 microns. When analysed, the fatigue life prediction drops from 31 000 hours to 23 189 hours. Unfortunately, no data exist with this type of damage to verify the severity of this proposed impact experimentally. For this reason, it is important to review the F-111 structure to determine which areas may be more prone to this type of damage formation.

The case that was found in service originally was in an area that had undergone compressive yield during the cold proof load test, which left a zone of residual tension (for more on this, see Mills et al. 2000) that could provide the sustained tensile stress necessary to cause SCC. Planned structural optimisation of the wing will reduce the risk areas for this type of residual stress thereby reducing the possibility of SCC in those locations, too.

6.4 Conclusions from sample application

This chapter provided two examples of applying the ECS concept to determine the remaining fatigue life (or inspection interval) for a component. As was described in the opening comments in this chapter, three things are necessary to use the ECS concept in practice:

- a reliable non-destructive method of determining pit size is needed.

- a solid knowledge of the stress distribution or at least the peak stress in the component is necessary.

- a solid knowledge of the stress spectrum experienced by a problem location is necessary.

In many situations, the second two items were very easy to come by. For that matter, in the laboratory, the first item is easy to assess. However, in the field, reliable NDI of a corrosion pit may be quite difficult. Successful NDI of corrosion pits, sufficient to give accurate measurements of depth and width, needs to be developed. In much the same way that NDI for Magnetic Rubber has been thoroughly assessed for probability of detection thresholds, so should some NDI technique for pitting. The probability of detection for pitting is typically quite good using magnetic rubber, for instance, but what really needs to be assessed is the fidelity of the measurements. We need to know not only where the pits are, but their shape and morphology.

The process demonstrated in this chapter appears lengthy, but only because every pit was evaluated at the exact stress at its location. To save time, and to provide extra conservatism, it seems logical to simply treat every pit as if it is in the worst possible stress location. Doing so in the sample applications cut the life prediction significantly, and so would adjust inspection intervals significantly, but in the scenarios investigated so far, these intervals have yet to encroach on intervals controlled by the CPLT schedule.

Also presented in this chapter was a discussion on the effects of stress corrosion cracking, or some form on intergranular damage, that may be undetectable at the base of a pit. This type of damage has been seen before in the fleet, although not routinely. Even a 40 micron intergranular crack can have a grave impact on the fatigue life of an

affected component. Therefore, it is important to assess the F-111 structure for areas where sustained tensile stresses may be sufficient to cause SCC. As always, hydrogen abatement should be a major goal associated with maintenance actions on D6ac components. Work by Grummet and Hinton (2001) give excellent guidance towards ensuring any hydrogen charging is eliminated in this very susceptible material.

7. Discussion of Overall Results

This research effort was designed to address the significance, within a more conventional fatigue lifing framework, of corrosion pitting in the F-111's D6ac steel structure, and this has been done with much success. The tool developed herein allows for the assessment of inspection intervals and maintenance intervals. For example, efforts to optimise the shape of the FFVH areas could increase inspection intervals from 500 flight hours to 2000 flight hours based on pure fatigue. This should only be done, though, if the unexpected occurrence of corrosion during those 2000 hours does not generate a structurally unsafe condition.

A number of important findings have come from this research project; however, some research remains, and this work should be tackled before the tools can be used in service.

The impact of the development of ECS on the F-111's management will be discussed in two different sections. First, it is important to know just how critical corrosion pitting will be to the primary structure of this aircraft. The results of this study shed some light on that question. Second, it is important to know how crucial this type of corrosion will be to the integrity of secondary structure.

7.1 Effect on primary structure of F-111

On the surface, it looks as though corrosion pitting will not be a major concern for the DADTA components of the F-111. If you peruse the ECS data for all the specimens tested, and if you peruse the fleet data from Appendix E, it becomes obvious that the ECS sizes for corrosion pitting are quite small. In almost every case, the ECS values are less than 125 microns (0.005 inch). Depending on the DADTA location, initial crack sizes for a traditional DADTA analysis are more on the order of 600 microns (0.02 inch) or even 1.25 mm (0.05 inch).

From this quick look, it is appears that a component that is unfortunate enough to be suffering corrosion in an exact location that is monitored by DADTA is relatively safe because the DADTA crack sizes are much larger than the ECS of corrosion pitting. However, there are sources for concern that need to be pointed out.

- The environment that causes the corrosion may be more severe than that characterised for use during the DADTA analysis. This could result in higher overall crack propagation rates through a corrosion fatigue mechanism. This would be exceptionally dangerous if some sort of chemical short crack effect was active, as the speed of crack propagation at small crack sizes has a profound effect on overall life. None of these experiments was conducted in anything other than dry air. Any impact of corrosion fatigue on fatigue performance and ECS distribution has not been characterised.

- In Chapter 6, the concern of SCC impacting overall life was raised. If SCC (or HE-induced intergranular cracking) becomes active in a pitted location and causes crack extension independent of flight hours, the predictive capability of this ECS tool is greatly undermined. The intergranular cracks would have to become quite large before they could be detected by traditional NDI. Although NDI would effectively betray the presence of pits, the ability to detect small intergranular damage at the base of the pits simply is not there.

- The ECS concept has only been validated in the case of stresses below the elastic limit. However, many of the F-111's trouble spots are linked to plastic compressive stresses that result in a residual tension field. Service history has shown that residual tension, plastic stresses, and pitting can join forces to cause cracking in quite a short amount of time (2000 hours or so). No life predictions using the DADTA 2b spectrum, the ECS values for the laboratory or fleet-detected pitting, and stresses bordering on plastic resulted in a fatigue life that short.

- There is potential for corrosion to occur in locations that are not the primary hot spot in a DADTA component. This could result in cracks developing in locations not typically inspected or analysed. The ECS concept could be used to address risks associated with this scenario.

- This model does not address the impacts of multiple cracks on the traditional DADTA analyses. For that matter, traditional DADTA analyses do not consider the possibility of multiple crack origins, either. The ECS development came from the assumption that one dominant pit was responsible for the cracking, since that is all that could be analysed. However, in many cases (particularly high stress cases) several pits formed cracks that joined to make the one crack that ultimately led to fracture. Multiple cracks in a fracture plane, or even crack shielding (from cracks above or below the main fracture plane) could have a profound effect on the predictions if they were incorporated into the model. Unfortunately, that cannot be done using the software supporting the F-111 DADTA.

7.2 Effect on secondary structure of F-111

The effects of corrosion pitting on the secondary structure in the F-111 is probably the greatest risk against meeting life-of-type goals. The ECS of corrosion damage is starting to encroach on the starting crack sizes for areas analysed as durability components, where initial crack sizes are closer to 125 microns (0.005 inch).

Here benefits and risks start to intrude into each others' territory. For instance, if corrosion damage is detected that puts a component at risk of not meeting its durability life goal, then a natural response is to remove that damage. However, this,

in many cases, may be more damaging to the structure than leaving the corrosion. Cleaning up the corrosion damage results in:

- The remaining protective scheme in the area (paint, primer, cadmium plating) which was slightly compromised to allow for the development of corrosion will now be completely eradicated to clean up the corrosion. Replenishment methods, such as cadmium brush plating, are not as good as the original protection scheme, and large repair areas run the risk of large area corrosion problems happening soon after a repair is completed.

- Rework of an area often result in a better-than-necessary surface finish, which tends to make recurring damage stand out even more when viewed with various NDI techniques such as acetate replicas or magnetic rubber. This can result in frequent and unnecessary maintenance actions.

Perhaps the main benefit of this research effort is to provide the groundwork for determining what levels of corrosion damage are tolerable in secondary structure, thus eliminating the need for constant, possibly more-damaging, maintenance.

A very useful way to address this is to look at areas of secondary structure in the F-111 and mix the ECS distributions, stress magnitudes and spectra to see if there are any structural hot spots that might threaten durability life if left alone (other than treatment to ensure that the corrosion does not grow).

8. Conclusions and Recommendations

The lack of adequate techniques to analyse corrosion fatigue interactions [Cole, Clark and Sharp 1997] gave rise to an AMRL research program into the effects of pitting on the fatigue behaviour in D6ac steel. The program contained several phases including:

- Constant amplitude fatigue of simple pitted coupons.

- Extensive fractography of the failed low-k_t specimens.

- Evaluation of material models and selection of appropriate crack growth modules based on stress levels.

- Identification of the Equivalent Crack Size (ECS) approach for pitting corrosion in D6ac steel.

- Use of ECS to predict lives in more complex fatigue specimens including simulated Fuel Flow Vent Hole (FFVH) 13 coupons and other plate-with-hole geometries.

The key result of this effort has been to apply the ECS as a method to incorporate corrosion damage into traditional fatigue life analysis techniques.

The basic development of the ECS concept required:

- Characterisation of key features of real corrosion pits that generate fatigue failures in laboratory coupons.

- Correlation of these features to the fatigue life of the coupons and, ultimately, to the ECS for those coupons.

The basic application of the ECS concept required the following:

- When corrosion damage is found in a real component, the key features of the corrosion damage must be measured, and an ECS is then calculated based on historical data from the coupon test program.

- By using a known stress spectrum for the part and an appropriate crack growth model, life from that ECS is calculated.

- In this way, residual life of the structure can be extracted from the basic as-detected damage dimensions.

The following subsections provide a quick snap-shot of the important conclusions from each chapter. Recommendations follow in the final sub-section.

8.1 Low-k_t test program.

This section of the report described a testing program that was used to establish the groundwork for Equivalent Crack Size (ECS) development in D6ac steel. The effort was centred on a constant amplitude fatigue program at three different stress levels using specimens with no stress concentration in the gauge section other than corrosion pits.

Corrosion pits of varying depth were used to provide variations in fatigue life that could be attributed to the different pit sizes. A number of observations came from this program, and they are summarised here.

- As would be expected, the lowest stress exhibited longest fatigue lives and the most scatter, whereas the highest stress exhibited the shortest fatigue lives and the least scatter.

- It is believed that the scatter in the fatigue lives is not entirely attributed to that normally associated with fatigue, as the specimens contained pits of varying depth, and it is reasonable to expect that pit size influenced scatter.

- Comprehensive fractography was completed on all the specimens that failed from corrosion pits. The main goal was to completely document all pit features so that they could be correlated to fatigue life and ECS values as discussed in the next section.

- Some of the specimens contained marker bands (to mark the fracture surface), so that crack growth curves could be generated post-mortem for the material used in this program.

8.2 ECS development

The ECS development process is the heart of this research effort. In this stage, correlations were sought between the ECS values generated by a selected material model and the pit features that caused fracture in the low-k_t coupons. The significant findings follow.

- Three different material models were investigated to see which was best for the purposes of ECS development.

- The three models were the original Forman curve fit used by LMTAS for DADTA management of the F-111, a mean-curve fit of the same data used to

develop the Forman fit, and a NASGRO data set as found in the USAF fracture code, AFGROW.

- The Forman curve fit was selected, as it matched the low K crack growth data quite well. The Forman curve fit has been used extensively over a long period by LMTAS in F-111 management.

- Using the Forman material model, the life of each low-k_t fatigue specimen was "back-predicted" to determine an ECS for that specimen. The different test stresses and fatigue lives provided a family of ECS values. This led to what may be the most important point in the entire study:

- *Any future ECS-based life predictions must use the fatigue crack growth rate model from which the ECS distribution was developed.* By using the Forman curve fit, the same material model can be used for the original DADTA work as well as any new work based on the corrosion pitting.

- Several pit features were studied to try to determine correlations with fatigue life. The strongest correlation was provided by the product of depth times aspect ratio, where aspect ratio is defined as depth over half width (a/c). This had a much stronger correlation than just pit depth.

- Once the best correlation of pit feature with fatigue life was found, the feature was plotted *vs.* ECS. The subsequent relationship was fitted with a mean curve and 95% and 99.95% confidence bands.

- All subsequent ECS validation was done using the mean curve for best estimates of life prediction along with the upper 99.95% confidence bound for more conservative estimates.

8.3 ECS validation

The purpose of the high-k_t test program was to validate the ECS distribution derived from the low-k_t experimental program. The key points of the high-kt program are as follows:

- Some tests were at constant amplitude (to see how the fatigue lives compared with the low-k_t program). Others sought to challenge the ECS model by making it perform under variable amplitude conditions and at stresses not previously tested.

- The fatigue lives of the high-k_t coupons were in line with those from the low-k_t program at similar stress levels. The relative severity of the corrosion pits seemed to influence the fatigue live predictably.

- The ECS values coupled with the AFGROW model did a reasonable job predicting the fatigue lives of the high-k_t constant amplitude specimens. In almost every case, the mean ECS over-predicted the experimental fatigue life, and the upper 99.95% confidence limit ECS under-predicted the experimental fatigue life.

- In only one case was there an unconservative result, where the fatigue life was shorter than that predicted by the most conservative 99.95% confidence limit ECS. This case involved a specimen with high plasticity, and since the analysis was done using an linear elastic fracture mechanics code, the results should be questioned, anyway. The result was unconservative by 1.6%.

- Eleven FFVH13 coupons were used to validate the ECS distribution under variable amplitude conditions.

- Again the ECS values derived from the low-k_t program did a good job predicting the fatigue life for this more demanding series of experiments.

- As with the constant amplitude experiments, the mean ECS tended to over-predict the experimental fatigue life, although in some cases it under-predicted — a very conservative result.

- As with the constant amplitude experiments, the upper 99.95% confidence limit ECS tended to under-predict the actual fatigue life. At the high stress levels, where the validity of AFGROW could be questioned, the actual life was quite close to the predictions by the upper limit.

- Three specimens were selected from a probability of detection study by Hugo and Harding at DSTO/AMRL to check the validity of the ECS distribution in predicting the lives of material corroded outside our control. This trial showed that the model was heavily challenged by small corrosion sizes, since there is such a wide spread in the life predictions between the mean and upper 99.95% confidence limit ECS values.

- The corrosion in the POD study was a lot smaller than the typical pitting corrosion found in the fleet as well as in the rest of the research program. In the one case where the corrosion was of the same magnitude, both the mean ECS (not surprisingly) and the upper 99.95% confidence limit ECS (surprisingly) over-predicted the experimental fatigue life.

- The upper 99.95% confidence limit ECS over-predicted the experimental fatigue life of the one POD coupon by +12.3%.

- This coupon was tested at a very high stress level, and in keeping with other observations where the model was unconservative, the validity of LEFM analysis in these cases is flagged as a probably source of error.

8.4 Sample application

The sample application sought to further illustrate application of the ECS concept. As repeatedly mentioned in this report, three things are necessary to use the ECS concept in practice:

- a reliable non-destructive method of determining pit size is needed. In this case magnetic rubber provided some success. Two part dental putties (such as Exaflex) and acetate replicas have been used successfully by NDTSL at RAAF Amberley.

- a solid knowledge of the stress distribution or at least the peak stress in the component is necessary.

- a solid knowledge of the stress spectrum experienced by a problem location is necessary.

The demonstration required extensive effort, but only because every pit was evaluated at the exact stress at its location. To save time, and to provide extra conservatism, it seems logical to simply treat every pit as if it is in the worst possible stress location. Doing so in the sample applications cut the life prediction significantly, and so would adjust inspection intervals significantly, but in the scenarios investigated so far, these intervals have yet to encroach on intervals controlled by the CPLT schedule.

Also presented here was a discussion on the effects of stress corrosion cracking, or some form on intergranular damage, that may be undetectable at the base of a pit. This type of damage has been seen before in the fleet, although not routinely. Even a 40 micron intergranular crack can have a grave impact on the fatigue life of an affected component.

8.5 Recommendations and limitations

Incorporating the ECS for pitting corrosion tool into the management of the F-111 fleet remains as a significant task. Before the tool is ready, a few things need to be addressed. In short, this tool is not a catch-all for corrosion situations in D6ac. A number of limitations (raised throughout this report) are mentioned here along with recommendations that, if addressed, will make the ECS tool much more robust.

8.5.1 Modelling Issues

- The first, and perhaps most important thing, to keep in mind is that this ECS distribution was built using the Modified Forman material model for D6ac that has long been used by Lockheed in management of the F-111. This material model must always be used in conjunction with the ECS curves presented in this report. If a new material model comes into use on the F-111, then a new ECS family will need to be developed.

- Because of limits in the corrosion protocol used to develop pitting, it was difficult to generate corrosion damage greater than 120 microns. This fact, coupled with limited specimen availability, meant that the ECS vs. pit metric curves developed in this program were sparsely populated in the 'upper-right' region of large pit metrics. Fleet corrosion data showed that corrosion damage of this size was certainly possible, so it would be wise to conduct more experiments to populate that region of the ECS curve and refine the mean and confidence bounds. Low-k_t constant amplitude experiments (at least three replicates at each of the three original stress levels) would be used to generate this data, just as they were used to generate the rest of the data on the curve.

- This model was developed to address corrosion pitting in D6ac steel. It is not valid for use on other corrosion morphologies (for example, crevice corrosion) and materials.

- Many of the problem areas in the F-111 structure are stressed beyond either compressive or tensile yield, particularly in the Cold Proof Load Test. As such, many of the specimens used in ECS development were deliberately stressed to levels at or exceeding monotonic yield. It was deemed important that the ECS distribution developed in this program be validated both in elastic stress cases as well as elastic — plastic cases.

- Unfortunately, the METLIFE computer code, which handles plasticity and stress/strain accumulation, was not ready at the time of these analyses, so the best thing available (the LEFM code, AFGROW) was used for all analyses. Still, the elastic-plastic cases need to be re-evaluated using METLIFE when that code is fully functional to determine the validity of the ECS in those cases. For now, we can only say that it is fully conservative in elastic cases.

- The ECS distribution in this report has been described by a 'mean curve,' or best estimate and a 3-sigma (upper 99.95%) confidence bound. Predictions based on the mean curve were typically unconservative, so use of the upper 99.95% confidence interval is recommended.

- Further conservatism than that allowed by the upper 99.95% confidence limit would come from proper application of the ECS engineering tool. To keep with

traditional application of damage tolerance analysis, an inspection interval of at least half that predicted by the upper bound would be applied in a fleet scenario.

- The ECS only provides a first approximation of life based on the damage as detected. For now, this approach does not take into account the possibility that the corrosion damage will continue to grow and evolve, thus changing the life prediction. This is important to recognise, since the purpose of the ECS modelling, in part, is to assess whether or not damage is safe to leave in place until either retirement or until a better maintenance opportunity. The adaptation of evolving damage states in this model requires knowledge of corrosion growth behaviour in D6ac steel, and others at DSTO/AMRL are working the corrosion kinetics issues.

- Any impact of corrosion fatigue on fatigue performance and ECS distribution has not been characterised. Such environmental effects could result in higher overall crack propagation rates through a corrosion fatigue mechanism. This would be exceptionally dangerous if some sort of chemical short crack effect was active, as the speed of crack propagation at small crack sizes has a profound effect on overall life.

- This model does not address the impacts of multiple cracks. The ECS development came from the assumption that one dominant pit was responsible for the cracking, since that is all that could be analysed. However, in many cases (particularly high stress cases) several pits formed cracks that joined to make the one crack that ultimately led to fracture. Multiple cracks in a fracture plane, or even crack shielding (from cracks above or below the main fracture plane) could have a profound effect on the predictions if they were incorporated into the model. Unfortunately, that cannot be done using the software supporting the F-111 DADTA.

8.5.2 Field application issues

- The demonstration of this technology in Chapter 6 brought to light an important issue. If the pits cannot be accurately described, they cannot be transformed into an ECS. Accurate description of corrosion pits is easy in laboratory, but not so easy in the field. Successful NDI of corrosion pits, sufficient to give accurate measurements of depth and width, needs to be developed. In this case, magnetic rubber provided an excellent NDI process.

- In Chapter 6, the concern of SCC impacting overall life was raised. If SCC (or HE-induced intergranular cracking) becomes active in a pitted location and causes crack extension independent of flight hours, the predictive capability of this ECS tool is greatly undermined. The intergranular cracks would have to become quite large before they could be detected by traditional NDI. Although

NDI would effectively betray the presence of pits, the ability to detect small intergranular damage at the base of the pits simply is not there.

- Thus, it is important to assess the F-111 structure for areas were sustained tensile stresses may be sufficient to cause SCC. And as always, hydrogen abatement should be a major goal associated with maintenance actions on D6ac components.

- On the surface, it looks as though corrosion pitting will not be a major concern for the DADTA components of the F-111. In almost every case, the ECS values are less than 125 microns (0.005 inch). Depending on the DADTA location, initial crack sizes for a traditional DADTA analysis are more on the order of 600 microns (0.02 inch) or even 1.25 mm (0.05 inch).

- There is potential for corrosion to occur in locations that are not the primary hot spot in a DADTA component. This could result in cracks developing in locations not typically inspected or analysed. The ECS concept could be used to address risks associated with this scenario.

- The effects of corrosion pitting on the secondary structure in the F-111 is probably the greatest risk against meeting life-of-type goals. The ECS of corrosion damage is starting to encroach on the starting crack sizes for areas analysed as durability components, where initial crack sizes are closer to 125 microns (0.005 inch).

- If corrosion damage is detected that puts a component at risk of not meeting its durability life goal, then a natural response is to remove that damage. However, this, in many cases, may be more damaging to the structure than leaving the corrosion. The ECS concept may realise its greatest benefit in preventing unnecessary maintenance which could be particularly 'detrimental.'

9. Acknowledgements

10. References

AAP 7002.043-36, NDT General Procedures, 25 Feb 99.

Aerostructures report (2001) F-111 Spectrum Review, Rev No 1, Report No. ER-F111-51-APM114, Aeronautical and Maritime Research Laboratory, March.

ASTM Standard G1-81, Preparing, Cleaning and Evaluating Corrosion Test Specimens, p. 507.

Ball, D.L. and Doerfler, M.T. (1996) Metallic Material Data for F-111 Durability and Damage Tolerance Analysis, LMTAS Report FZS-12-626.

Buntin, W.D. (1971) Concept and Conduct of Proof Test of F-111 Production Aircraft, Presented to Royal Aeronautical Society, London, England.

Cole G.K., Clark G. and Sharp P.K., (1997) The Implications of Corrosion with respect to Aircraft Structural Integrity, DSTO-RR-0102, March.

Cox, A. (1985) Fatigue Cracking in the Upper Plate of Wing Pivot Fittings in RAAF F-111 Aircraft, Defect Assessment & Failure Analysis Report (ARL Letter Report No. M34/85).

Eklund, G., (1994) The relationship between Slag Inclusions and Corrosion, *Localised Corrosion*, NACE-3, Houston, Texas USA.

Feddersen, C.E., Moon, D.P. and Hyler, W.S. (1972) Crack Behaviour in D6ac Steel; An Evaluation of Fracture Mechanics Data for the F-111 Aircraft, MCIC Report number 72-04, ARL Ref. 70908, Damage Tolerance Design Handbook Reference 82543.

Grummet, S. and Hinton, B. (2001) Personal communications about hydrogen embrittlement abatement in high strength steels, DSTO/AMRL Fishermans Bend.

Harter, J.A. (2000) Online help discussions from US Air Force Research Laboratory crack growth code, AFGROW.

Harter, J.A. (2001) Online help discussions from US Air Force Research Laboratory crack growth code, AFGROW.

Heller M, Burchill M, McDonald M and Watters K.C. (2001), Shape Optimisation of Critical Stiffner Runouts in the F-111 Wing Pivot Fitting, DSTO-TR-1119, April

Heller M, Burchill M, McDonald M and Watters K.C. (2001), Shape Optimisation of Critical Fuel Vent Holes in the F-111 Wing Pivot Fitting, DSTO-TR-1120, April.

Holden, G. (1999) Characterisation of Pitting Corrosion In D6ac Steel, Vacation Student Report, DSTO Fishermen's Bend.

Ives M.B. (1992) Metallography of Pitting Corrosion, *Materials Charactisation*, No. 28, pg 257-270.

Kowal, E. and Heller, M. (1999) Microgrid Plastic Analysis of a Representative F-111C Fuel Flow Vent Hole 13 Coupon, DSTO-TR-0951.

Laffe and Sutherland, B.J. (1994) F-111 Cold Temperature Proof Testing, Interest Item, Lockheed Memorandum.

Loader, C. and Sharp, P.K. (2001) Review of Pitting Corrosion and Pitting Effects on Structural Integrity, DSTO Technical Report, publication pending.

Manning S.D., Speaker S.M.,Gordon D.E., Yang J.N. and Shinozuka M. (1979-1984) Durability Methods Development, Volume 1 to Volume VII, AFFDL-TR-79-3118, AFRL, Wright-Patterson AFB, Ohio USA.

Manning S.D. and Yang J.N. (1987) Advanced Durability Analysis, Volume 1, AFWAL-TR-86-3017, AFRL, Wright-Patterson AFB, Ohio USA.

Melchers, R.E. (1984) Pitting Corrosion in marine Environments – A Review, Research report 101-07-1994, University of Newcastle, NSW, Australia

Mills, T., Clark, G., Sharp, P.K., Loader, C. and Schmidt, R. (2001) Review of F-111 Structural Materials, DSTO-TR-1118.

Mills, T., and Loader, C. (2000) Pitting Corrosion Procedure for use in F-111 Full Scale Wing Test, DSTO-TN-0326.

Murtagh, B.J. and Walker, K.F. (1997) Comparison of Analytical Crack Growth Modelling and the A-4 Wing Fatigue Test Experimental Results for a Fatigue Crack in an F-111 Wing Pivot Fitting Fuel Flow Hole Number 58, DSTO-TN-0108.

Newman, J.C., Jr., Raju, I.S. (1986) Stress-Intensity Factor Equations for Cracks in Three-Dimensional Finite Bodies Subjected to Tension and Bending Loads, *Chapter 9: Computational Methods in the Mechanics of Fracture*, ed. Atluri, S.N.

Nguyen, H.C. (1991) Failure Analysis of F-111E P/N 68-043 Wing Carry-Thru-Box and Upper Plate, General Dynamics Report FZM-12-14705.

Ruijini G., Srivastava S.C. and Ives M.B. (1989) Pitting Corrosion Behavior of UNS N08904 Stainless Steel in Chloride/Sulfate Solution, *Corrosion*, November, pg 874-882.

Sharp P.K. (2001), EIFS Modeling of 7050 Aluminium Alloy Corrosion Pitting and its Implications for Aircraft Structural Integrity, DSTO Research Report, to be published May 2002.

Srivastava S.C. and Ives M.B. (1987), , *Corrosion*, Vol 43, pg 687.

Walker, K. (2000) Personal Communication, DSTO/AMRL Fishermans Bend.

Appendix A. Tabular Crack Growth Data

Modified LMTAS Mean Curves

The following table is the tabular data used in the AFGROW modelling while developing ECS values based on Modified LMTAS Mean curve fits. Lockheed document FZS-12-626 [Ball and Doerfler 1996] contains most of this same data, although the table has been extrapolated down to ΔK of 2.18 MPa $\sqrt{m}$ (2 ksi $\sqrt{in}$) to lower the threshold per Lockheed DADTA practice.

Table A1. Tabular da/dN v ΔK data for Modified LMTAS Mean curves (continued next page).

ΔK (ksi $\sqrt{in}$)	da/dN (in./cycle)	ΔK	da/dN	ΔK	da/dN
R = 0.1		R = 0.5		R = 0.8	
2.1	1.03E-09	-	-	-	-
2.2	1.39E-09	-	-	-	-
2.4	2.03E-09	2.0	1.66E-09	-	-
2.6	2.87E-09	2.1	2.06E-09	-	-
2.8	3.95E-09	2.3	3.06E-09	-	-
3.0	5.32E-09	2.5	4.41E-09	2.0	4.30E-09
3.1	6.13E-09	2.7	6.17E-09	2.1	5.35E-09
3.3	8.04E-09	2.9	8.43E-09	2.2	6.59E-09
3.5	1.00E-08	3.0	1.00E-08	2.4	1.00E-08
4.1	2.00E-08	3.5	2.00E-08	2.8	2.00E-08
4.5	3.00E-08	3.9	3.00E-08	3.1	3.00E-08
4.8	4.00E-08	4.1	4.00E-08	3.3	4.00E-08
5.0	5.00E-08	4.4	5.00E-08	3.5	5.00E-08
5.3	6.00E-08	4.6	6.00E-08	3.6	6.00E-08
5.4	7.00E-08	4.7	7.00E-08	3.7	7.00E-08
5.6	8.00E-08	4.9	8.00E-08	3.8	8.00E-08
5.8	9.00E-08	5.0	9.00E-08	3.9	9.00E-08
5.9	1.00E-07	5.1	1.00E-07	4.0	1.00E-07
6.9	2.00E-07	6.0	2.00E-07	4.7	2.00E-07
7.6	3.00E-07	6.6	3.00E-07	5.2	3.00E-07
8.1	4.00E-07	7.0	4.00E-07	5.5	4.00E-07
8.6	5.00E-07	7.4	5.00E-07	5.8	5.00E-07
8.9	6.00E-07	7.7	6.00E-07	6.0	6.00E-07
9.4	7.00E-07	8.0	7.00E-07	6.2	7.00E-07
10.0	8.00E-07	8.2	8.00E-07	6.4	8.00E-07
10.5	9.00E-07	8.4	9.00E-07	6.6	9.00E-07
11.0	1.00E-06	8.6	1.00E-06	6.7	1.00E-06

Table A1 cont.   Tabular da/dN v ΔK data for Modified LMTAS Mean curves.

ΔK (ksi √in)	da/dN (in./cycle)	ΔK	da/dN	ΔK	da/dN
	R = 0.1		R = 0.5		R = 0.8
14.7	2.00E-06	11.0	2.00E-06	7.8	2.00E-06
17.4	3.00E-06	13.0	3.00E-06	8.5	3.00E-06
19.5	4.00E-06	14.6	4.00E-06	9.0	4.00E-06
21.3	5.00E-06	15.9	5.00E-06	9.7	5.00E-06
22.9	6.00E-06	17.0	6.00E-06	10.3	6.00E-06
24.4	7.00E-06	18.0	7.00E-06	10.9	7.00E-06
25.7	8.00E-06	18.9	8.00E-06	11.4	8.00E-06
26.9	9.00E-06	19.8	9.00E-06	11.8	9.00E-06
28.0	1.00E-05	20.6	1.00E-05	12.2	1.00E-05
36.3	2.00E-05	26.2	2.00E-05	14.9	2.00E-05
41.9	3.00E-05	29.9	3.00E-05	16.5	3.00E-05
46.3	4.00E-05	32.6	4.00E-05	17.6	4.00E-05
49.8	5.00E-05	34.8	5.00E-05	18.4	5.00E-05
52.8	6.00E-05	36.6	6.00E-05	19.1	6.00E-05
55.4	7.00E-05	38.1	7.00E-05	19.6	7.00E-05
57.7	8.00E-05	39.5	8.00E-05	20.0	8.00E-05
59.8	9.00E-05	40.6	9.00E-05	20.4	9.00E-05
61.7	1.00E-04	41.6	1.00E-04	20.7	1.00E-04
74.0	2.00E-04	48.1	2.00E-04	22.4	2.00E-04
81.0	3.00E-04	51.3	3.00E-04	23.2	3.00E-04
85.7	4.00E-04	53.4	4.00E-04	23.6	4.00E-04
89.1	5.00E-04	54.7	5.00E-04	23.8	5.00E-04
91.6	6.00E-04	55.8	6.00E-04	24.0	6.00E-04
93.7	7.00E-04	56.5	7.00E-04	24.1	7.00E-04
95.4	8.00E-04	57.2	8.00E-04	24.2	8.00E-04
96.8	9.00E-04	57.7	9.00E-04	24.3	9.00E-04
97.9	1.00E-03	58.1	1.00E-03	24.4	1.00E-03
98.0	4.00E-03	59.0	4.00E-03	23.3	4.00E-03
98.0	1.00E-02	59.0	1.00E-02	23.3	1.00E-02

Appendix B. Load Spectra

This appendix contains the load spectra used during the fatigue tests for all specimens. These same spectra were used for AFGROW and METLIFE predictions of fatigue test results. The spectra are all normalised for stress.

Constant amplitude testing:

Constant amplitude is a bit of a misnomer in some cases, since so many of the specimens contained marker bands. The marks involved variable amplitude loading, but as a rule, most of the damage in the specimens was generated using constant amplitude loading, and the marker band spectra impacted overall life by less than 1%. Table A1 shows the marker band spectra for the different constant amplitude stresses used throughout this research program. The normalised stress level of 1.0 corresponds to the main load level of the test; the marker bands do use overloads at times, and these are represented as greater than 1.0. As a rule, they all follow the same pattern and load ratios with the exception that the constant amplitude blocks are adjusted based on stress level and expected fatigue life to provide at least 10 marker bands on a fracture surface. Also, at the higher stresses, the typical 11% overload block of 50 cycles (see Table B1) is reduced to 5%. One pass through the spectrum involved one set of constant amplitude cycles, one underload block, and one overload block. Depending on stress level, one pass through the spectrum involved 500, 1000, 2000, or 4000 total cycles.

Table B1. Load spectra used for the different stress levels of constant amplitude testing.

Max stress	Constant Amplitude			Underload Block			Overload Block		
MPa (ksi)	max	min	cycles	max	min	cycles	max	min	cycles
896 (130)	1.0	0.1	3900	0.75	-0.15	50	1.11	.15	50
1144 (166)	1.0	0.1	1900	0.75	-0.15	50	1.11	.15	50
1214 (176)	1.0	0.1	900	0.75	-0.15	50	1.11	.15	50
1310 (190)	1.0	0.1	400	0.75	-0.15	50	1.05	.15	50
1351 (196)	1.0	0.1	400	0.75	-0.15	50	1.05	.15	50
1386 (201)	1.0	0.1	400	0.75	-0.15	50	1.05	.15	50

The AFGROW spectrum file names for these different sequences are:

d6acmark 130.sp3
d6acmark 13001.sub

d6acmark 166.sp3
d6acmark 16601.sub

d6acmark 176.sp3
d6acmark 17601.sub

d6acmark 190.sp3
d6acmark 19001.sub

d6acmark 196.sp3
d6acmark 19601.sub

d6ac mark 201.sp3
d6acmark 201.sub

Hi-K_t Spectrum Testing:

For the variable amplitude testing, a frequently used F-111 spectrum was employed since many computer analysis efforts at DSTO have used the same one. This made it easy to cross check solutions to make sure the crack growth modelling used for this research program was correctly tuned.

The spectrum used was for DADTA Item 86 (DI 86), which is at vent hole 58 in the lower plate of the wing pivot fitting in the F-111. Details of the DI86 are given in, Aerostructures (2001), but they do not really apply to this effort. The DADTA-2b spectrum was used for this study, but not in its full form. The original spectrum has 1 949 652 turning points, which makes it cumbersome to handle with the computer and makes testing time inordinately long, since most of those turning points are very minor load excursions that contribute little to crack growth. Thus, it was decided to filter the spectrum at 10% mean spectrum stress (MSS). The MSS used for DI86 was 740 MPa (107 ksi), and filtering reduced the number of turning points to 104 806 and produced a final count of 52 403 cycles per pass. In terms of flight hours on the F-111, one pass of the spectrum equates to 500 simulated flight hours.

Figure B1 is a plot of the filtered spectrum. As with the constant amplitude spectra, it has been normalised to provide simplified use at several different stress levels, both for test frame control and for computer modelling purposes.

The AFGROW spectrum files associated with this load sequence are:

di86-trun-10MSS.sp3
di86-trun-10MSS01.sub
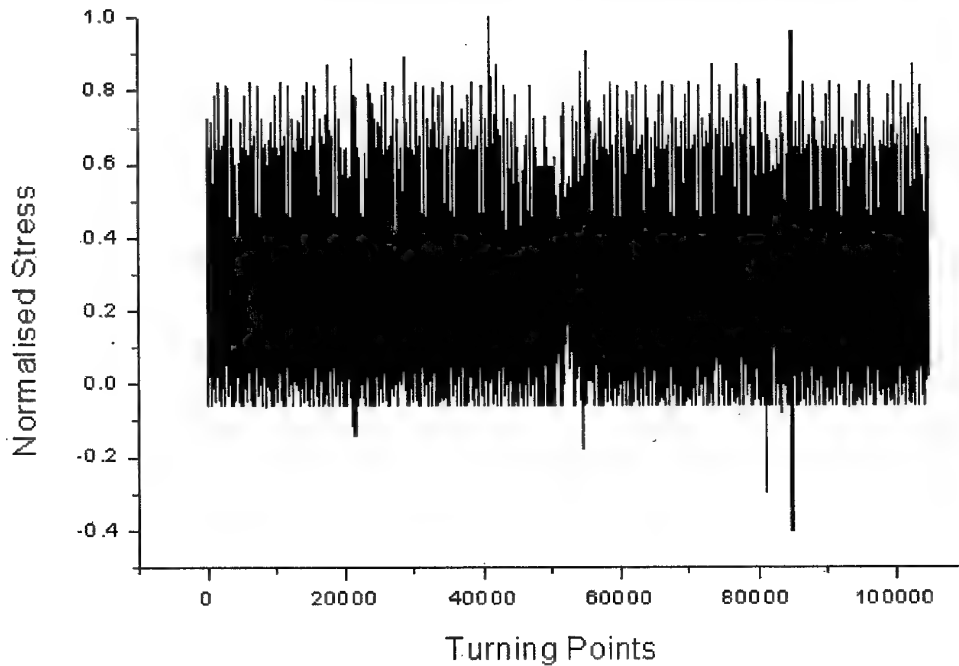
Figure B1. Normalised DADTA-2b spectrum for DI86 in the F-111 wing pivot fitting lower plate. This spectrum has been truncated at 10% MSS to reduce overall number of turning points.

POD Specimen Spectrum:

This spectrum is essentially another filtered version of the DADTA2b sequence discussed in the previous section on the high-k_t specimens. This variation of DADTA2b was used by Hugo and Harding (DSTO/AMRL) to generate cracks in pitted specimens. The specimens were cracked as part of a major testing program designed to generate an updated probability of detection (POD) distribution for magnetic rubber inspection on D6ac.

In addition to being heavily filtered to the point that it only had 18 742 turning points (vs. 52 403 in the previous iteration of the spectrum), the POD spectra was also clipped to take out all loads that were either negative or zero.

The AFGROW spectrum files associated with this load sequence are:

pod nclip.sp3
pod nclip01.sub
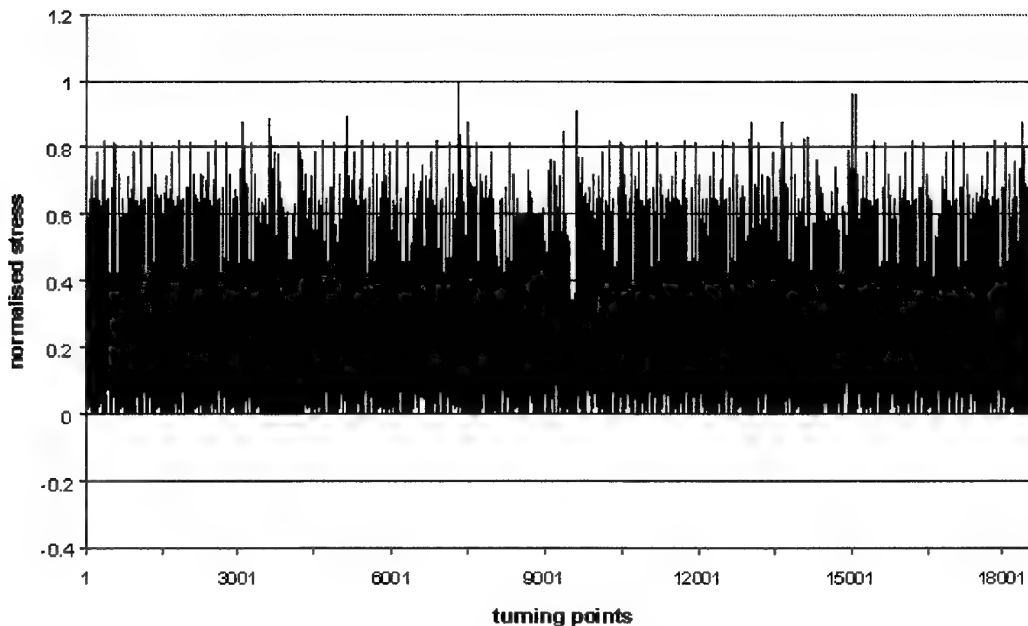
Figure B2. DADTA2b spectrum variation used for POD trial.

DI36 Spectrum with CPLT:

Figure B3 shows the DI36 spectrum (full name DI36+D2b) used in the last series of high-k_t experiments (k_t=3.1). Unfortunately, all of these tests had high levels of plasticity in them, so it was not possible to do any predictions at the time of this writing, because the METLIFE computer code was not functioning at the necessary level. Therefore, the load spectrum is simply shown here for future reference. The next appendix has the rest of the test details, so that the DI36 specimens can be analysed with METLIFE when that software becomes available.

The maximum stress associated with the normalised level of 1.0 in the DI36 spectrum was 1018MPa (147.7ksi) for these coupons. Each repeat block through the spectrum represents 500 simulated flight hours. Every four spectrum block repeats, a cold proof load sequence was applied. These stresses peaked 1814MPa (263.3ksi) and the specifics of the CPLT sequence is shown in Table B2.
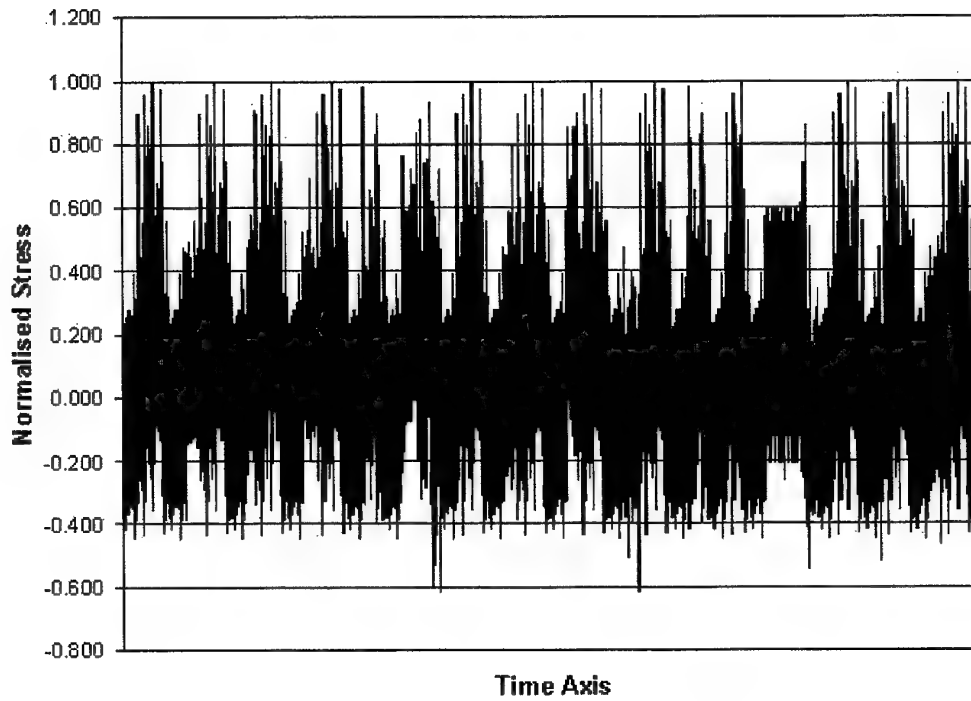
Figure B3. DI36 load spectrum used in final high-kt tests.

Table B2. CPLT sequence repeated every four spectrum passes (2000 hours).

Turning Point	Stress (MPa)	Stress (ksi)	Aircraft load factor (g)
1	0	0	1
2	1815	263	-2.4
3	-1815	-263	+7.33
4	567	82	-3.0
5	-1053	-152	+7.33
6	0	0	1

Appendix C. Load Interaction Calibration

Many of the experiments in this program used spectrum loading. In order to make accurate predictions of the test results, and to make this predictive tool useful for fleet applications, it was necessary to calibrate the load interaction models within AFGROW. The best way to do this was by trying to recreate experimental crack growth behaviour in AFGROW by iterating key parameters in different load interaction models.

Two models were calibrated for the purpose of future modelling.

1) Closure Model
2) Willenborg Model

Both are available in AFGROW, and one is available in the ADAMSYS and METLIFE codes. The Closure Model is unique to AFGROW and was developed by Harter from early work by Erdogan and Elber, and Creager and Sunder [Harter 2000]. The online help in AFGROW gives the details of this model.

The Willenborg retardation model is a very common retardation model that is used in many crack growth codes. According to Harter (2000), many crack growth codes use the Chang acceleration model to account for the effect of compressive stress cycles in reducing the effectiveness of previous overloads on retarding crack growth. AFGROW uses a technique that simply reduces the size of the plastic zone (thus, the effectiveness of subsequent retardation) when compressive loads occur in a sequence. Again, the online help in AFGROW details this model.

ADAMSYS and METLIFE also have provisions for using the Willenborg retardation model.

To calibrate the load interaction parameters, an earlier DSTO Technical Note by Murtagh and Walker (1997) was consulted. In this document, a study was made of crack prediction code performance using a fracture in an old F-111 full scale fatigue test article as the 'target result.'

In the A4 wing fatigue test, as the experiment was called, a crack grew in what is now DADTA Item 58 from 0.0075 inch to failure in 5680 spectrum hours. The goal here was to use load interaction parameter that gave similar life when coupled with the original modelling parameters used by then-General Dynamics.

For all the AFGROW model inputs, one is referred to Murtagh and Walker (1997). For the purposes of this report, though, a closure level of 0.235 gave a predicted life of 5516 hours. This value of 0.235 was brought forward into all subsequent crack growth predictions in this research program. However, while this value and model works well in AFGROW, a small realisation that this an AFGROW-unique retardation model

required that a suitable Willenborg parameter also be determined. The following table shows how the predictions using a Willenborg parameter of 2.7 compares with the predictions derived from the Closure Model parameter of 0.235. A low stress and high stress specimen were chosen from the high-k_t test program for this comparison.

Table C1. Comparison between Willenborg parameter and Closure Model in life prediction.

Retardation Model	Specimen ID	Predicted life mean ECS	Predicted Life upper 99.95% ECS	Actual Life (SFH)
Willenborg 2.7	FP78AD (low)	50 610	34 974	47 184
Closure 0.235		52 106	35 194	
Willenborg 2.7	EM47AF2B (hi)	15 404	9449	10 195
Closure 0.235		15 255	8735	

Appendix D. DI36 / CPLT Specimens

This appendix provides details of the final D6ac steel coupon testing undertaken in this research program. This portion of the test program was designed to demonstrate the validity of the ECS under elastic-plastic conditions using the METLIFE fracture code. Unfortunately, at the time of writing, the METLIFE software was still undergoing development, so this appendix is now relegated to recording information so that the analyses can be performed in the future.

Five tests were conducted, as these were all the specimens available at the time. The designs were simple, a concave dogbone with a hole in the middle. The coupons were 185 mm (7.28 inch) long, 57 mm (2.24 inch) wide, and 6.3 mm (0.25 inch) thick in the gauge section. The specimens contained a 10 mm (0.4 inch) diameter hole in the centre of the gauge section.

All of the specimens contained corrosion pits around the entire perimeter of the bore of the hole. Corrosion at the corner between the bore and the specimen face was avoided to make sure that all modelling efforts were focused on surface thumbnail cracks like with the other high-k_t and low-k_t experiments in this program. Corrosion pitting in the first four specimens targeted depths of 90 microns. However, since the pitting was allowed to occur all along the bore of the hole, the largest pits were not guaranteed to be in the zone of maximum stress. As such, the testing really covered a random variety of pit sizes. The fifth specimen was corroded for longer to reach a target pit size of 130 microns.

During testing, all of the specimens developed cracks on both sides of the holes. In Table D1, the appropriate side of the hole is bold-typed if the crack was markedly longer than its counterpart. If the two sides were close to equal, then the data are not highlighted. The two sides of the hole are separated by the dashed line in the table.

In the table, information is given for every pit in the fracture plane. Pits with significant size had their ECS determined. In this way, in the future, the load spectrum can be combined with the Forman material model and specimen dimensions and ECS to generate a life prediction for the coupon. The actual lives are also listed in Table D1.

When using the ECS, the dimension given is for a and c, since the starting aspect ratio for these cracks is assumed to be unity.

It is obvious by looking at Table D1 that many of these specimens developed cracks from both sides of the hole. Unfortunately, all the previous analysis has been done for cracks out of only one location. Multiple pits causing multiple cracks should be addressed if the model is to continue to increase in predictive accuracy.

Table D1. Pit metric and ECS information for the five DI36/CPLT coupons. These specimens will not have their lives predicted until METLIFE is functioning fully.

Specimen ID	Pit Depth (a) microns	Pit Width (2c) microns	Metric (a^2/c) microns	ECS mean (microns)	ECS upper 99.95%CL (microns)	Experimental Life in Hours
EL6AD2	**101**	**171**	**119**	**63.5**	**93**	
	36	77				
	72	119	87	34.5	64	
EL6AJ2	56	91	69	24.5	54.1	
	36	56				
	65	77	110	52.8	82.6	
EL6AG2	51	149	35	12.7	42.5	
	55	134				
	68	141	66	22.7	52.5	
	62	105	73	27	56.5	
EL5AD1	**61**	**155**	**48**	**16.8**	**46**	
	48	106	43	14.7	44.2	
	55	133	45	15.3	45.1	
EL3AG1	105	223	99	43.5	73.1	
	61	114				
	67	73	122	66.1	96.1	
	82	162				
	82	153				
	60	200				

Appendix E. Pitting in F-111 Fleet vs. Laboratory

This appendix contains the details of several examples of pitting in the F-111 fleet and compares the features to the pitting generated in the laboratory during this experimental program.

Laboratory Pitting

For the artificial corrosion, 134 different pits were characterised during the experimental program. Based on experimental fatigue results, it was decided to not collect depth information for pits less than 30 microns deep. The largest pit generated in the laboratory was 105 microns deep at the time of data collection. A subsequent effort (on a scrap piece of D6ac) generated pitting 120 microns deep, but it must be kept in mind that the maximum depth of the pitting was carefully controlled by the electrochemical process described in Chapter 2.

Even if it was possible to grow still deeper pits, the power law nature of the pit growth kinetics means that diminishing returns were reached quite quickly. For instance, 60 micron pits took 375 seconds to grow, 90 micron pits took 845 seconds to grow, and the grand target of 135 microns required 1680 seconds (28 minutes), but the depth in that one trial fell short at 120 microns (the case mentioned above). This probably happened because a fair amount of general attack and a little crevice corrosion started to occur at the extended exposure time. There does appear to be a practical limit to the pitting using this method — at least using the parameters selected for this trial.

The laboratory pits were measured using two different techniques. In some cases, the fracture plane of a fatigue specimen passed through a pit or several pits, and the depth and aspect ratio was easily measured using a scanning electron microscope (SEM). In other cases, the pits had not caused fracture, so pit depth and aspect ratio was determined using an optical measuring microscope. This led to some differences in aspect ratio data in many cases.

Virtually every pit that had very high aspect ratios ($a/c > 2$) were found in the SEM. These pits tended to have a very small surface opening. The optical microscope could not see into similar pits well enough to get an accurate depth measurement, so they were not analysed. The optical microscope was much better at measuring pits with $a/c < 2$. This can be seen clearly in Figure E1.

Because of the high aspect ratio of some of the pits, some pit metrics were quite large for the laboratory data. The maximum was 171 microns (depth * aspect ratio), but this was the result of a 43 micron deep pit that had an aspect ratio nearing four. A clear trend seen in Figure C1 is that as pits get deeper, the aspect ratios tend to decrease (as indicated by the dotted line on the figure). Although shallow pits have a wide variety of aspect ratios, the deeper pits very seldom have a high aspect ratio. For instance, at

100 microns depth, aspect ratios greater than one are a rarity. This happens because pits driven to these great depths tend to link with neighbouring pits and form low aspect ratios. A good example of this is shown in Figure 27 in Chapter 4.

In-service data are also shown in Figure E1 chart, and their significance is discussed in the following paragraphs.

In-service Corrosion

Around 100 pits were characterised from in-service damage in F-111 aircraft. The areas where information was available included wing pivot fitting (WPF) upper and lower plates, stiffener runouts in the WPF, a D6ac pylon fitting, and the horizontal tail pivot shaft. The information WPF and horizontal tail pivot shaft was all lifted from replicas (acetate and dental putty), and the damage to the pylon fitting was characterised from SEM micrographs.

The greatest pit depth recorded from in-service damage was a cavernous 672 microns. This occurred in the horizontal tail pivot shaft pistol fitting. Fortunately, the pit was in an innocuous area because stress was so low. The damage in the pivot fitting was consistently deeper than the other areas mapped, and many pits approached 200 microns in depth. However, their morphology was very different from all the other areas investigated, as they had very wide aspect ratios, which led to very small pit metrics. In Figure E1, the horizontal tail damage is noticeably separate from the rest of the data, and whether to even call this damage pitting is worthy of debate. It may have been more some sort of localised general attack that had been working for a very long time.

The pitting damage determined from the wing and pylon fitting matched very well with the laboratory grown corrosion (Figure E1). Again, pits with very high aspect ratios (a/c > 2) were rare, a couple of exceptions being found in the micrographs from the pylon fitting. The replica techniques used on the rest of the pits probably would not be able to not resolve this type of morphology.

Since the damage in the horizontal tail was so noticeably different from pits in other areas, those data were excluded from the following comparisons. Furthermore, the largest pit (672 microns – in horizontal tail) was excluded from Figure E1 as it compressed the left side of the graph too much. It is important to note that the original work is based on modelling the effects of pitting corrosion in the WPF not the horizontal tail.

Pit Feature Comparisons

Figure E2 shows a comparison histogram of 134 laboratory-grown pits versus 59 pits measured from the F-111. The shapes of the histograms are quite similar, although the pits in-service can reach slightly greater depths than what was achieved in the

laboratory (discussed earlier). This is not cause for great concern, as the pit metric (depth * aspect ratio) used to determine ECS covers a greater range in the laboratory damage than the in-service damage. This is shown in Figure E3.

Limitations

Keeping the damage in the horizontal tail pivot shaft in mind, it is obvious that corrosion damage in the F-111 can reach depths much greater than 135 microns. However, it is questionable as to whether or not that damage was actually pitting. As such, it should be stated here that the modelling efforts in this research report cover pitting corrosion. The ECS process is not meant to cover crevice corrosion or heavy general attack. While the approach may work, it has by no means been validated for these other damage morphologies.

Also, most of the damage investigated from the aircraft was done using replicas. This will continue to be the case in the future, since the liberty is not likely to be granted (obviously) to cut parts out of the airplane for a full destructive examination of the corrosion damage. The replica techniques can easily be questioned as to their resolution, mostly in their ability to measure depths accurately, particularly when pits are narrow (high aspect ratio). Corrosion products in the base of pits could further throw off depth estimates. It is because of these problems that it is probably wise to use the upper bound of the ECS correlation curve, as it adds in a healthy safety factor to cover limitations of NDI.
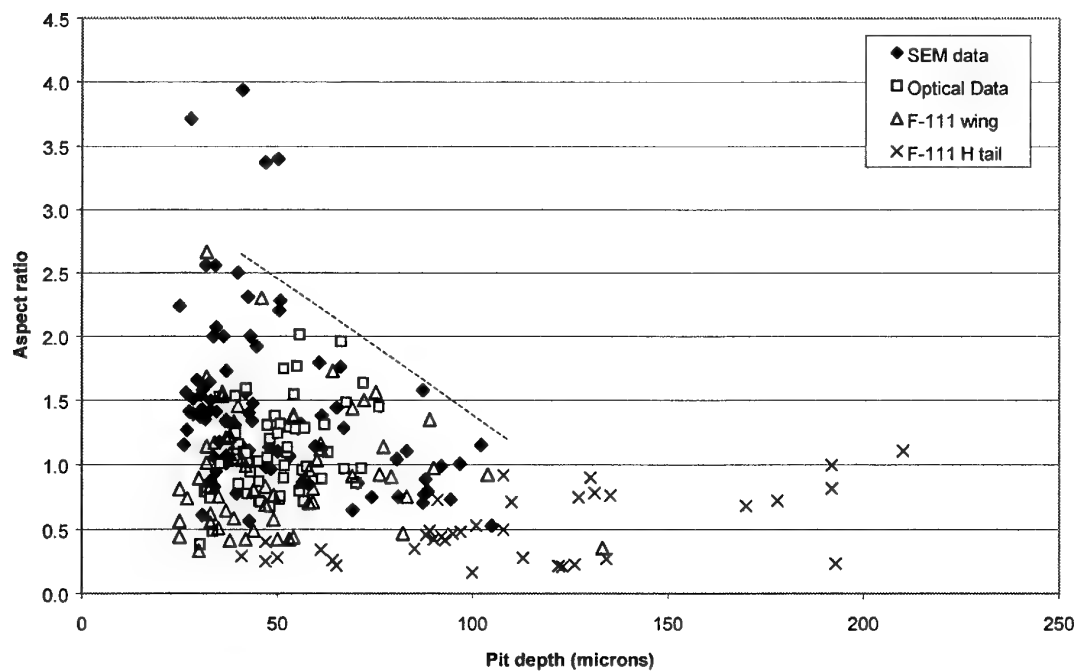
Figure E1. Pit depth vs. aspect ratio for laboratory and in-service corrosion.
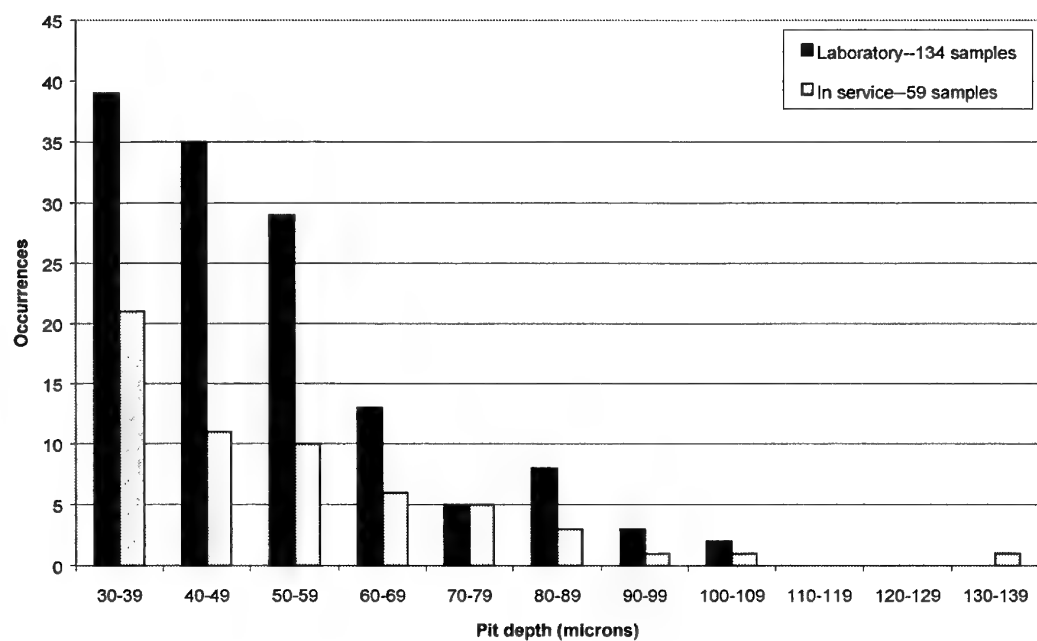
Figure E2. Pit depth histogram for laboratory vs. in-service pitting.
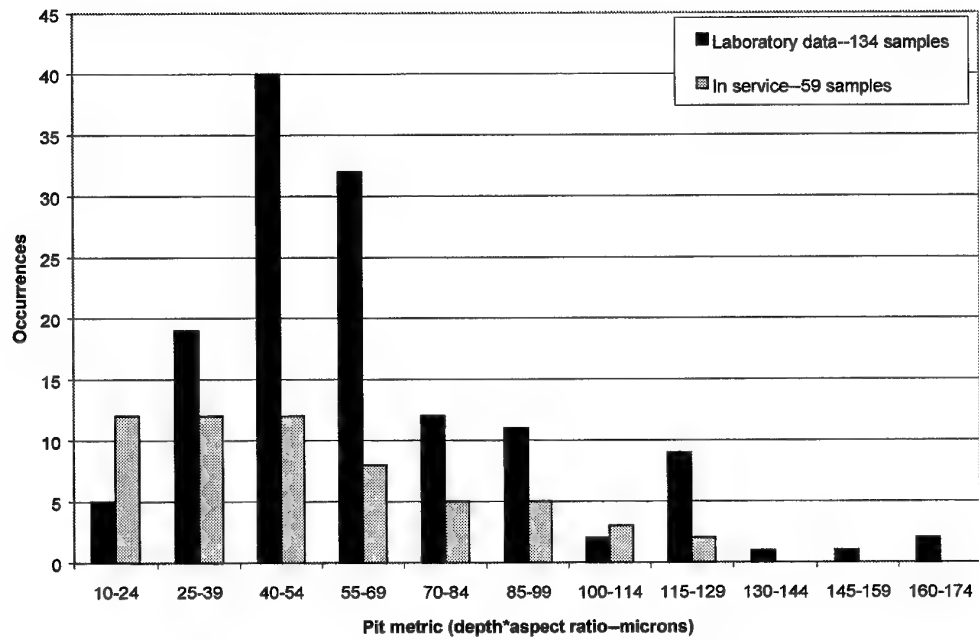
Figure E3. Pit metric histogram for laboratory vs. in–service pitting.

Appendix F. Summary of FP78AD Pitting

The following tables summarise all the pit locations, depths, and aspect ratios for the 57 pits investigated in specimen FP78AD for the low stress sample application discussed in Section 6.1. Also included are the stresses at the location of each pit, the mean ECS values, the upper 99.95% confidence limit ECS values, and the life predictions associated with each of these ECS curves.

In the second table, life predictions shaded in grey (80 000 hours) were not actually run (to save time). Life in the cases is at least 80 000 hours. The entry that is highlighted in light grey with bold type was the shortest life for the upper and mean curve ECS cases in this specimen.

Table F1. Pit locations and morphologies in specimen FP78AD.

pit	X (mm)	Y (mm)	pit depth (microns)	metric (depth*AR)
1	0.5652	1.9429	30.3	11.7
2	0.5856	1.386	31.4	16.2
3	-0.6264	3.376	31.9	24.3
4	-0.968	1.3208	32.8	25.0
5	-1.9376	3.0924	33.5	25.3
6	0	1.9728	35.2	32.5
7	-1.9276	0.7048	35.4	32.5
8	-4.3972	0.8848	39.3	32.7
9	0.7172	2.7128	39.3	32.9
10	-4.696	1.3936	39.8	34.2
11	0	1.6612	39.8	35.8
12	-2.2922	3.3228	40.1	37.1
13	-3.8484	2.3764	40.1	38.4
14	-0.5332	3.118	41.4	39.5
15	0.2512	2.1768	42.1	40.7
16	-1.4472	2.9764	42.1	40.7
17	-2.9892	1.2592	42.3	41.6
18	-0.7864	1.3884	43.1	44.0
19	-4.816	0.9656	44.8	44.4
20	-3.8636	1.7028	45.2	45.6
21	-1.9376	3.2852	45.3	45.9
22	-2.1828	1.8324	45.3	46.0
23	-4.6972	1.5984	45.7	46.2
24	-4.358	2.6204	47.4	46.5
25	0.0004	2.5808	47.4	46.5
26	-0.5548	3.2732	48	48.9
27	-2.8848	1.18	48.1	50.2
28	-0.3716	1.3522	49.4	51.4
29	-0.1088	2.782	50	53.9
30	-4.7476	2.3204	50.5	54.1
31	-1.1004	0.5616	50.6	54.7

Table F1 cont. Pit locations and morphologies in specimen FP78AD.

pit	X (mm)	Y (mm)	pit depth (microns)	metric (depth*AR)
32	-1.5856	3.4176	50.6	56.6
33	-4.4644	1.1048	51.5	57.5
34	-1.7156	1.85	51.5	57.8
35	-0.8564	2.2236	51.7	59.7
36	-0.8116	3.4216	52.3	60.1
37	0.008	1.0676	52.5	60.3
38	-3.398	2.954	53	62.1
39	0.6916	1.7376	54.1	62.2
40	0.1896	3.084	54.5	64.9
41	-4.4436	2.66	54.8	66.7
42	-0.9488	3.342	55.5	67.1
43	-3.42	0.9416	55.6	68.2
44	-3.274	1.7936	56.3	68.5
45	-1.8264	0.5696	56.6	69.0
46	0.5716	3.064	56.8	69.4
47	-0.0564	3.134	57.3	69.7
48	0.3316	1.1096	61.2	73.0
49	-4.7476	2.1012	61.9	81.2
50	-0.9812	0.702	62.7	83.6
51	-0.3164	1.3776	66.1	90.1
52	-0.7028	1.2244	66.9	96.9
53	-0.0172	0.5988	67.4	100.1
54	-2.9936	0.7248	69.9	109.8
55	-4.8404	1.3248	71.3	112.0
56	-3.1524	2.67	71.7	117.4
57	-4.1624	2.6916	75.7	129.7

Table F2. ECS values and life predictions for specimen FP78AD.

pit	ECS upp 99	ECS mean	Stress at point	life from AFGROW (hrs) ECS upp99	Predicted life from mean ECS
1	38.1	8.2	0.993	55195	80000
2	39.0	8.9	0.993	53695	80000
3	40.6	10.4	0.977	55694	80000
4	40.7	10.5	0.965	58195	80000
5	40.8	10.6	0.942	64195	80000
6	42.2	12.1	1.000	48695	80000
7	42.2	12.1	0.943	61695	80000
8	42.2	12.2	0.782	80000	80000
9	42.2	12.2	0.991	50195	80000
10	42.5	12.5	0.750	80000	80000
11	42.8	12.9	1.000	47695	80000
12	43.1	13.2	0.927	64695	80000
13	43.4	13.6	0.835	80000	80000

Table F2 cont. ECS values and life predictions for specimen FP78AD.

pit	ECS upp 99	ECS mean	Stress at point	life from AFGROW (hrs) ECS upp99	Predicted life from mean ECS
14	43.6	13.8	0.981	50695	80000
15	43.8	14.2	0.997	47195	80000
16	43.9	14.2	0.953	56695	80000
17	44.0	14.4	0.894	73695	80000
18	44.6	15.1	0.971	52195	80000
19	44.7	15.2	0.737	80000	80000
20	44.9	15.5	0.834	80000	80000
21	45.0	15.6	0.942	58195	80000
22	45.0	15.7	0.932	60695	80000
23	45.1	15.7	0.749	80000	80000
24	45.1	15.8	0.786	80000	80000
25	45.1	15.8	1.000	45195	80000
26	45.7	16.5	0.980	48695	80000
27	46.0	17.0	0.899	69195	80000
28	46.4	17.4	0.987	46695	80000
29	47.0	18.2	0.996	44404	80000
30	47.1	18.3	0.744	80000	80000
31	47.2	18.5	0.962	51195	80000
32	47.8	19.2	0.951	52695	80000
33	48.0	19.5	0.774	80000	80000
34	48.1	19.6	0.948	53195	80000
35	48.7	20.3	0.969	48195	80000
36	48.8	20.5	0.971	47695	80000
37	48.9	20.6	0.999	42195	80000
38	49.4	21.3	0.866	74695	80000
39	49.4	21.3	0.992	43195	80000
40	50.3	22.4	0.998	41695	80000
41	50.9	23.2	0.776	80000	80000
42	51.1	23.4	0.966	46695	80000
43	51.5	23.9	0.865	72195	80000
44	51.6	24.0	0.875	68905	80000
45	51.8	24.2	0.945	50195	80000
46	52.0	24.5	0.993	40695	80000
47	52.1	24.6	0.998	40195	80000
48	53.3	26.2	0.996	39195	80000
49	56.9	30.6	0.744	80000	80000
50	58.2	32.0	0.945	44695	80000
51	61.6	36.2	0.989	35195	55195
52	65.9	41.2	0.975	35195	56695
53	68.1	43.8	0.999	31195	47195
54	75.6	52.6	0.894	43695	61695
55	77.5	54.9	0.734	80000	80000
56	82.5	60.8	0.883	42695	59195
57	95.7	76.8	0.807	53195	65195

Appendix G: NDI of Corrosion Pits in D6ac Steel

Repeatedly identified in this report is the need for reliable NDI of corrosion pits. This capability is a hinge for the ECS concept developed here, as the equivalent crack size of a corrosion pit is directly related to the pit's physical depth and aspect ratio.

Although no specific effort was undertaken to develop or even evaluate NDI as part of this study, some other recent efforts (associated with pitting the F-111 full-scale wing fatigue test article) have shed some light on the subject. Full details of this activity are found a report by Mills and Loader (2001), but some of the information has been extracted and placed into this appendix along with a couple other thoughts.

In addition to the effort mentioned above, NDTSL at RAAF Amberley has a lot of experience taking replicas of pits using acetate as well as two-part dental putty, such as Exaflex.

Cleaning the Pits for NDI

A crucial part of the pit measurement process is ensuring that the pits are cleaned of corrosion product. This is not always simple, as the corrosion products associated with dissolution of D6ac can be tenacious. If the pits do not clean out easily (which may be difficult to discern) then Clarke's reagent can be used to remove corrosion products. Use of Clarke's was necessary in the laboratory, where the electrochemical corrosion process formed tight oxide caps over the pits. With these caps in place it was not possible to determine anything other than pitting location using NDI.

Clarke's reagent is a strong acid, so its use must be approached with caution to avoid personal injury as well as to avoid hydrogen embrittlement of the steel.

The recipe for 200 ml of Clarke's reagent is: 200 ml hydrochloric acid, 4 g of antimony trioxide (Sb_2O_3), and 10 g of stannous chloride ($SnCl_2$) (ASTM Standard G1-81).

Removing the corrosion product from the pits is simple. It requires a well agitated solution of Clarke's reagent, cotton buds, and ethanol. The Clarke's reagent is used to wet a cotton bud; the recently corroded area is swabbed for 60 seconds, and then vigorously rinsed with ethanol. Proper safety equipment, to include nitrile gloves, is necessary for this step.

Exposure Trial

The 'safe time limit' of 60 seconds for swabbing with Clarke's reagent was determined using the following experiment. A simple study assessed the impact of Clarke's reagent on the surface condition of the D6ac steel. The steel was exposed to the solution from times ranging between 30 seconds and 10 minutes. The times and

physical observations are listed below. The solution was allowed to sit for about four days before use, so it would weaken some.

- 10 minutes—solution caused pitting up to 12 microns deep. Surface etching was very evident and accompanied by dark discolouration. Increased shallow pitting activity was prevalent near the edges of the affected area, likely the result of differential aeration.
- 5 minutes—solution caused pitting less than one micron deep. Surface etching was evident, but discolouration was less. The effects of differential aeration at the edge of the wetted area were still noticeable.
- 2 minutes—no pitting was present. Surface etching was still apparent but very light. Evidence of differential aeration at the edge of wetted area could not be found. The region was still discoloured.
- 90 seconds—very benign. Etching was minimal along with the discolouration.
- 60 seconds—scattered etching and minimal discolouration.
- 45 seconds—benign.
- 30 seconds—benign.

From the results of this experiment, it appears that exposure times to the Clarke's reagent can range from 30 seconds to 60 seconds without adversely affecting the material.

Hydrogen Embrittlement

Using a strong acid on high strength steel can be cause for concern if done improperly, as it can lead to hydrogen embrittlement (HE). Research by Grummet and Hinton (2001) shows that the risk for HE abates depending on the time and temperature history. In 4340 steel, 16 days at room temperature is adequate to ensure HE will not occur. Since D6ac is less susceptible to HE than 4340, the time required to avoid HE is less in this alloy. Although no data yet exist for room temperature, results at 50 °C confirm this behaviour. If less time is available, 24 hours at 50 °C will drive hydrogen out of D6ac. This can be accomplished by placing heat blankets on the affected areas. To lower the risk of HE, the amount of Clarke's reagent used should be minuscule, and the exposure time should be kept to less than 60 seconds.

Replica Technique for Measuring Pits

The purpose for cleaning the corrosion pits is so an accurate replica can be made of the pits. The replica technique described here is magnetic rubber casting. Mixing of the compound followed the procedures from AAP 7002.043-36, NDT General Procedures. This compound is mixed together then poured into a aluminium tape dam affixed around the FFVH. In about 20 minutes, the compound becomes firm, and the replica

can be taken from the component directly to an optical microscope for pit measurement. On a flat specimen containing pits, a high degree of pit depth accuracy was achieved with the magnetic rubber material, as shown in Table G1. The small discrepancies in the observations results from variability in determining at what depth the feature was last in focus.

Table G1. Comparison of actual pit depths to depths replicated by magnetic rubber on a simple specimen. Actual pit depths were determined using an optical microscope.

Location	Actual Depth (microns)	Replicated Depth (microns)	Percent Difference
1	82	83	1.2
2	97	99	2.0
3	86	89	3.3
4	72	74	2.7

Many locations in the F-111 WCTB and WPF are lot more geometrically complex. Thus, a simulated FFVH was pitted three different times in the laboratory. The complex geometry presented more of a challenge for making magnetic rubber castings, and several problems were encountered. The main difficulty was with the magnetic rubber material tearing off in the pits when being removed from the FFVH, since the casting could not be lifted straight off the surface.

As shown in Table G2, the first result seemed reasonable. In the second try, the magnetic rubber underestimated the depth, and it is not clear whether material was sheared off in the pit or if the replica was damaged in a different way. The final try for that specimen (Location 3) was ruined when the replica tore off in the pit.

Locations 4-6 were in a second practice FFVH, and the dam for the magnetic rubber was modified to allow the replica to be lifted off the surface of the steel as directly as possible. Location 4 had the shallowest corrosion damage, and it was almost all crevice corrosion because of trouble encountered applying the corrosion damage. The magnetic rubber replicated this damage with ease, and no material was left in the crevices. Location 5 worked very well, but in Location 6, some of the magnetic rubber remained in the pits. The shallower pits (50 microns or less) were clean; the two deeper main pits (92 and 71 microns) retained some of the magnetic rubber material.

In all, the second batch of experiments (Locations 4-6) met with much more success. The technique is still not perfect, but it should provide valuable information. This appears to be a very delicate process, so more care will lead to more success.

Table G2. Comparison of actual versus replicated pit sizes using magnetic rubber in two practice FFVHs.

Location	Actual Depth (microns)	Replicated Depth (microns)	Percent Difference
1	38	36	5
2	58	42	28
3	74	27	64
4	33	31	6
5	70	65	7
6	92	76	17

DISTRIBUTION LIST

The Incorporation of Pitting Corrosion Damage into F-111 Fatigue Life Modelling

T. Mills, P.K. Sharp and C. Loader

AUSTRALIA

DEFENCE ORGANISATION

Task Sponsor
DGTA-ASI
S&T Program
    Chief Defence Scientist
    FAS Science Policy   } shared copy
    AS Science Corporate Management
    Director General Science Policy Development
    Counsellor Defence Science, London (Doc Data Sheet)
    Counsellor Defence Science, Washington (Doc Data Sheet)
    Scientific Adviser to MRDC Thailand (Doc Data Sheet)
    Scientific Adviser Joint
    Navy Scientific Adviser (Doc Data Sheet and distribution list only)
    Scientific Adviser - Army (Doc Data Sheet and distribution list only)
    Air Force Scientific Adviser
    Director Trials

Aeronautical and Maritime Research Laboratory

    Research Leader (Doc Data Sheet and Distribution List Only
    Task Manager

T. Mills (5 copies)	J. Boyes
K. Sharp (6 copies)	B. Crawford
C. Loader	T. Van Blaricum
G. Clark	G. Swanton (DSTOSO Amberley)
K. Watters	G. Hugo (MPD)
K. Walker	

DSTO Library and Archives
    Library Fishermans Bend
    Library Edinburgh 1 copy
    Australian Archives

Capability Systems Staff
    Director General Maritime Development (Doc Data Sheet only)
    Director General Aerospace Development

Knowledge Staff

Director General Command, Control, Communications and Computers (DGC4) (Doc Data Sheet only)

Army

ABCA National Standardisation Officer, Land Warfare Development Sector, Puckapunyal (4 copies)

SO (Science), Deployable Joint Force Headquarters (DJFHQ) (L), Enoggera QLD (Doc Data Sheet only)

NPOC QWG Engineer NBCD Combat Development Wing, Puckapunyal, VIC (Doc Data Sheet relating to NBCD matters only)

Air Force

DGTA

ASI4: Dr Madabhushi Janardhana (2 copies)

SRSPO CENGR (Amberley) WGCDR M. Benfer

Intelligence Program

DGSTA Defence Intelligence Organisation

Manager, Information Centre, Defence Intelligence Organisation

Defence Libraries

Library Manager, DLS-Canberra

Library Manager, DLS - Sydney West (Doc Data Sheet Only)

UNIVERSITIES AND COLLEGES

Australian Defence Force Academy
    Library
    Head of Aerospace and Mechanical Engineering
Serials Section (M list), Deakin University Library, Geelong, VIC
Hargrave Library, Monash University (Doc Data Sheet only)
Librarian, Flinders University

OTHER ORGANISATIONS

National Library of Australia
NASA (Canberra)
AusInfo

OUTSIDE AUSTRALIA

INTERNATIONAL DEFENCE INFORMATION CENTRES
US Defense Technical Information Center, 2 copies
UK Defence Research Information Centre, 2 copies
Canada Defence Scientific Information Service, 1 copy
NZ Defence Information Centre, 1 copy

ABSTRACTING AND INFORMATION ORGANISATIONS
Library, Chemical Abstracts Reference Service
Engineering Societies Library, US
Materials Information, Cambridge Scientific Abstracts, US
Documents Librarian, The Center for Research Libraries, US

INFORMATION EXCHANGE AGREEMENT PARTNERS
Acquisitions Unit, Science Reference and Information Service, UK
Library - Exchange Desk, National Institute of Standards and Technology, US
National Aerospace Laboratory, Japan
National Aerospace Laboratory, Netherlands

SPARES (5 copies)

Total number of copies: 67

| DEFENCE SCIENCE AND TECHNOLOGY ORGANISATION DOCUMENT CONTROL DATA | | 1. PRIVACY MARKING/CAVEAT (OF DOCUMENT) | |

2. TITLE The Incorporation of Pitting Corrosion Damage into F-111 Fatigue Life Modelling	3. SECURITY CLASSIFICATION (FOR UNCLASSIFIED REPORTS THAT ARE LIMITED RELEASE USE (L) NEXT TO DOCUMENT CLASSIFICATION) Document (U) Title (U) Abstract (U)

4. AUTHOR(S) T. Mills, P.K. Sharp and C. Loader	5. CORPORATE AUTHOR Aeronautical and Maritime Research Laboratory 506 Lorimer St Fishermans Bend Vic 3207 Australia

6a. DSTO NUMBER DSTO-RR-0237	6b. AR NUMBER AR-012-354	6c. TYPE OF REPORT Research Report	7. DOCUMENT DATE June 2002

8. FILE NUMBER M1/9/936	9. TASK NUMBER AIR 00/139 A20926	10. TASK SPONSOR RAAF ASI2-DGTA	11. NO. OF PAGES 157	12. NO. OF REFERENCES 22

13. URL on the World Wide Web http://www.dsto.defence.gov.au/corporate/reports/DSTO-RR-0237.pdf	14. RELEASE AUTHORITY Chief, Airframes and Engines Division

15. SECONDARY RELEASE STATEMENT OF THIS DOCUMENT

Approved for public release

OVERSEAS ENQUIRIES OUTSIDE STATED LIMITATIONS SHOULD BE REFERRED THROUGH DOCUMENT EXCHANGE, PO BOX 1500, EDINBURGH, SA 5111

16. DELIBERATE ANNOUNCEMENT

No Limitations

17. CASUAL ANNOUNCEMENT	Yes

18. DEFTEST DESCRIPTORS
Fatigue life modelling, Pitting corrosion damage, F-111, Equivalent initial flow size EIFS, Equivalent cack size modelling, high strength steel

19. ABSTRACT   In this report, an Equivalent Crack Size (ECS) model is developed for corrosion pitting in D6ac steel. Relationships between physical corrosion morphology and fatigue life of laboratory coupons were established that allowed corrosion pits to be described as cracks to provide input for durability and damage tolerance analyses. Using the ECS relationship, fatigue lives were accurately predicted in complex coupons tested under spectrum loading. Details are provided on all the corrosion procedures, the developmental testing program, and the validation testing program. So far, the ECS model for corrosion pitting is only valid for areas of the structure that do not experience yielding. A portion of this testing program was meant to examine the application of ECS to cases that experience compressive and tensile yield, but that has been placed on hold until final development of the appropriate analysis software. The impacts of this research on F-111 fleet management can be quite positive by helping avoid unnecessary maintenance and helping to reach a life-of-type goal of 2020.